
Quantification of the water balance and experimental evaporation studies, Lake Urmia, Iran

Dissertation

Doctoral thesis submitted in fulfilment of the requirements
for the degree Doctor rerum naturalium (Dr. rer. nat.)
at the
Department of Materials- and Geosciences
Technische Universität Darmstadt



TECHNISCHE
UNIVERSITÄT
DARMSTADT

Submitted by

Sahand Farhangdarehshouri

born on 18 September 1985 in Shiraz, Iran

Referee 1: Dr. Stephan Schulz

Referee 2: Prof. Dr. Andreas Henk

Examiner 1: Prof. Dr. Christoph Schüth

Examiner 2: Prof. Dr. Boris Lehmann

Darmstadt 2023

Farhangdarehshouri, Sahand

Title: Quantification of the water balance and experimental evaporation studies, Lake Urmia, Iran

Darmstadt, Technische Universität Darmstadt

Publication on TUpriints: 2023

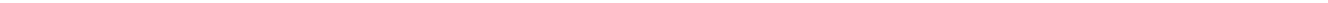
Submission: 2 June 2023

Thesis defense: 2 August 2023

URN: urn:nbn:de:tuda-tuprints-244668

Licence information: Veröffentlicht unter Urheberrecht / Published under Copyright

Urheberrechtlich geschützt / In copyright <https://rightsstatements.org/page/InC/1.0/>



Declaration of authorship

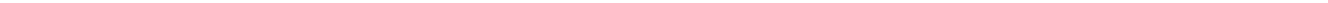
I hereby declare that the presented dissertation is based on original research and is the result of my own work. I certify that this dissertation contains no material that has been accepted for the award of any other degree in my name, in any university or other tertiary institution and, to the best of my knowledge and belief, contains no material previously published or written by another person, except where due reference has been made in the text.



Sahand Farhangdarehshouri

02.06.2023

Darmstadt,



Foreword

The drying up of Lake Urmia is one of the major environmental crises in Iran and I am honoured to have had the opportunity to study it. There is a debate among scientists regarding the causes of the lake's level decline, with some attributing it to the increase in agricultural activities and some changes in climatic conditions. This thesis aims to piece together the puzzle to get a better understanding of the reasons for the decline in water level as well as to propose development scenarios for the lake Urmia.

This cumulative dissertation includes three studies listed in the International Scientific Indexing (ISI) Journals. I had the privilege of writing my PhD thesis as an international DAAD student at the Institute of Applied Geosciences at TU-Darmstadt, under the supervision of Dr. Stephan Schulz and Prof. Dr. Christoph Schüth. Furthermore, we worked with Prof. Dr. Massoud Tajrishy from the Department of Civil Engineering at Sharif University of Technology, who is leading the Lake Urmia Restoration Programme (ULRP).

I would like to extend my appreciation to the German Academic Exchange Service (DAAD) for funding my studies through the NaWaM Study Scholarships and Research Grants 2015 (57156376) provided by the Federal Ministry of Education and Research (BMBF). I also want to express my gratitude to my dear colleagues Dr. Nils Michelsen and Dr. Elmira Hassanzadeh for their unconditional support.

ISI publications that are part of this cumulative thesis:

Schulz, S., Darehshouri, S., Hassanzadeh, E., Tajrishy, M., Schüth, C., 2020. Climate change or irrigated agriculture – what drives the water level decline of Lake Urmia. *Scientific Reports* 10 (1): 236 <https://doi.org/10.1038/s41598-019-57150-y>

Darehshouri, S., Michelsen, N., Schüth, C., Schulz, S., 2020. A low-cost environmental chamber to simulate warm climatic conditions. *Vadose Zone Journal* 19 (1): 1–6 <https://doi.org/10.1002/vzj2.20023>

Darehshouri, S., Michelsen, N., Schüth, C., Tajrishy, M., Schulz, S., 2022. Evaporation from the dried-up lake bed of Lake Urmia, Iran. *Science of The Total Environment*: 159960 <https://doi.org/10.1016/j.scitotenv.2022.159960>

Associated ISI publication (not part of this cumulative thesis):

Schröder, T., Hassanzadeh, E., Darehshouri, S., Tajrishy, M., Schulz, S., 2022. Satellite based lake bed elevation model of Lake Urmia using time series of Landsat imagery. *Journal of Great Lakes Research*. <https://doi.org/10.1016/j.jglr.2022.08.016>

Abstract

The first study (Schulz et al., 2020) deals with the quantification of the water balance components of Lake Urmia and their temporal development over the last five decades. It shows that the fluctuations in the water level of Lake Urmia in the period we studied were mainly triggered by climatic changes. However, under current climatic conditions, agricultural water abstraction is significant compared to the remaining inflow of surface water. Changes in agricultural water abstraction would have a significant impact on the lake volume and could lead either to a stabilisation of the lake or to its complete collapse.

The second study deals with the construction and testing of a low-cost climate chamber for simulating warm climate conditions (Darehshouri et al., 2020). The climate chamber enables reliable regulation of temperature and relative humidity in a typical range of warm climate conditions. Climate chambers are widely used in various disciplines (e.g., salt weathering of rocks, nutrient leaching in soils, water repellency of soils or in evaporation studies, as well as in testing monitoring equipment, etc.). This study also includes step-by-step instructions for building a low-cost DIY climate chamber. The use of the climate chamber allowed us to conduct a series of evaporation experiments to estimate evaporation from the lake surface (Schulz et al., 2020) and the dried lake bed (Darehshouri et al., 2022) of the Lake Urmia and accordingly determine a better water balance for the lake.

The third study (Associated ISI publication, Schröder et al., 2022) presents a lake bed elevation model of Lake Urmia. In the course of model generation, a time series of the extent of the lake surface was derived from 129 satellite images with different acquisition dates based on the Landsat sensors Thematic Mapper (TM), Enhanced Thematic Mapper Plus (ETM+), and Operational Land Imager (OLI). Due to the rapid shrinking of the lake during the last two decades, lake surface areas ranging from 890 km² to 6125 km² could be covered. The water edge of the various lake extents was then linked to the observed water level on the day of the satellite image acquisition. The resulting contour lines, covering water levels between 1270.04 m and 1278.42 m a.s.l. and thus representing the lakebed morphology in its shallow parts, were merged with existing data (deeper parts) and interpolated to generate a lake bed elevation model. Finally, Lake Urmia's Level-Area-Volume relationships were derived from the lake bed elevation model and compared to bathymetric data previously published.

In the fourth study (Darehshouri et al., 2022) we quantified the amount of evaporation from the dried up lake bed of Lake Urmia. The decline in the lake's water level between 1998 and 2020 has formed an area of more than 4,000 km² (i.e., in September 2015) of dried up lake bed, which is covered with precipitated salt on the surface. Although several studies have analysed the water balance of the lake in recent decades, evaporation from the dried up lake bed has not been taken into account. Considering that large areas dried up, we assumed that evaporation from the dried up lake bed might also play a role in the overall water balance of the lake. We applied a transferable multi-methods approach using laboratory column experiments and field data to determine the evaporation from the

dried up lake bed of Lake Urmia. The column experiment was conducted with undisturbed soil columns taken from the dried up lake bed of Lake Urmia. The columns were placed in a climate chamber and exposed to daily temperature and humidity cycles to simulate the climatic conditions of Lake Urmia, while monitoring weight and water level changes due to evaporation. Our results show that the estimated evaporation from the dried up lake bed during the dry season (June to August) ranges from 0.12 mm per day to 0.2 mm per day, accounting for up to more than 6% (0.07 km^3) of the total evaporation from Lake Urmia, depending on the lake level.

Table of contents

| | |
|---|----|
| Declaration of authorship | 4 |
| Foreword | 6 |
| Abstract | 7 |
| Table of contents | 9 |
| List of figures | 11 |
| List of tables | 15 |
| List of abbreviations | 16 |
| 1 Introduction | 19 |
| 1.1 Background | 19 |
| 1.2 Study area | 24 |
| 1.3 Climate | 25 |
| 1.4 Geology | 26 |
| 1.4.1 Structural geology | 26 |
| 1.5 Hydrogeology | 28 |
| 1.5.1 Groundwater systems | 28 |
| 1.6 Surface water | 30 |
| 1.6.1 Reservoirs | 31 |
| 1.7 Development of the water sector | 31 |
| 1.7.1 Land use | 31 |
| 1.7.2 Water consumption | 32 |
| 1.8 References | 35 |
| 2 Climate change or irrigated agriculture – what drives the water level decline of Lake Urmia | 38 |
| 2.1 Abstract | 38 |
| 2.2 Introduction | 39 |
| 2.3 Methods | 42 |
| 2.3.1 Data | 42 |
| 2.3.2 Level-area-volume relationship | 42 |
| 2.3.3 Salt water evaporation | 42 |
| 2.3.4 Statistics | 44 |
| 2.4 Results and discussion | 44 |
| 2.4.1 Lake Urmia's water balance. | 44 |
| 2.4.2 Changing climate vs. irrigation water consumption | 46 |
| 2.4.3 Reservoirs and discharge | 49 |
| 2.4.4 Implications on future perspectives | 49 |
| 2.5 Conclusion | 51 |

| | |
|---|-----|
| 2.8 Supplementary data | 52 |
| 2.9 References | 52 |
| 3 A Low-cost Environmental Chamber to simulate warm Climatic Conditions | 57 |
| 3.1 Abstract | 57 |
| 3.2 Introduction | 58 |
| 3.3 Design | 58 |
| 3.4 Test | 60 |
| 3.5 Concluding remarks | 64 |
| 3.6 Acknowledgments | 65 |
| 3.7 Supplementary data | 65 |
| 3.8 References | 65 |
| 4 Evaporation from the dried-up lake bed of Lake Urmia, Iran | 68 |
| 4.1 Abstract | 68 |
| 4.2 Introduction | 69 |
| 4.3 Study area | 70 |
| 4.4 Materials and methods | 72 |
| 4.4.1 Water level monitoring and soil core sampling | 72 |
| 4.4.2 Column experiment | 73 |
| 4.4.3 Upscaling and regionalization of evaporation data | 75 |
| 4.5 Results and Interpretation | 75 |
| 4.5.1 Column experiment | 75 |
| 4.5.2 Implications for water balance calculations | 78 |
| 4.6 Conclusion | 80 |
| 4.7 Authorship contribution statement | 80 |
| 4.8 Data availability | 80 |
| 4.9 Acknowledgments | 81 |
| 4.10 Supplementary data | 81 |
| 4.11 References | 81 |
| 5 Outlook | 85 |
| 6 Conclusions | 87 |
| Supplementary information 1 | 90 |
| Supplementary information 2 | 94 |
| Supplementary information 3 | 111 |

List of figures

- Fig. 1-1.** a) Overview map of the study area, including the elevation of the catchment area and boundaries of the Lake Urmia. b) Geographical location of the Lake Urmia catchment area. **17**
- Fig 1-2.** Images of Lake Urmia, Iran (1992) view from Kaboodan Island. a) Main islands in the southern part of Lake Urmia are marked on a Landsat-5 image (acquisition date: 2nd of September 1995). The photos (b-e) show a lively lake (Photos by Bijan Darehshouri, 1992). **18**
- Fig. 1-3.** a) Water level of Lake Urmia from 1965 to 2021 (data ULRP, 2021). b) Satellite images showing the lake level decline, the lake area was extracted from satellite images, using its extent in 1995 as a reference. The images include Landsat image from 1976, (Landsat-2), 1986, 1995, 2000, 2005, (Landsat-5) and the most recent images, from 2013 to 2022, (Landsat-8). The acquisition dates were displayed on top of each image. **20**
- Fig. 1-4.** Images of Lake Urmia, Iran (September, 2017). a) Direction of the images, are market on a Landsat-8 image (acquisition date: 14th of September 2017) facing north, east and west highlights the extent of the drying and the dramatic transformation of the once vast body of water. The photos (b-e) show the devastating impact of decreased water levels on the once vibrant lake. **21**
- Fig. 1-5.** a) Precipitation intensity in the Lake Urmia catchment area. b) Average temperature and relative humidity in Lake Urmia from 1952 to 2020, and average monthly precipitation from 1952 to 2017 (Data source: WRMC, 2021). c) Annual precipitation in Urmia City from 1952 to 2020. **24**
- Fig. 1-6.** Simplified geological map of the Lake Urmia catchment area grouping rock units based on similar lithology into a single unit, regardless of their geological ages. **25**
- Fig. 1-7.** Geographical location of the main aquifers around the Lake Urmia (data ULRP, 2017). **27**
- Fig. 1-8.** a) Main rivers in the Lake Urmia catchment area, as well as the locations of discharge stations near the river mouth. b) Annual inflow of the main rivers into Lake Urmia, representing the average discharge over 18 years (1996-2014). c) Total surface water discharge into Lake Urmia from 1953 to 2017 (data from ULRP, 2017), based on measurements taken at the discharge stations. **28**
- Fig. 1-9.** a) Area of irrigated farming and the location of major dams b) Capacity of major dams in the catchment area c) Area of irrigated farming and surface water use for agriculture 1970 to 2016 (data source: WRMC, 2021). **30**
- Fig. 1- 10.** Groundwater and surface water consumption in the Lake Urmia catchment area in 2014 (ULRP, 2014). It is essential to note that the above figures are based on permitted wells (Fig. 1-13) and designated areas for surface water extractions. **31**
- Fig. 1-11.** Distribution of the 93,000 wells and measurements of electrical conductivity values that were conducted by the WRMC in 2014. **32**
- Fig. 2-1.** Geographic overview of Lake Urmia basin. (a) Location of monitoring stations, and minimum and maximum lake extent, and extent at lowest lake level (1274 m a.s.l.) before 1995. (b) Regional overview. (c) Number of hydrometric stations over time. **38**

- Fig. 2-2.** Impact of lake volume on evaporation. (a) Relationship of salinity and lake volume (Karbassi et al., 2010). (b) Relationship of the empirical ratio α and salinity; error bars for α from the evaporation experiment of Salhotra et al., (1985, 1987) show the standard deviations for a range ($n = 24$) of different temperatures (16–35 °C) and humidities (29–62%). **41**
- Fig. 2-3.** Water balance of Lake Urmia. Temporal evolution of Lake Urmia's water balance components (seasonal sums) and observed lake volume (seasonal average). A hydrological season in the Lake Urmia basin extends from October to September of the following year. **43**
- Fig. 2-4.** Statistical analysis of runoff and weather time series. (a) Temporal evolution of 12-months SPEI and SRI (moving average filter with a kernel size of 12 months). A pointing up and down triangle shows a significant positive and negative Mann-Kendall trend, respectively. A dot means no significant trend ($p = 0.05$). (b) Relationship between discharge weighted monthly mean SPEI and SRI values. (c) Probability density plot of the linear regression slope of the SRI-SPEI relationship based on bootstrap sampling. (d) Temporal evolution of anthropogenic influences affecting Lake Urmia's water budget. (a–d) The colour code used refers to the periods defined in Figs. 2-3 and 2-4a and grey coloured lines or dots representing the period 1954–1965. **44**
- Fig. 2-5.** Morphology of Lake Urmia. (a) Cross section of Lake Urmia with a vertical exaggeration (VE) of 150 and 3000 above and below 1278.4 m a.s.l., respectively. The location of the cross section is displayed in Fig. 2-1. (b) Volume-area relationship; the blue area shows the range of monthly values between 2013 and 2018. **46**
- Fig. 2-6.** Development scenarios for Lake Urmia. Climatic best-case (mean precipitation, potential evaporation and inflow of period 3), status quo (mean of period 6) and worst-case (mean of seasons 1999/00 to 2000/01) scenarios. (a–c) Scenarios assuming current irrigation water extraction. (d–f) Scenarios assuming a reduced irrigation water extraction by $1.2 \text{ km}^3 \text{ a}^{-1}$ (50% of current surface water extraction for irrigation). **48**
- Fig. 3-1.** (A) Operating environmental chamber with activated infrared lamps; opening can be closed with a transparent acrylic glass panel (for bill of materials and construction manual, see, Supplementary data 2); (B) Schematic sketch of the air circulation. **58**
- Fig. 3-2.** Target and measured temperature (left axis) and relative humidity (right axis) over the 48 days testing period. **59**
- Fig. 3-3.** Temperature and relative humidity ranges that can be simulated with the environmental chamber (grey box). **61**
- Fig. 4-1.** Overview of the study area, with location of monitoring well and sampling sites, and distribution of annual average temperature (Data source: WRMC, 2021). Moreover, selected lake extents are shown, at initial (May 1995), lowest (Sept 2015), and recent (May 2019) lake levels between 1995 and 2020 (Data source: ULRP, 2021). b) Regional geographic overview. c) Climatic data for Urmia, incl. Mean temperature and relative humidity data and monthly precipitation sums (2012–2017; Data source: WRMC, 2021). **69**
- Fig. 4-2.** Groundwater levels (daily mean) in the monitoring well during the 2016 rainy season and the 2017 dry season. For comparison, also the Lake Urmia water level is shown. **71**
- Fig. 4-3.** Climate chamber and column experiment setup. **73**

| | |
|---|------------|
| Fig. 4-4. a) Temperature and relative humidity in the climate chamber. b) Water level development in the two columns C1 and C2. c) Cumulative mass loss (12 h median). d) Photo documentation of column tops (after 0, 4, 9, and 37 d) showing increasing salt precipitation on the soil surfaces. | 75 |
| Fig. 4-5. Lake Urmia level compared to dried lake bed area (monthly mean) from 1998 to 2020. | 77 |
| Fig. 4-6. Evaporation from the dried-up lake bed area (blue, orange) and open lake surface (grey) for the three summer months in the period 1998–2020. For better overview, also corresponding fractions are displayed (hatched areas; right axis). | 77 |
| Fig 5-1. Temperature changes under five emission scenarios considering, different levels of CO ₂ and greenhouse gas emissions (Data: IPCC, 2021). Bar represent the best estimate of the projected temperature change and error bars represent estimate of the uncertainty associated with the projections. For example, range for the temperature change in the near term (2021-2040) under the SSP1-1.9 scenario is 1.2 to 1.7°C. This means that there is a high degree of confidence that the temperature change will fall within this range. Best estimate represents the value that is considered to have the highest probability. For example, the best estimate for the temperature change in the near term (2021-2040) under the SSP1-1.9 scenario is 1.5°C. | 83 |
| Supplemental Fig. S1-1. Simulated Lake volume evolution. Simulated lake volume evolution from 1971 to 2017 for observed inflow rates and natural inflow rates (inflow + irrigation water extraction). | 89 |
| Supplemental Fig. S1-2. Mann-Kendall trends and mean annual flow rates for discharge stations. a, Upstream of reservoirs or before reservoir construction. b, Downstream of operating reservoirs. | 90 |
| Supplemental Fig. S1-3. Interannual runoff variability. Interannual runoff variability of normalized mean runoff rates before and after dam construction. | 90 |
| Supplemental Fig. S2 1.1. Cutting templates | 96 |
| Supplemental Fig. S2-1.2. Assembly of the heavy-duty shelf, sliding in the climate chamber walls (1 to 6) and application of the sealing materials | 98 |
| Supplemental Fig. S2 1.3. Cooling unit assembly: The wiring of the Peltier elements (7), application of the thermally conductive glue on the Peltier elements (8), mounting of the water-cooling blocks (9), mounting of the aluminium heat sinks and fans (10). | 99 |
| Supplemental Fig. S2-1.4. Air circulation and humidifier assembly: Construction of the moistening unit (11), perforation of the PVC pipe (12), installation of the inline fan (Ø 100 mm) (13), connection of PVC pipes with elbows and pipe connectors (14), installation of pressure reducing and solenoid valves (15). | 100 |
| Supplemental Fig. S2 1.5. Mounting of the pre-assembled units into the environmental chamber: Aluminium sheet installation (16), humidifier and air circulation unit installation (17), infrared heating lamps installation (18), controlling board platform & access port installation (19), temperature and relative humidity sensors installation (20), cooling unit installation (21) | 101 |
| Supplemental Fig. S2-1.6. Detailed photographs | 102 |
| Supplemental Fig. S2-2.1. Vertical distribution of temperature data loggers. | 103 |

| | |
|---|------------|
| Supplemental Fig. S2-2.2. Vertical temperature deviation from target temperature at 25°C (a), 30°C (b), 35°C (c), 40°C (d), 45°C (e), and 50°C (f). | 104 |
| Supplemental Fig. S2-2.3. Horizontal distribution of temperature data loggers. | 105 |
| Supplemental Fig. S2-2.4. Horizontal temperature deviation from target temperature at 25°C (a), 30°C (b), 35°C (c), 40°C (d), 45°C (e), and 50°C (f). | 105 |
| Supplemental Fig. S2-3.1. Temperature and relative humidity control ranges that can be simulated, for selected commercially available devices and for the DIY environmental chamber presented in this study. All commercial environmental chambers were tested at an ambient temperature of 23°C and the DIY environmental chamber was at an ambient temperature between 21 and 22°C. | 107 |
| Supplemental Fig. S3-1. Estimating the approximate elevation of monitoring well; (a) overview location of the monitoring well, (b) elevation estimation of the wellhead using classified Landsat-5 image (acquisition date: 2nd of October 2006) showing the closest lake shoreline to our monitoring well, and the lake level at that date was 1,272.80 m a.s.l. (data source; ULRP, 2021). | 111 |
| Supplemental Fig. S3-2. Sampling procedure; (a) column 1 at 37.128°N, 45.760°E, and (b) column 2 at 37.114°N, 45.458°E were collected in October 2016 from the southwestern and southern part of the dried up lake bed, respectively. (c) the excavated lakebed, consisting of fine silty sediments that also contain clay. | 112 |
| Supplemental Fig. S3-3. Grain size distribution curve, Samples collected in October 2016 from the southern (C1) and southwestern (C2) part of Lake Urmia (Fig. 1) at 0 (a) to 0.5 m (b) depth. The sediments consist mainly of clayey silt (clSi) and fine sandy, clayey silt (fsaclSi). | 113 |
| Supplemental Fig. S3-4. Lake Urmia level compared to lake area (monthly mean) from 1998 to 2020. | 117 |
| Supplemental Fig. S3-5. Influence of temperature on sensors; (a) simulated diurnal temperature and humidity, corresponding (b) water level changes and (c) weight changes. | 118 |
| Supplemental Fig. S3-6. Estimated yearly evaporation compared to summer (June, July and August) evaporation from the open lake surface. | 119 |

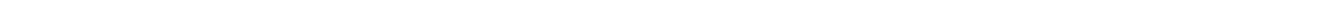
List of tables

| | |
|---|------------|
| Table 2.1. Climatic boundary conditions. Climatic boundary conditions for the simulations of development | 48 |
| Supplemental Table S2-1.1. Bill of materials, prices and suppliers. | 93 |
| Supplemental Table S2-3.1. Temperature and humidity control ranges for commercial environmental chambers and the DIY environmental chamber presented in this study. | 106 |
| Supplemental Table S3-1. Chemical composition of the lake's water and the extracted groundwater sample from our monitoring well | 110 |
| Supplemental Table S3-2. Averaged Lake volume, water level of the lake and the saltwater evaporation coefficient as ratio between saline and freshwater evaporation. | 116 |
| Supplemental Table S3-3. Estimated evaporation amounts from lake surface and dried up lakebed area of the Lake Urmia for three summer months (June, July and August) in the period 1998–2020). | 120 |

List of abbreviations

| | |
|-----------------------------|--|
| °C | degree Celsius |
| a | Year |
| a.s.l. | Above sea level |
| BC | Before Christ |
| BMBF | Federal Ministry of Education and Research |
| BP | Before present |
| Col. | Column |
| d | Day |
| DIY | Do it yourself |
| E | Evaporation (<i>E</i>) from the lake surface |
| E_{fresh} | Freshwater evaporation |
| E_{sal} | Salt water evaporation |
| g | Gram |
| g d^{-1} | Grams per day |
| gL^{-1} | Grams per litre |
| h | Hour |
| kHz | Kilohertz |
| km | Kilometre |
| km^2 | Kilometre square |
| km^3 | Kilometre cube |
| $\text{km}^3 \text{a}^{-1}$ | Kilometre cube per year |
| m a.s.l. | Meters above sea level |
| mg | Milligram |
| mm d^{-1} | Millimetre per day |
| mm | Millimeter |
| n | Number |
| P | Precipitation |
| P.V.C | Poly Vinyl Chloride |
| Q | Inflow into the lake |
| DoE | Department of Environmental agency |
| SPEI | Standardized Precipitation Evaporation Index |
| SRI | Standardized Runoff Index |
| SDI | Standardized Discharge Index |
| dS | Changes in water storage |
| E | Evaporation from the lake surface |
| WGS | World Geodetic System |
| VE | Vertical exaggeration |
| l/s | Liter per second |
| R^2 | Coefficient of determination |
| RH | Relative humidity |
| T | Temperature |
| Temp. | Temperature |
| ULRP | Urmia Lake restoration program |
| W | Watt |
| WRMC | Water Resources Management Company |
| ϑ_{tar} | Target temperature [$^{\circ}\text{C}$] |

φ True relative humidity [%]
 φ_{tar} Target relative humidity [%]



1 Introduction

1.1 Background

1.1.1 Socio-ecological relevance of Lake Urmia

Lake Urmia (known as Darya-Che Orumiyeh in Persian) is located in the northwest of Iran (Fig. 1-1). It is the largest saline lake in Iran and a critical habitat for numerous bird species. The lake provides significant ecological, cultural, and economic benefits to the surrounding communities. Lake Urmia also has a fascinating history. Lake Urmia's earliest historical reference dates back to 850's BC, where an Assyrian King is said to have documented it (Potts, 2021). One of the most significant archaeological sites in the Lake Urmia region is Tepe Hasanlu (Hasanlu Hill) (37.00°N, 45.46°E), an ancient city located 12 km to the southwest of Lake Urmia (Fig. 1-1a), and dating back to the 12th century BC (Dyson, 1989).

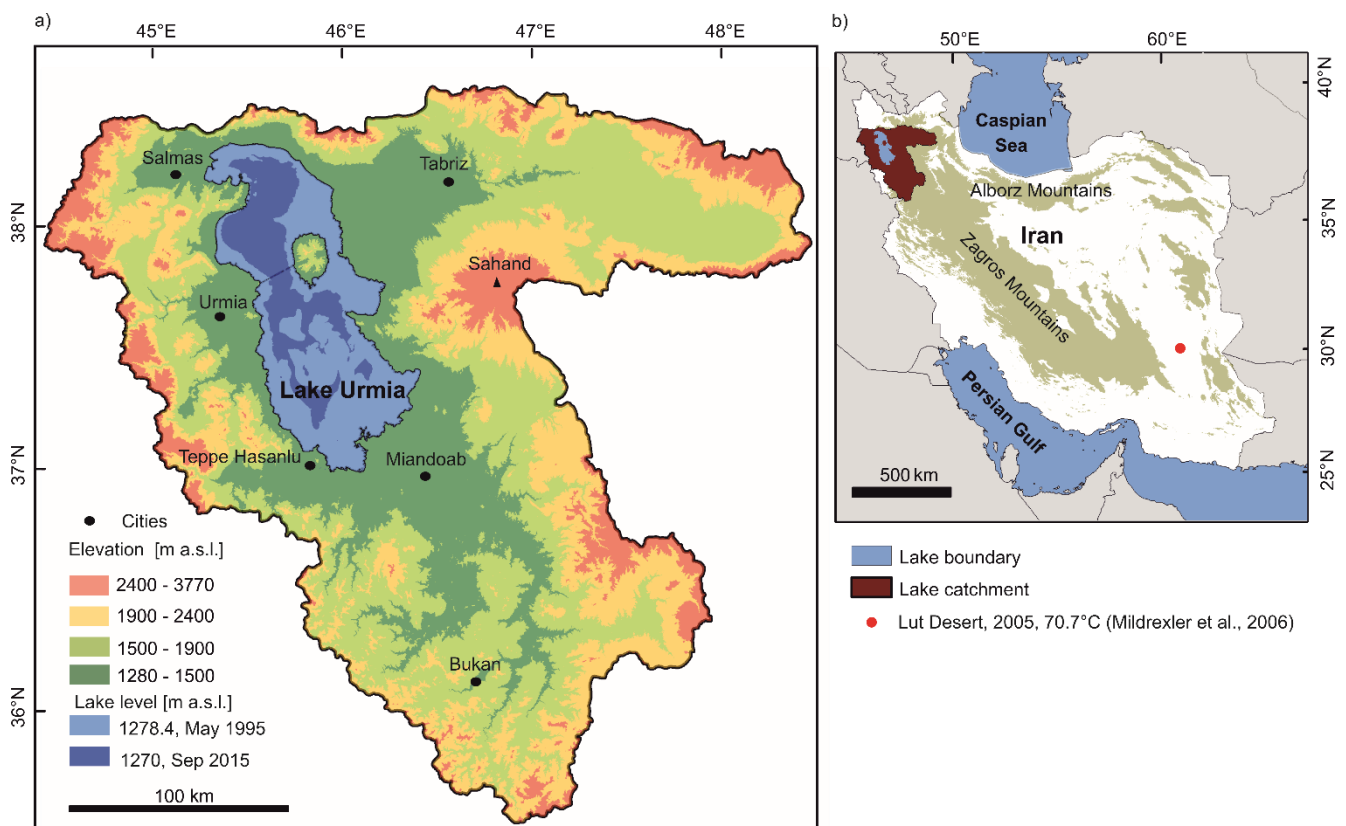


Fig. 1-1. a) Overview map of the study area, including the elevation of the catchment area and boundaries of the Lake Urmia. b) Geographical location of the Lake Urmia catchment area.

Lake Urmia catchment area has been an important location for settlements for centuries and remains an essential ecological asset for the region today. Lake Urmia and its surrounding lagoons have been designated as a "Wetland of International Importance" and are listed in UNESCO's World Network of Biosphere Reserves (UNESCO, 2019). The area is home to approximately 180 plant species, nearly 25 mammals, and over 115 bird species. The Lake itself includes several islands. Islands in the south

of the lake such as Kaboodan and Ashk Islands (Fig. 1-2), are playing a crucial role in the breeding and reproduction of local birds, as well as providing a sanctuary for migratory birds (Asem et al., 2014).



Fig 1-2. Images of Lake Urmia, Iran (1992) view from Kaboodan Island. a) Main islands in the southern part of Lake Urmia are marked on a Landsat-5 image (acquisition date: 2nd of September 1995). The photos (b-e) show a lively lake (Photos by Bijan Darehshouri, 1992).

1.1.2 Drying of the Lake Urmia

The observed Lake Urmia water level measurements (Fig 1-3a) indicate a significant increase in the lake level between 1965 and 1970. Afterward, the lake level remained relatively stable from 1970 to 1990, followed by another sharp increase between 1990 and 1995. Subsequently, there was a steep

decrease in the lake level from 1995 to 2001, and a moderate decrease between 2002 and 2015. These changes can be observed by comparing series of Landsat images captured from Lake Urmia in this period (Fig. 1-3b). Between 1995 and 2015, the lake experienced a significant reduction in its volume and surface area, losing up to 90% of its volume and 60% of its surface area, as reported by Schulz et al. (2020). This created up to more than 4000 km² of dried-up lake bed (Fig 1-4), for example, in September 2014 and 2015 (Darehshouri et al., 2022). Decrease in the lake's volume also caused an increase in the natural salinity of the lake. The salinity increased from 160 gL⁻¹ in 1995 (Karbassi et al., 2010) to about 340 gL⁻¹ in 2008 (Karbassi et al., 2010). The lake's ecology has been severely impacted by the increase in salinity, resulting in a reduction in the reproductive rate of *Artemia Urmiana*. This species plays a vital role in the lake's ecosystem, serving as a food source for many bird species (Agh et al., 2008). The reduction in the reproductive rate of *Artemia Urmiana* has resulted in decline of migratory bird populations (Sima et al., 2021). Bird species such as flamingos, pelicans, egrets, and ducks have nearly vanished from Lake Urmia (Weiss, 2018).

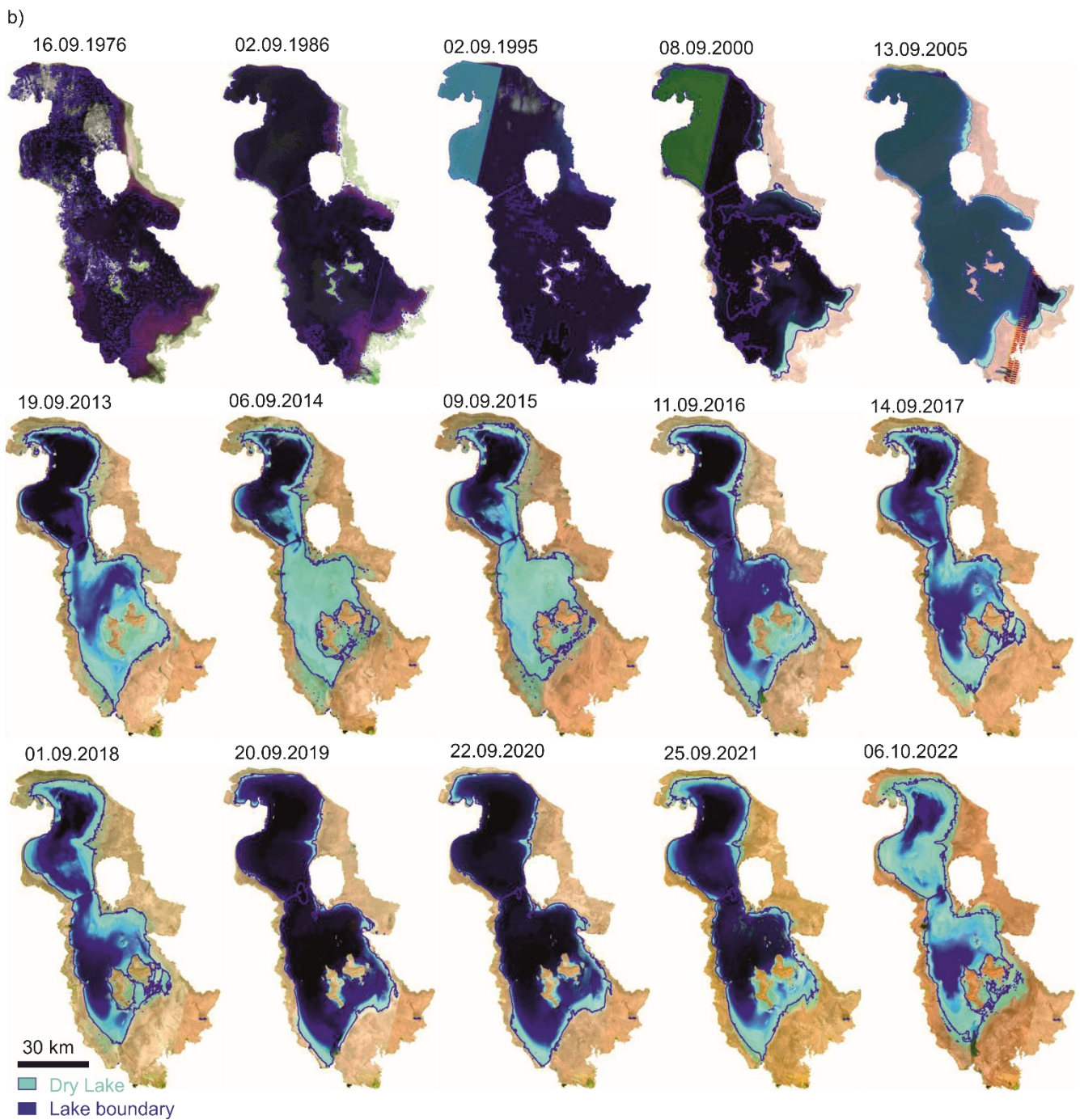
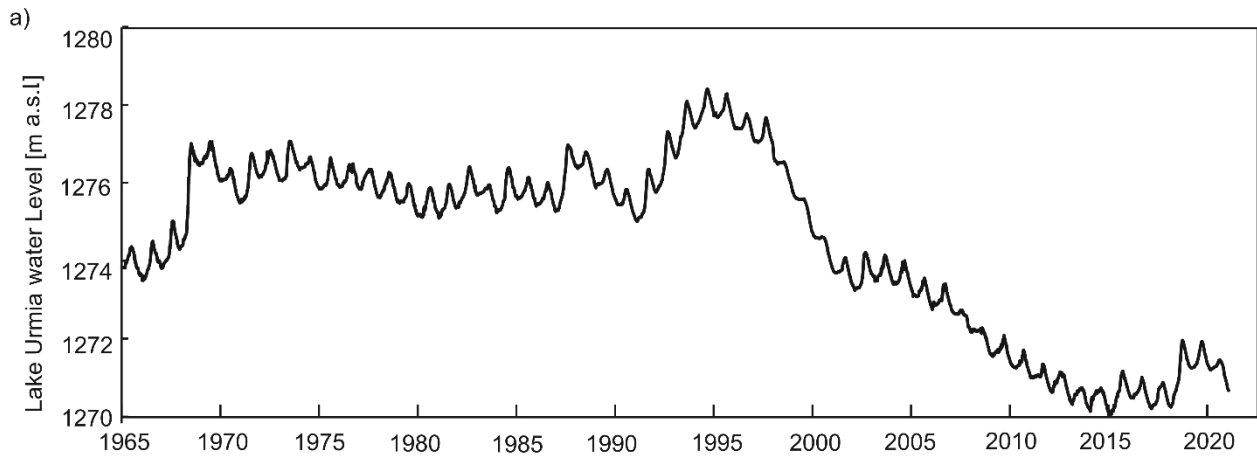


Fig. 1-3. a) Water level of Lake Urmia from 1965 to 2021 (data ULRP, 2021). b) Satellite images showing the lake level decline, the lake area was extracted from satellite images, using its extent in 1995 as a reference. The images include Landsat image from 1976, (Landsat-2), 1986, 1995, 2000, 2005, (Landsat-5) and the most recent images, from 2013 to 2022, (Landsat-8). The acquisition dates were displayed on top of each image. Additionally, the variation in colour in the images from 1995 and 2000 (combined with Landsat-5 on 11.09.1995 and 30.08.2000) are because of combination with an additional satellite image from the neighbouring orbit, which captures the northwest region of the lake.

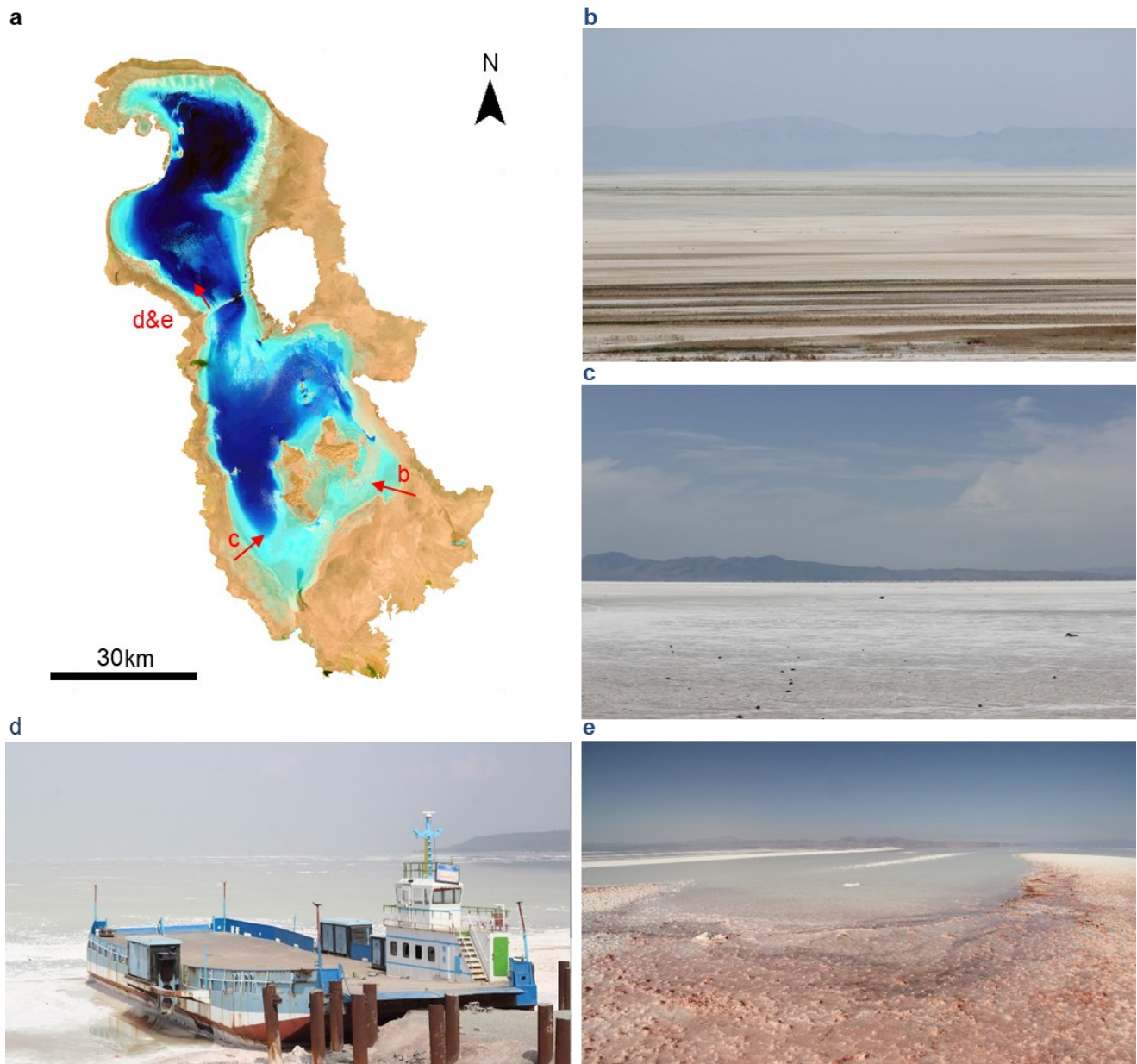


Fig. 1-4. Images of Lake Urmia, Iran (September, 2017). a) Direction of the images, are market on a Landsat-8 image (acquisition date: 14th of September 2017) facing north, east and west highlights the extent of the drying and the dramatic transformation of the once vast body of water. The photos (b-e) show the devastating impact of decreased water levels on the once vibrant lake.

Several studies investigated the reason behind the Lake Urmia decline, Hassanzadeh et al. (2012) has been studied the Lake Urmia catchment through a system dynamics model. The findings indicated that the reduction in lake volume was accelerated by human activities such as the increase in agricultural land, over-extraction of surface water resources, and the building of dams. Another study by Schulz et al. (2020) evaluated the water balance of Lake Urmia by examining its inflow, precipitation, evaporation and storage changes over the past 50 years suggests that human activities influence alone may not be the sole factor driving the decrease in Lake Urmia's water level, as fluctuations in lake levels are impacted by meteorological boundary conditions. The findings by Schulz et al. (2020) also shows that although fluctuations of lake level follow the meteorological boundary conditions, human activities correspondingly have a great influence.

1.1.3 Study aim

Development of an experimental method to measure the evaporation rate of Lake Urmia under controlled climatic conditions. This involved quantifying the amount of evaporation from both the lake surface and the dried up lake bed. In addition, the study quantified the water balance components of Lake Urmia and their temporal variations over the last five decades. The aim of these study is to establish a more accurate water balance for the Lake Urmia catchment.

1.2 Study area

Lake Urmia, located in the northwest of Iran, is situated in a closed basin surrounded by mountainous areas with elevations ranging from 1,270 to 3770 m a.s.l. (Fig. 1-1). The lake has a catchment area of approximately 52,000 square kilometers and a lake area of around 5,500 km² (mid-1990s) (Alesheikh et al., 2007). The lake itself is extremely shallow, about 11 m deep, with an average area-volume ratio of about 900 km⁻¹, considering a lake level range of 1267.1 to 1278.4 m a.s.l. (Schulz et al., 2020).

The region is one of the most densely populated areas in Iran, with a large number of cities and towns that depend on water supply. The most populated city in the western part of the Lake, Urmia city, has a population of one million. Tabriz, on the eastern side of the lake has a population of 1.6 million. Salmas, located in the north western part, has a population of around 100,000. Miandoab and Bukan, both situated in the southern part of Lake Urmia, have populations of 135,000 and 295,000, respectively (Fig. 1-1). Miandoab is the heart of agricultural activities in the region, which comprises about 480 km² of agricultural areas and gardens (MoE, 2013).

1.3 Climate

Iran has a diverse climate with the majority of the country has a dry, hot summer and a relatively cold winter. The coast along the Caspian Sea is milder, with higher humidity and more rainfall. Most settlements in Iran are situated in the Zagros and Alborz Mountain ranges, including the capital city of Tehran, which benefits from the favourable climate of the Alborz Mountains compared to the central Iranian deserts. These deserts are known to be among the hottest and driest regions on the planet. The climate in these deserts is barely habitable, in 2005, the temperature in the Lut Desert (29.9°N, 59.1°E) (Fig. 1-1a) reached a record high of 70.7°C (Mildrexler et al., 2006). The catchment area of Lake Urmia is located in the northwest of the country, at the Zagros Mountains (Fig. 1-1). The climate in this region is influenced by westerly Mediterranean moist air, the Zargros mountain range, and the lake itself, creating a unique microclimate that is relatively cold and wet during the winter months and hot and dry during the summer months. The average temperature in the catchment area ranges from 5°C in winter to 30°C in summer, with the hottest months being July and August. During the winter months, the relative humidity in the region is relatively high, above 70%, whereas during the summer months, it is lower than 35% (Fig. 1-5a).

Based on Köppen-Geiger climate classification system the catchment area of Lake Urmia has a cold 'Dsa' and arid 'BSk' climate (Peel et al., 2007). Dsa signifies cold temperatures with dry and hot summers. BSk represents an arid climate with dry summers and cold mean annual temperature. The precipitation is unevenly distributed throughout the year, with most rainfall occurring in winter and spring. During the summer months, precipitation is scarce and the region is prone to drought. The annual precipitation in the region ranges from 350 to 550 mm. The mountainous areas in the catchment area receive more precipitation compared to the areas at lower altitudes. In the western and southwestern parts of the catchment area, areas at higher elevations receive over 800 mm of precipitation annually (Fig. 1-5b), compared to the lower altitude regions. For example, in Urmia city, the mean annual precipitation is about 450 mm (Fig. 1-5c).

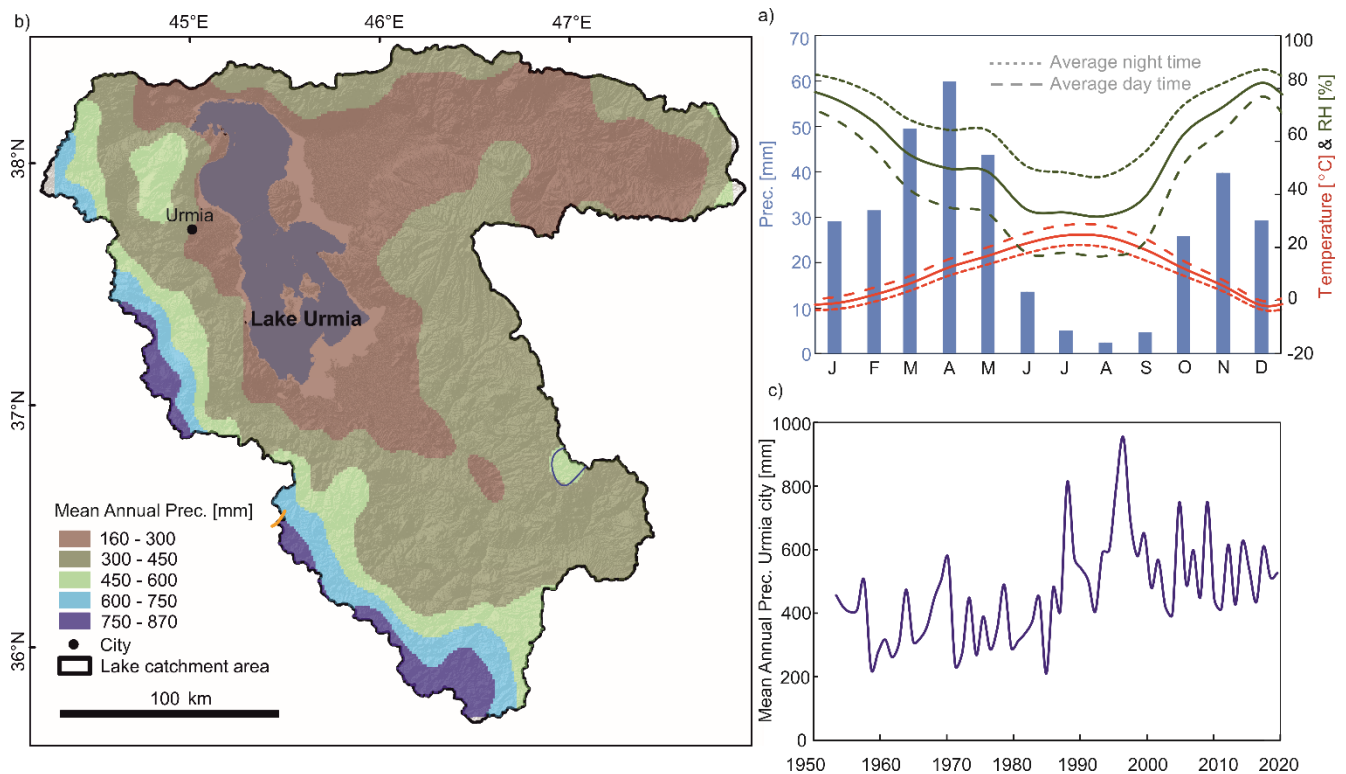


Fig. 1-5. a) Precipitation intensity in the Lake Urmia catchment area. b) Average temperature and relative humidity in Lake Urmia from 1952 to 2020, and average monthly precipitation from 1952 to 2017 (Data source: WRMC, 2021). c) Annual precipitation in Urmia City from 1952 to 2020.

1.4 Geology

1.4.1 Structural geology

The geological setting of Lake Urmia is characterized by the presence of several geological features, including volcanic and sedimentary rock formations, tectonic plate boundaries, and a complex network of faults and fractures. The Lake Urmia region is located in a tectonically active area known as the Zagros fold-thrust belt. According to Sharifi et al., (2018), the region is affected by various tectonic forces, including the convergence of the Arabian and Eurasian plates, as well as internal deformation within the Zagros fold-thrust belt. These forces have resulted in the development of several major tectonic features in the region, including the North Tabriz Fault (Fig. 1-6).

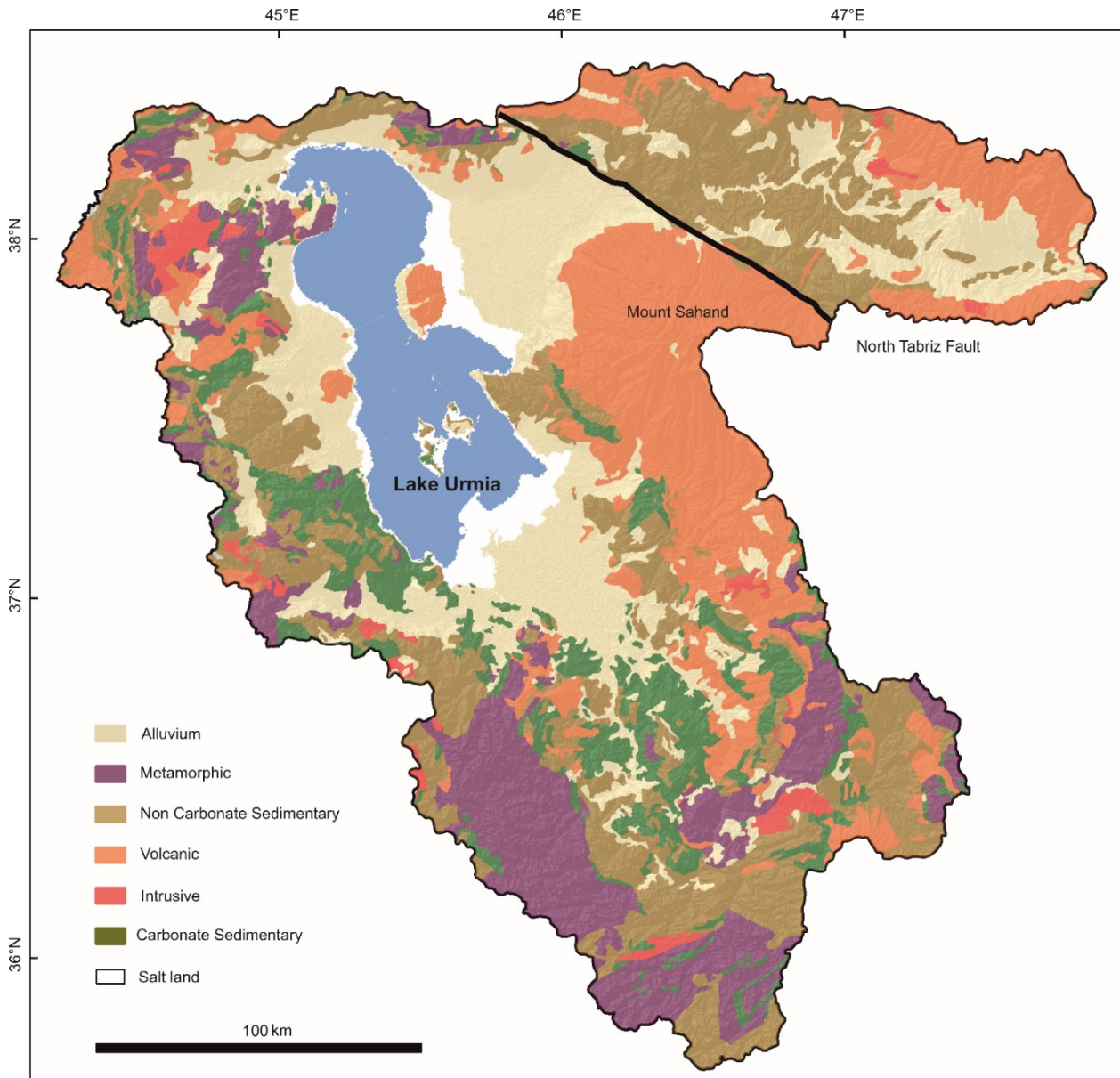


Fig. 1-6. Simplified geological map of the Lake Urmia catchment area grouping rock units based on similar lithology into a single unit, regardless of their geological ages (data URRP, 2017).

Nogole-Sadat (1993) in the Seismotectonic map of Iran categorizes the area around Lake Urmia as being in the Central Metamorphic Zone, with the eastern part being in the Central Magmatic Zone where volcanic extrusive rocks are prevalent (JICA, 2016). Volcanic rocks resulting from eruptions are widespread, particularly in the eastern part of the lake, which dates back to the Tertiary to Quaternary Era. The western and southern parts of the lake are mainly covered by pre-Cambrian, Palaeozoic, and Mesozoic formations. Travertine, from fissures are also distributed in this area (JICA, 2016).

Sedimentology

Sediments of the Lake Urmia shows significant variation, with the dominant size fraction being silt. However, sand and sandy-silt are mainly present in the northwest part of the lake where intrusive rock units occur. Clay-bearing siliciclastics are prevalent in the central and southern parts of the lake, with the highest concentration of clay found in the narrow middle section of the lake near the causeway (Sharifi et al., 2018). Our lake bed sediment samples from the southern and southwestern parts of the lake primarily consist of clayey silt (clSi) and fine sandy, clayey silt (fsaclSi) (Fig S3-3).

1.5 Hydrogeology

1.5.1 Groundwater systems

The Lake Urmia catchment area has several aquifers that provide water for drinking, irrigation, and industry. The alluvial aquifers around the lake cover an area of about 13,000 km². The Urmia and Miandoab aquifers are the largest in the region, covering an area of approximately 1,500 km² (Fig. 1-7).

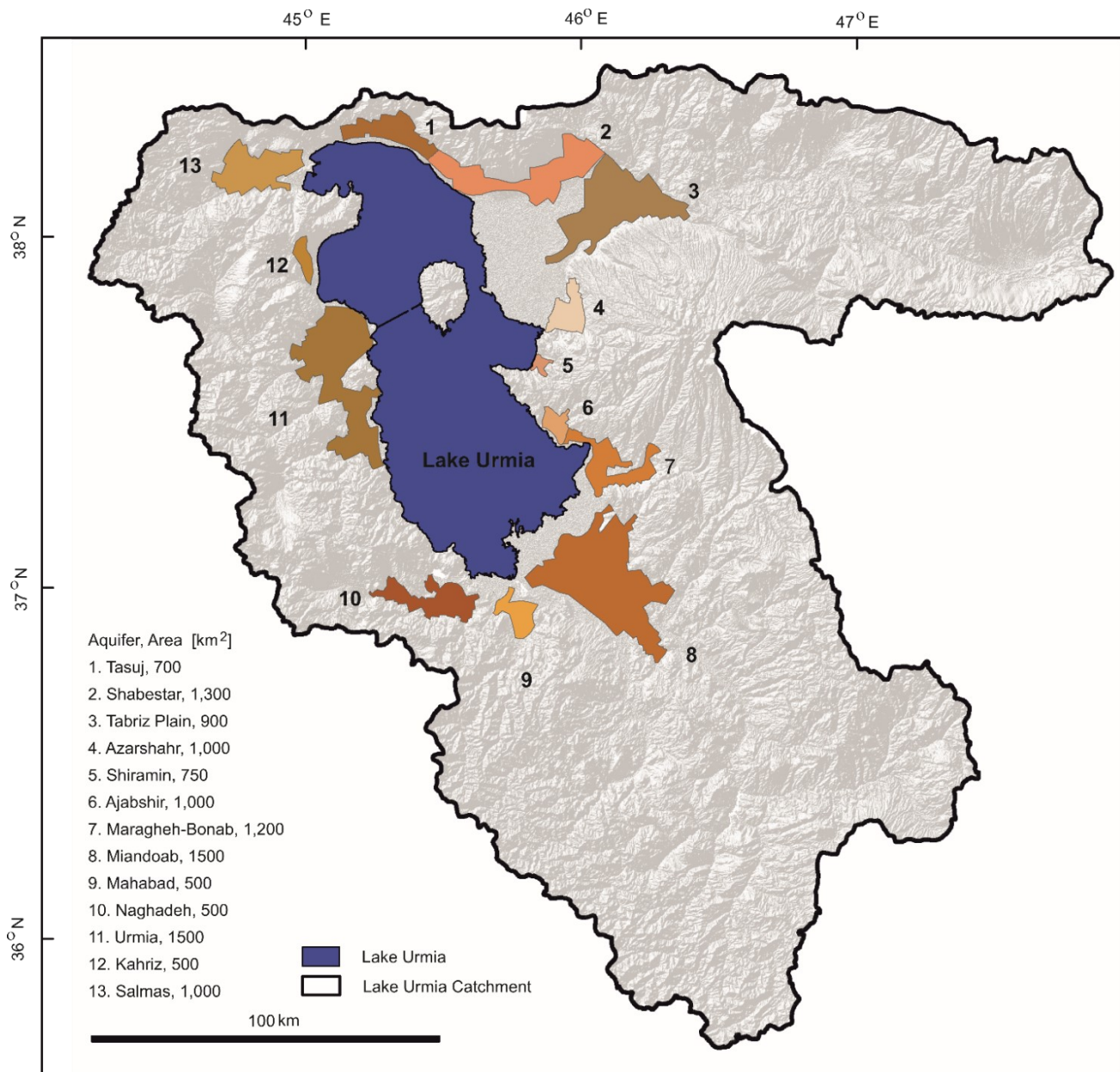


Fig. 1-7. Geographical location of the main aquifers around the Lake Urmia (data ULRP, 2017).

There are various studies investigating the hydrological interactions between Lake Urmia and its catchment area. A recent study by Sheibani et al. (2022) investigates the interaction of hypersaline lake and groundwater and how sediment deposit affects this relationship. The results indicate that sediment thickness and hydraulic conductivity play a significant role in preventing saltwater from entering the aquifer, and changes in hydraulic conductivity of the aquifers does not have a noticeable effect on saltwater entrance rate but affects the salinity at the transition zone. Sheibani et al. (2022) also investigated the response of the groundwater flow regime to a 10-year water level decline of the lake and subsequent rise in lake level. The results suggest that as the lake level declines, the

saltwater inflows to the aquifer decreases, and the freshwater flow towards the lake's boundary flows directly into the lake.

1.6 Surface water

The Urmia Lake catchment is home to several important rivers, covering a total area of about 52,000 km². The lake itself covers about 5,500 km² (mid-1990s) (Alesheikh et al., 2007) which accounts for up to more than 10% of the total area of the entire lake catchment area. The rivers in the region support rich ecosystems and serve as important habitats. The Aji River catchment with an area of about 13,000 km², accounting for 24% of the entire lake catchment area. The second-largest area is the Zarrineh River catchment with an area of about 12,000 km², representing 23% of the lake catchment. The Zarrineh and Simineh Rivers in the south have significant ecological and economic value for the surrounding region. For instance, the Zarrineh River is a major source of irrigation water for agriculture, while the Simineh River provides drinking water for local communities (Fig. 1-8a).

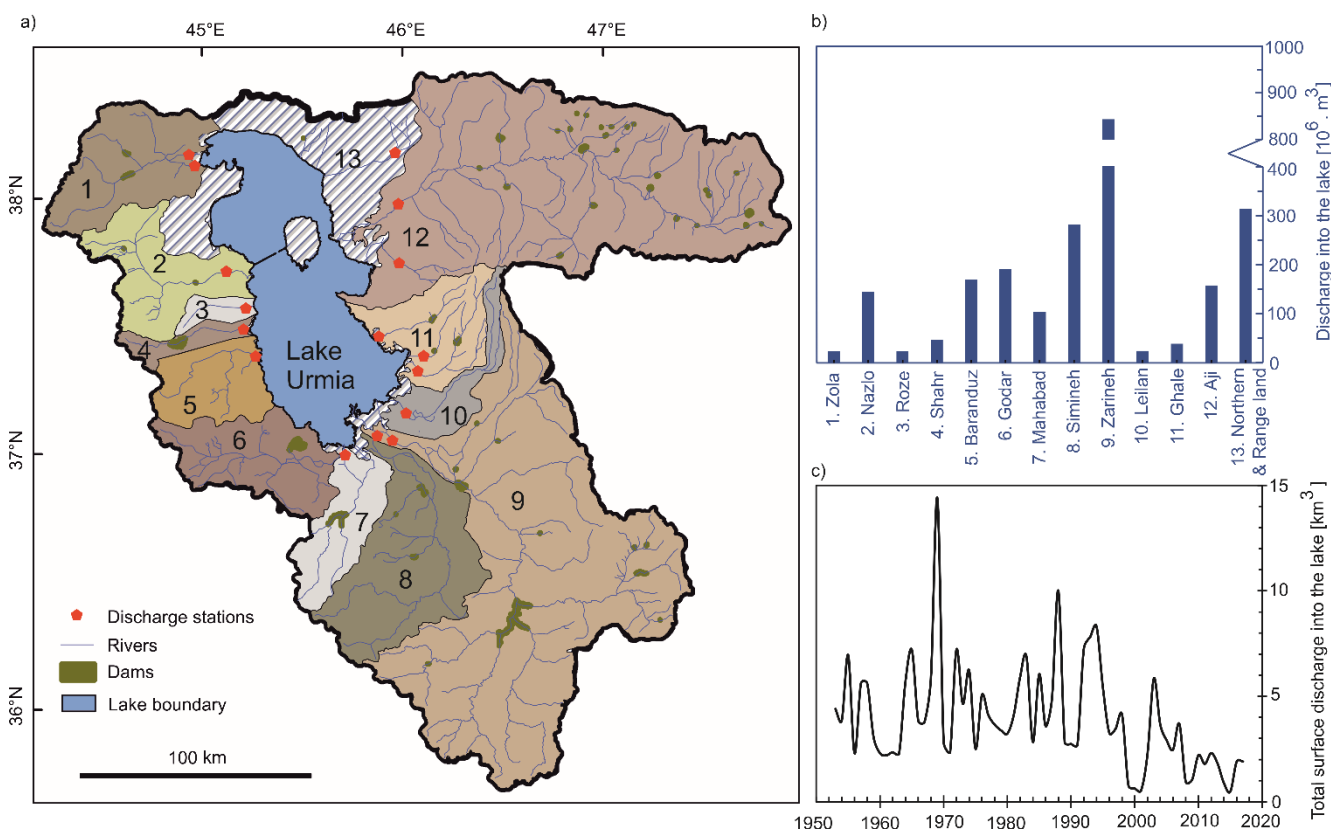


Fig. 1-8. a) Main rivers in the Lake Urmia catchment area, as well as the locations of discharge stations near the river mouth. b) Annual inflow of the main rivers into Lake Urmia, representing the average discharge over 18 years (1996-2014). c) Total surface water discharge into Lake Urmia from 1953 to 2017 (data from ULRP, 2017), based on measurements taken at the discharge stations.

The Zarineh and Simineh rivers, together are providing approximately 50% of the total surface water inflow to Lake Urmia (Fig. 1-8 b). These rivers play a crucial role in the lake's catchment area. Since 1995, the surface water inflow into Lake Urmia has decreased (Fig. 1-8 c), and the lake has experienced a drastic decrease in water levels over the past two decades. Several factors have contributed to this reduction, including damming of rivers, diversion of surface water for agriculture, and climate change. Chapter 2 provides an extensive analysis of the impact of these factors on the changes in the lake's water volume.

1.6.1 Reservoirs

There are several important reservoirs in the catchment area of the Lake Urmia that play a critical role in meeting the region's water supply, irrigation, and hydroelectric power generation needs. Some of the key reservoirs in this area include the Mahabad and Bukan dams (Fig 1-9a). The construction of dams in the Lake Urmia Basin started with the Mahabad Dam in 1970, and today there are 34 dams in the region with the Bukan Dam being the largest one, having a capacity of 0.8 km³ (Fig. 1-9b).

1.7 Development of the water sector

1.7.1 Land use

The land use in the Lake Urmia catchment is a combination of agricultural, industrial, and urban areas. Agricultural land covers a large portion of the catchment (Fig. 1-9). Additionally, there are also some areas of protected natural habitat, such as forests, nature conservation parks (e.g., IEW, 2023) and wetlands, which provide important ecosystem services and are critical for the preservation of biodiversity.

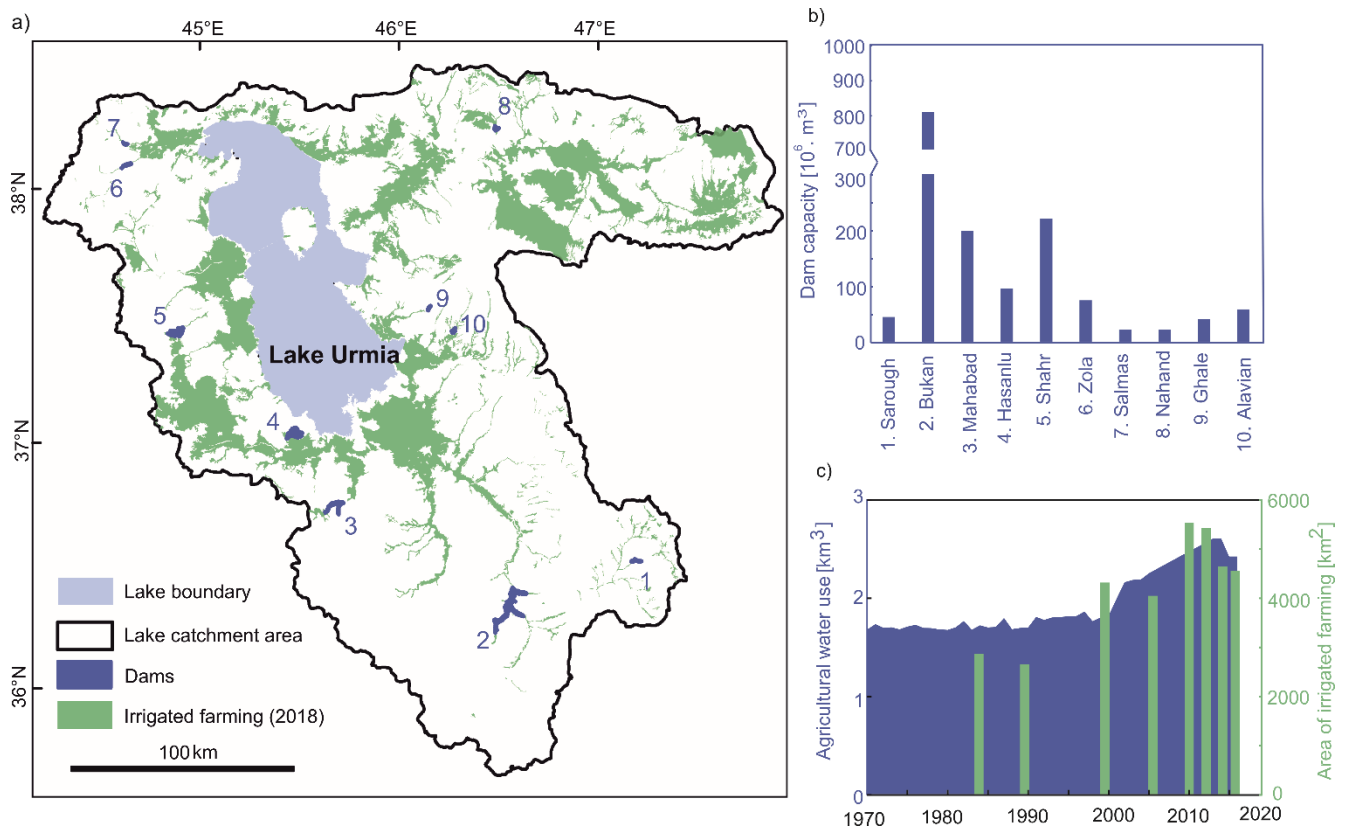


Fig. 1-9. a) Area of irrigated farming and the location of major dams b) Capacity of major dams in the catchment area c) Area of irrigated farming and surface water use for agriculture 1970 to 2016 (data source: WRMC, 2021).

Agricultural activities play a crucial role in the catchment area of Lake Urmia and have undergone significant changes over the past few decades. An analysis of land use changes by JICA (2016) within a twenty-year period between 1987 and 2007, using data from Iran Water Resources Management Company (WRMC), showed a 40% increase in the total area of agricultural land, expanding from approximately 8,200 km² to about 11,600 km². JICA (2016), estimated that these changes led to an increase in the total water demand for agricultural activities, rising from around 2.5 km³ in 1987 to 4.3 km³ in 2007. Although the highest percentage of agricultural water use is consumed by irrigated farming, more recent data from WRMC, (2019) indicates an increase in both the area of irrigated land and surface water consumption for agriculture (Fig 1-9c).

1.7.2 Water consumption

Surface water consumption

According to the Ministry of Energy's Master Plan Report on Agricultural Water Supply (MoE, 2013), an analysis of water consumption in the Lake Urmia catchment area estimated that the renewable water resources and water consumption is about 7 and 4.8 km³a⁻¹ respectively. These values are

based on water consumption data from 2007 to 2013. Agricultural activities, industries, and domestic use, consume 70% of the renewable water resources in the Lake Urmia catchment area. The agricultural water demand accounts for approximately $4.3 \text{ km}^3 \text{ a}^{-1}$, which is roughly 60% of the total renewable water resources and 90% of the overall water consumption in the catchment area. Surface water resources contribute 2.2 km^3 (57%) to the annual water demand for agriculture (JICA, 2015). For instance, in 2014, the Zarineh River had the highest surface water consumption within the Lake Urmia catchment area, amounting to $0.74 \text{ km}^3 \text{ a}^{-1}$ (Fig 1-10).

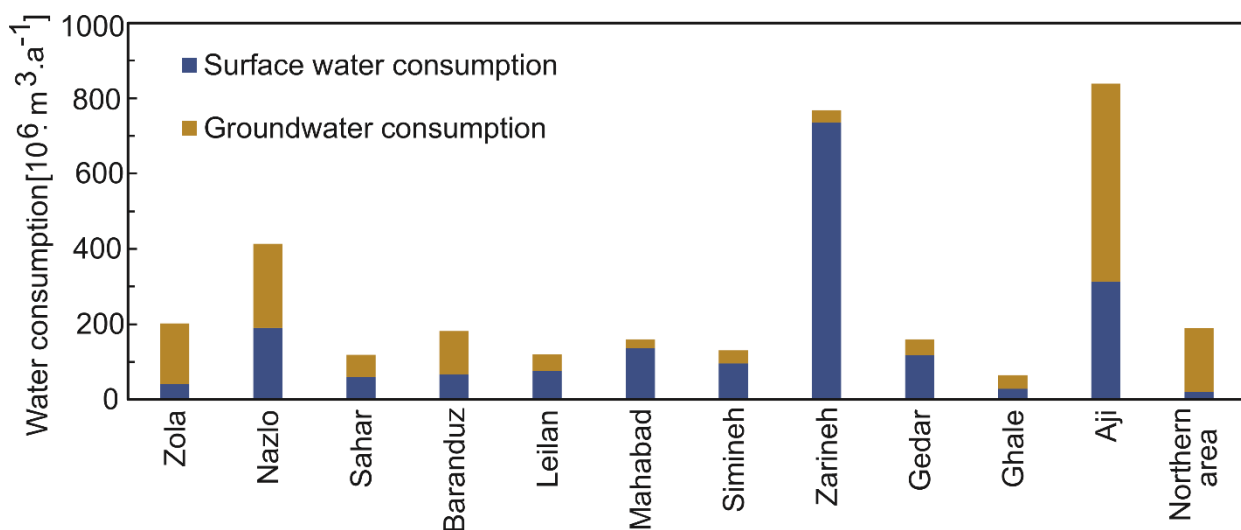


Fig. 1- 10. Groundwater and surface water consumption in the Lake Urmia catchment area in 2014 (data: ULRP, 2014). It is essential to note that the above figures are based on permitted wells (Fig.1-13) and designated areas for surface water extractions.

Groundwater consumption

The region heavily depends on groundwater, and over the years, its usage has intensified in the catchment area. Irrigation consumes a major portion of the groundwater. In recent decades, the number of wells drilled in the region has increased significantly to meet the growing demand for water. Around 93,000 wells have been constructed, mostly situated in the plain areas near the Lake Urmia and near the rivers (Fig. 1-11). About $1.6 \text{ km}^3 \text{ a}^{-1}$ (43%) of the annual water demand for agricultural supply from groundwater (JICA, 2015).

For example, in 2014, in the Aji River catchment area, over 0.52 km^3 of groundwater was withdrawn and primarily used for agricultural activities, accounting for approximately 90% of the groundwater consumption. Remarkably, in the catchment area of Nazlo, Baranduz, and Aji Rivers, the groundwater consumption exceeds the surface water consumption. The combined surface water and groundwater consumption in the Aji River catchment area is the highest compare to the other catchments of Lake Urmia, reaching approximately $0.84 \text{ km}^3 \text{ a}^{-1}$ (Fig. 1-10).

The Iran Water Resources Management Company (WRMC) has reported a decline in the groundwater level of Tabriz aquifer between 2004 and 2014. Moreover, significant water level declines have also been observed in Salmas and Tasuj aquifers since 1995. According to WRMC's analysis of groundwater for salinity, some wells in the area have electric conductivity levels higher than $10,000 \mu\text{S cm}^{-1}$, indicating high salinity. Groundwater salinization is predominantly observed on the eastern side of the lake and in the Miandoab region in the south (Fig. 1-11).

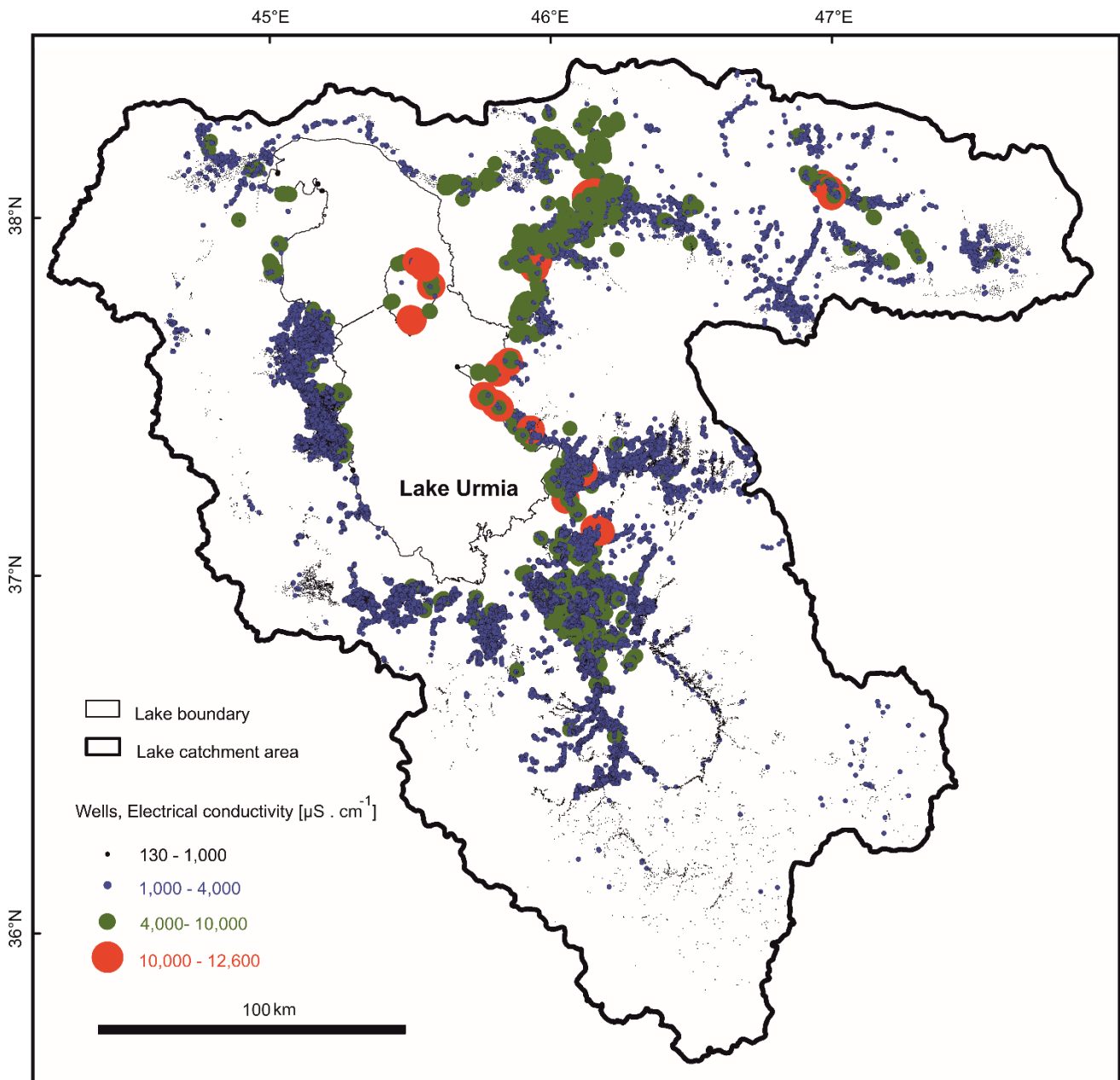


Fig. 1-11. Distribution of the 93,000 wells and measurements of electrical conductivity values that were conducted by the WRMC in 2014.

1.8 References

- Agh, N., Van Stappen, G., Bossier, P., Yari, A.M., Rahimian, H., Sorgeloos, P., 2008. Life cycle characteristics of six *Artemia* populations from Iran. *Pak. J. Biol. Sci.* 11, 854–861. <https://doi.org/10.3923/pjbs.2008.854.861>
- Alesheikh, A.A., Ghorbanali, A., Nouri, N., 2007. Coastline change detection using remote sensing. *Int. J. Environ. Sci. Technol.* 4 (1), 61–66. <https://doi.org/10.1007/BF03325962>
- Asem, A., Eimanifar, A., Djamali, M., De los Rios, P., Wink, M., 2014. Biodiversity of the hypersaline Urmia Lake national park (NW Iran). *Diversity* 6 (1) <https://doi.org/10.3390/d6010102>
- Danesh-Yazdi, M., Ataie-Ashtiani, B., 2019. Lake Urmia crisis and restoration plan: planning without appropriate data and model is gambling. *J. Hydrol.* 576, 639–651. <https://doi.org/10.1016/j.jhydrol.2019.06.068>
- Darehshouri, S., Michelsen, N., Schüth, C., Schulz, S., 2020. A low-cost environmental chamber to simulate warm climatic conditions. *Vadose Zone Journal* 19 (1): 1–6 <https://doi.org/10.1002/vzj2.20023>
- Darehshouri, S., Michelsen, N., Schüth, C., Tajrishy, M., Schulz, S., 2022. Evaporation from the dried-up lake bed of Lake Urmia, Iran. *Science of The Total Environment*: 159960 <https://doi.org/10.1016/j.scitotenv.2022.159960>
- Djamali, M., de Beaulieu, J-L., Shah-hosseini, M., Andrieu-Ponel, V., Ponel, P., Amini, A., Akhani, H., Leroy, S.A.G., Stevens, L., Lahijani, H., Brewer, S., 2008. A late Pleistocene long pollen record from Lake Urmia, NW Iran, *Quaternary Research*. <https://doi.org/10.1016/j.ygres.2008.03.004>
- Dyson, R.H. Jr., 1989 – The Iron Age architecture at Hasanlu: An essay. *Expedition* 31,2-3: 107-127. Available here: <https://www.penn.museum/sites/expedition/the-iron-age-architecture-at-hasanlu-an-essay/>
- Hassanzadeh, E., Zarghami, M., Hassanzadeh, Y., 2012. Determining the main factors in declining the Urmia Lake level by using system dynamics modeling. *Water Resources Management*. 26, 129–145. <https://doi.org/10.1007/s11269-011-9909-8>
- Hu, Z. Li, Q. Chen, X. Teng, Z. Chen, C. Yin, G. Zhang, Y., 2016. Climate changes in temperature and precipitation extremes in an alpine grassland of Central Asia. *Theoretical and Applied Climatology*, 126(3–4), 519–531. <https://doi.org/10.1007/s00704-015-1568-x>
- IEW 2023. Iran Environment and Wildlife watch, Sahand Protected Area | nature conservation park, <https://www.iew.ir/1391/06/11/1313>
- IPCC, 2021: Climate Change 2021: The Physical Science Basis. Contribution of Working Group I to the Sixth Assessment Report of the Intergovernmental Panel on Climate Change [Masson-Delmotte, V., P. Zhai, A. Pirani, S.L. Connors, C. Péan, S. Berger, N. Caud, Y. Chen, L. Goldfarb, M.I. Gomis, M. Huang, K. Leitzell, E. Lonnoy, J.B.R. Matthews, T.K. Maycock, T. Waterfield, O. Yelekçi, R. Yu, and B. Zhou (eds.)]. Cambridge University Press, Cambridge, United Kingdom and New York, NY, USA, 2391 pp. <https://doi:10.1017/9781009157896>
- JICA, 2016. Japan international cooperation agency, data collection survey on hydrological cycle of lake Urmia basin in the Islamic Republic of Iran final report hydrological cycle of lake. 268.
- Karbassi, A., Bidhendi, G.N., Pejman, A., Bidhendi, E., 2010. Environmental impacts of desalination on the ecology of Lake Urmia. *J. Great Lakes Res.* 36, 419–424. <https://doi.org/10.1016/j.jglr.2010.06.004>

Kong, L., Sauer, D., Wang, X., Li, Y., Pourkermani, M., Yang, J., 2022. 30,000 Years of the southwestern Lake Urmia (Iran) paleoenvironmental evolution inferred from mineralogical indicators from lake and watershed sediments. *Palaeogeography, Palaeoclimatology, Palaeoecology*, 610, 110814. <https://doi.org/10.1016/j.jseaes.2022.105387>

Mildrexler, DJ., Zhao, M., Running, SW., 2006. Where are the hottest spots on Earth? *Eos* 87 (43) <https://doi.org/10.1029/2006EO430002>

MoE, 2013, Master Plan Report of the Ministry of Energy (Ministry of Energy, Water and Wastewater Macro-Planning Office; Studies on Updating National Water Master Plan in Basins of Aras, Urmia, Talesh-Anzali Wetland, Greater Sefidrood, Haraz-Ghareh Sou, Gorganrood and Atrak. Fourth Volume: Report on Surface Water Resources (Quantitative and Qualitative) Urmia Watershed (in Persian).

Nogole Sadat, M., 1993. Seismotectonic map of Iran (scale 1: 1 000 000), Geological Survey of Iran, Tehran.

O'Neill, B., Carter, T., Ebi, K., Harrison, P., Kemp-Benedict, E., Kok, K., Kriegler, E., Preston, B., Riahi, K., Sillmann, J., 2020. Achievements and needs for the climate change scenario framework. *Nature Climate Change*, 10, 1074–1084 (2020). <https://doi.org/10.1038/s41558-020-00952-0>

Peel, M.C., Finlayson, B.L., McMahon, T.A., 2007. Updated world map of the Köppen-Geiger climate classification. *Hydrol. Earth Syst. Sci.* 11, 1633–1644. <https://doi.org/10.5194/hess-11-1633-2007>

Potts, D.T., 2021. The Sea of Zamua. In *Nomina in Aqua Scripta*, by A.J. Domínguez Monedero, C. del Cerro Linares, F.J. Villalba Ruiz de Toledo, & F.L. Borrego Gallardo. Homenaje a Joaquín María Córdoba Zoilo. Madrid, Spain: ISBN: 978-84-8344-762-8.

Schröder, T., Hassanzadeh, E., Darehshouri, S., Tajrishy, M., Schulz, S., 2022. Satellite based lake bed elevation model of Lake Urmia using time series of Landsat imagery. *Journal of Great Lakes Research*. <https://doi.org/10.1016/j.jglr.2022.08.016>

Schulz, S., Darehshouri, S., Hassanzadeh, E., Tajrishy, M., Schüth, C., 2020. Climate change or irrigated agriculture – what drives the water level decline of Lake Urmia. *Scientific Reports* 10 (1): 236 <https://doi.org/10.1038/s41598-019-57150-y>

Shadkam, S., Ludwig, F., van Oel, P., Kirmit, Ç., Kabat, P., 2016. Impacts of climate change and water resources development on the declining inflow into Iran's Urmia Lake. *J. Great Lakes Res.* 42, 942–952. <https://doi.org/10.1016/j.jglr.2016.07.033>

Sharifi, A., Shah-Hosseini, M., Pourmand, A., Esfahaninejad, M., Haeri-Ardakani, O., 2018. The Vanishing of Urmia Lake: A Geolimnological Perspective on the Hydrological Imbalance of the World's Second Largest Hypersaline Lake, in: *Handbook of Environmental Chemistry*. https://doi.org/10.1007/978-3-319-7359-2_359

Sheibani, S., Ataie-Ashtiani, B., Safaie, A., Simmons, C.T., 2020. Influence of lakebed sediment deposit on the interaction of hypersaline lake and groundwater: a simplified case of Lake Urmia, Iran. *J. Hydrol.* 588, 125110. <https://doi.org/10.1016/j.jhydrol.2020.125110>

Sima, S., Rosenberg, D.E., Wurtsbaugh, W.A., Null, S.E., Kettenring, K.M., 2021. Managing Lake Urmia, Iran for diverse restoration objectives: moving beyond a uniform target lake level. *J. Hydrol. Reg. Stud.* 35, 100812. <https://doi.org/10.1016/j.ejrh.2021.100812>.

Stone, R., 2015. Feature: Saving Iran's great salt lake. *Science* (80-). <https://doi.org/10.1126/science.349.6252.1044>

Sun, Q., X. Zhang, F. Zwiers, S. Westra, and L. Alexander, 2021: A Global, Continental, and Regional Analysis of Changes in Extreme Precipitation. *Journal of Climate*, 34(1), 243–258, <https://doi.org/10.1175/jcli-d-19-0892.1>

ULRP 2021. Urmia Lake Restoration programme. Daily Lake Urmia level data. Available at: <https://www.ulrp.ir/fa/> (Accessed 26 November 2021).

UNDP & DoE 2008. An Independent Review: The Status of Water Resources in the Lake Urmia Basin.

UNESCO 2019. Lake Oromeeh Biosphere Reserve, Islamic Republic of Iran. <https://en.unesco.org/biosphere/aspac/lake-oromeeh>. (Accessed 8 May 2022).

Weiss, K. R. 2018, (April 3). Iran's tarnished gem: Lake Urmia was once a haven for birds and bathers. Now, its piers lead nowhere. What happened? National Geographic. <https://www.nationalgeographic.com/photography/article/lake-urmia-iran-drought>

WRMC 2021. Water Resources Management Company (WRMC) of Iran Ministry of Energy. Data available upon request, more info: <https://www.ulrp.ir>

Zhang, M. Chen Y. Shen Y. Li Y., 2017. Changes of precipitation extremes in arid Central Asia. Quaternary International 436: 16–27. <https://doi.org/10.1016/j.quaint.2016.12.024>

2 Climate change or irrigated agriculture – what drives the water level decline of Lake Urmia

Stephan Schulz ^{a,*}, Sahand Darehshouri ^a, Elmira Hassanzadeh ^b, Massoud Tajrishy ^c, Christoph Schüth ^a

^a Technische Universität Darmstadt, Institute of Applied Geosciences, Schnittspahnstr. 9, 64287, Darmstadt, Germany

^b Polytechnique Montréal, Department of Civil, Geological and Mining Engineering, Montreal, Canada.

^c Sharif University of Technology, Urmia Lake Restoration Program, Department of Civil Engineering, Azadi Ave, P.O.Box: 11155, 9313, Tehran, Iran.

*Corresponding author: Stephan Schulz, schulz@geo.tu-darmstadt.de

Published in **Scientific Reports**, 2020, Vol. 10, Article number: 236 (2020),

<https://doi.org/10.1038/s41598-019-57150-y>

2.1 Abstract

Lake Urmia is one of the largest hypersaline lakes on earth with a unique biodiversity. Over the past two decades the lake water level declined dramatically, threatening the functionality of the lake's ecosystems. There is a controversial debate about the reasons for this decline, with either mismanagement of the water resources, or climatic changes assumed to be the main cause. In this study we quantified the water budget components of Lake Urmia and analysed their temporal evolution and interplay over the last five decades. With this we can show that variations of Lake Urmia's water level during the analysed period were mainly triggered by climatic changes. However, under the current climatic conditions agricultural water extraction volumes are significant compared to the remaining surface water inflow volumes. Changes in agricultural water withdrawal would have a significant impact on the lake volume and could either stabilize the lake, or lead to its complete collapse.

2.2 Introduction

Lake Urmia is an endorheic lake located in north-west of Iran (Fig. 2-1). With an average original surface area of about 5,000 km² it is one of the largest hypersaline lakes on earth (Eimanifar and Mohebbi, 2007; Kabiri *et al.*, 2012; Stone, 2015). Considering its original extent, Lake Urmia has more than one hundred islands, which are vital for the reproduction of various local birds, but also as a safe breeding refuge of migratory birds such as Flamingos and White Pelicans (Eimanifar and Mohebbi, 2007). The main islands are an ideal habitat for endangered species such as the Iranian yellow deer and Armenian mouflon (Asem *et al.*, 2014). Despite its very high natural salinity of 140–280 gL⁻¹ (Karbassi *et al.*, 2010; Sharifi *et al.*, 2018) the lake itself constitutes a living space for diverse bacterial communities, halophilic phytoplankton, or the brine shrimp *Artemia Urmiana* (Asem *et al.*, 2014). Starting in 1995, Lake Urmia experienced a strong decline in lake level. Between 1995 and 2013 the lake lost about 60% of area and even more than 90% of its volume (Delju *et al.*, 2013; Tourian *et al.*, 2015; Alizadeh-Choobari *et al.*, 2016; Shadkam *et al.*, 2016). Although the interannual variability of the lake level has always been high, the extreme decline in the 90 s is a singular event, at least in the last 100 years (Golabian, 2011; Wurtsbaugh *et al.*, 2017). This loss of volume has negative impacts on the lake's ecosystems, such as a significant reduction of the aquatic habitat accompanied by an increase of salinity to more than 300 gL⁻¹ (Eimanifar and Mohebbi, 2007), which has caused a severe slowdown of the reproduction rate of *Artemia Urmiana* (Agh *et al.*, 2008). Moreover, most islands have disappeared and the deposition of sand dunes and evaporites on the dried-up lake bed has formed a vast salty desert.

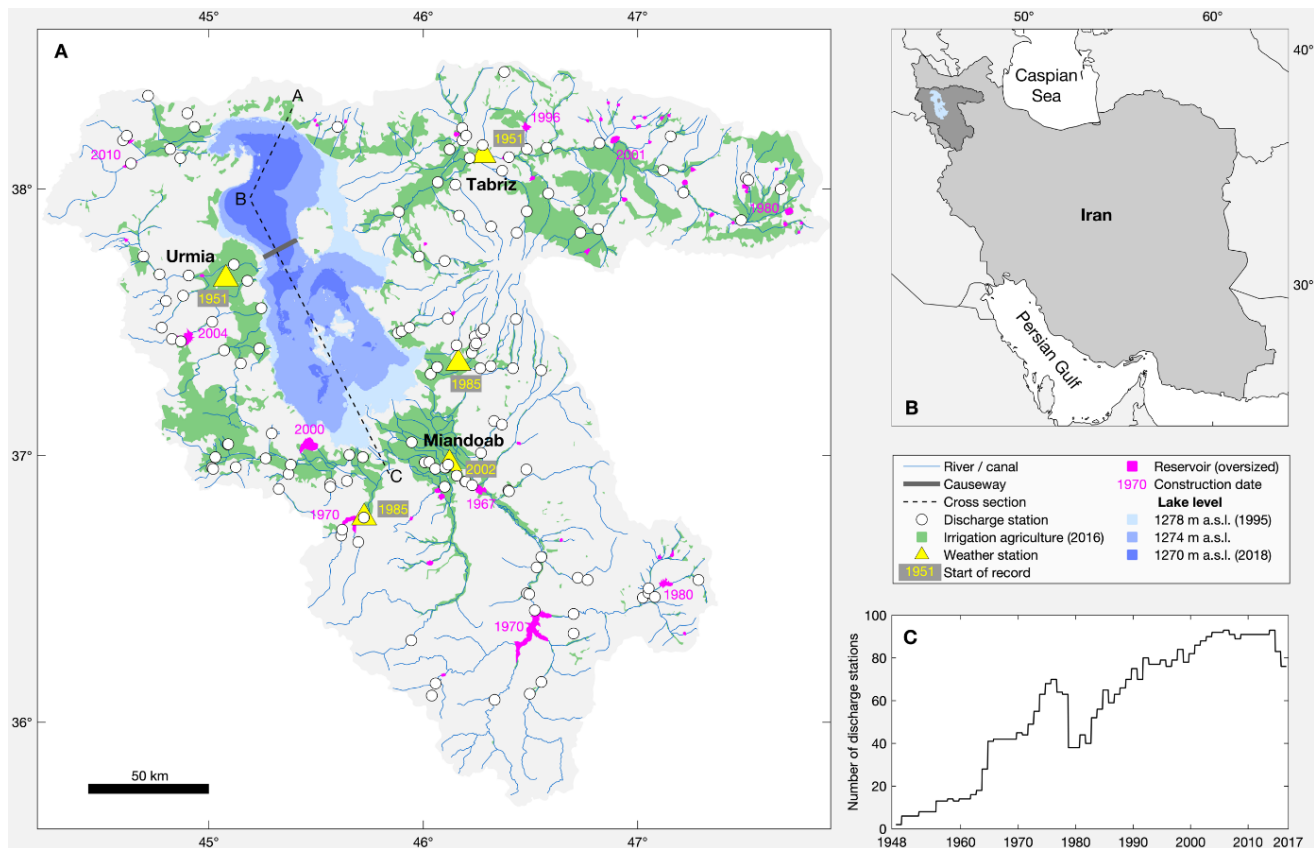


Fig. 2-1. Geographic overview of Lake Urmia basin. (a) Location of monitoring stations, and minimum and maximum lake extent, and extent at lowest lake level (1274 m a.s.l.) before 1995. (b) Regional overview. (c) Number of hydrometric stations over time. (Plots and maps are generated using MATLAB R2019b, www.mathworks.com).

The reasons behind the pronounced water level decline during the past two decades are controversial. Several studies state that the reduction of surface water inflow due to agricultural extraction predominantly caused the lake level decline (Hassanzadeh *et al.*, 2012; Aghakouchak *et al.*, 2015; Hesami and Amini, 2016; Jalili *et al.*, 2016; Nouri *et al.*, 2017; Alborzi *et al.*, 2018; Ghale *et al.*, 2018; Chaudhari *et al.*, 2018; Khazaei *et al.*, 2019). This was mainly triggered by an uncontrolled growth of the irrigated area, accompanied by the extensive construction of reservoirs, and poor agricultural water use efficiency. Several studies base their conclusions on trend analysis of hydro-meteorological data sets (Zoljoodi and Didevarasl, 2014; Alizadeh-Choobari *et al.*, 2016; Jalili *et al.*, 2016; Khazaei *et al.*, 2019). While Jalili *et al.*, (2016) and Khazaei *et al.*, (2019) identified only weak correlations between meteorological variables and lake level and hence concluded that mainly anthropogenic changes caused the lake level decline, Alizadeh-Choobari *et al.*, (2016) and Zoljoodi and Didevarasl, (2014) could identify more pronounced trends in climate variables, i.e. increasing temperatures and decreasing precipitation over the last decades. Interestingly, the studies from the former authors base on rather large-scale satellite products, while the latter have used records of local weather stations. Three of the studies mentioned above even provide quantitative estimates of anthropogenic impacts. Alizadeh Govarchin Ghale *et al.*, (2018) concluded on the basis of a time

series analysis comparing the water balance of the lake with agricultural water consumption that about 80% of the shrinkage in the period 1998–2010 was man-made. Using a hydrological model, (Chaudhari *et al.*, 2018) found that 86% of the shrinkage of the lake in the period 1995–2010 can be explained by human activities. Hassanzadeh *et al.*, (2012) used a system dynamics model (Simonovic, 2009) to analyse the influence of different management and climate scenarios on the lake volume. Their model results suggest that the influence of the reservoirs (at a storage volume of about 1 km³), the changes in precipitation directly above the lake, and the reduced inflow due to overuse of surface water are responsible for 25%, 10% and 65% of the volume loss, respectively. Other studies conclude that changes in climate, i.e., reduced precipitation and increased temperatures, are mainly responsible for lowering the lake level (Delju *et al.*, 2013; Fathian *et al.*, 2015; Arkian *et al.*, 2016; Malekian and Kazemzadeh, 2016; Shadkam *et al.*, 2016). Generally, these studies based their assumptions on similarities between trend patterns of climate and inflow into the lake. Fathian *et al.*, (2015) showed that decreasing discharge trends can already be observed in the headwater catchment areas, which indicate climate-induced changes, and that the reservoirs do not seem to have a significant influence.

Shadkam *et al.*, (2016) analysed the relative contribution of climate change and water management to the water balance of the lake using a variable infiltration capacity model. They also conclude that reservoirs have no significant impact on the reduced lake inflow and that climate and irrigation have an impact of 60% and 40% respectively. Furthermore, they state that the increased irrigation water demand results from stronger and longer periods of drought and thus establish a direct correlation between the increasing agricultural water demand and climatic changes.

The future of Lake Urmia is at stake. The relevance and interplay of global and regional factors, i.e., climate change and local water management, will determine its fate. Although our ability to influence climatic changes seems to be rather limited, at least on a short time scale, an optimization of agricultural practices has a proven potential for immediate water savings (Mostafa *et al.*, 2017). However, to encourage and justify related water savings requires a prediction of their potential benefits based on scientifically sound future projections. To this end, we quantify the components of the water budget of Lake Urmia over the last five decades and analyse their temporal evolution and interplay. Based on the water balance, we perform a series of simulations of different development scenarios to analyse whether and to what extent local agricultural water saving could contribute to the restoration and conservation of Lake Urmia.

2.3 Methods

2.3.1 Data

The lake volume evolution as well as the quantification and further analysis of the different water balance components (inflow, precipitation, evaporation and change of storage) base on a series of different data sets. These include: (i) mean monthly and annual lake level for the period 1965–2018 and 1931–2017, respectively (Iran Water Resources Management Company); (ii) monthly and annual inflow into the lake for the period 1965–2016 and 1953–2017, respectively (Ministry of Energy); (iii) monthly river runoff for a total of 132 gauging stations with records between 1952 and 2016 (Ministry of Energy); (iv) monthly potential evaporation, calculated based on routine weather data using a simplified version of the Penman equation (Valiantzas, 2006), for Tabriz from 1952 to 2017 (Iran Meteorological Organization); (v) monthly precipitation for the stations Tabriz (1951–2017), Urmia (1951–2017), Sahand (1985–2017), Mahabad (1985–2017) and Miandoab (2002–2017) (Iran Meteorological Organization); (vi) monthly river water extraction for irrigation from 1970 to 2016 (Ministry of Agriculture); (vii) evolution of total area for irrigation agriculture in the Lake Urmia catchment between 1984 and 2016 (Ministry of Agriculture); (viii) information about the 41 principal reservoirs in the catchment, i.e. construction date and capacity (Ministry of Energy); (ix) bathymetry of Lake Urmia with a resolution of 30×30 m, surveyed in 2017 by an echo sounding (50–200 kHz) mapping campaign (by the Ministry of Energy's Water Research Institute on request of Urmia Lake Restauration Program).

2.3.2 Level-area-volume relationship

The lake area and volume are calculated based on the lake level and the raster data set of the bathymetry. To calculate the area, the number of pixels, which are equal or lower than the corresponding lake level, is multiplied with the pixel size (900 m^2). Subsequently, the mean depth is calculated by subtracting the mean elevation of the pixels, which are equal or lower than the lake level, from the lake level. Multiplying the mean depth with the area results the lake volume.

2.3.3 Salt water evaporation

Evaporation from saline water bodies depends on meteorological variables, but also on the salinity and the ionic composition. As the salinity increases, the free energy of the water molecules is reduced, resulting in a decrease in the saturation vapor pressure above the water surface and thus a decrease in evaporation (Salhotra *et al.*, 1985a, 1987). Here, the relationship of actual salt water evaporation (E_{salt}) to freshwater evaporation (E_{fresh}) can be represented by the salinity dependent empirical ratio α (Salhotra *et al.*, 1985a, 1987) Eq. (2).

$$\alpha = \frac{E_{\text{salt}}}{E_{\text{fresh}}} \quad \text{Eq. (2)}.$$

Lake Urmia is an endorheic basin and therefore the salt concentration depends strongly on the lake volume. A linear regression model, based on a number of observations (Karbassi *et al.*, 2010), explains this dependence of the salinity on the lake volume quite well (Fig. 2-2a). In order to determine the empirical ratio α , we performed evaporation experiments for eight different salt solutions and a fresh water reference. The ionic composition of the salt solution used was similar to that of Lake Urmia (Karbassi *et al.*, 2010) and the initial salt concentrations ranged from 5% to 38%. During the experiment, temperature and relative humidity were kept constant at 30 °C and 20%, respectively, by means of an environmental chamber. The experiment lasted 7 days and each day the evaporation loss was measured gravimetrically. For the expected concentration range, based on the range of observed volumes (Fig. 2-2a), a linear regression model is used to describe the relationship between α and salinity (Fig. 2-2b). Subsequently, actual salt water evaporation rates for Lake Urmia were estimated by multiplying potential evaporation rates with the corresponding value for α , which was derived from the introduced linear models.

It should be noted that this approach constitutes a simplification. Actually, α not only depends on the salinity, but it is also influenced by meteorological variables. Two studies of (Salhotra *et al.*, 1985a, 1987) have analysed this influence. They experimentally determined α for a range (n = 24) of different temperatures (16–35 °C) and humidities (29–62%) for three concentrated Mediterranean Sea water samples with about 5.4%, 20%, and 23.3% salinity.

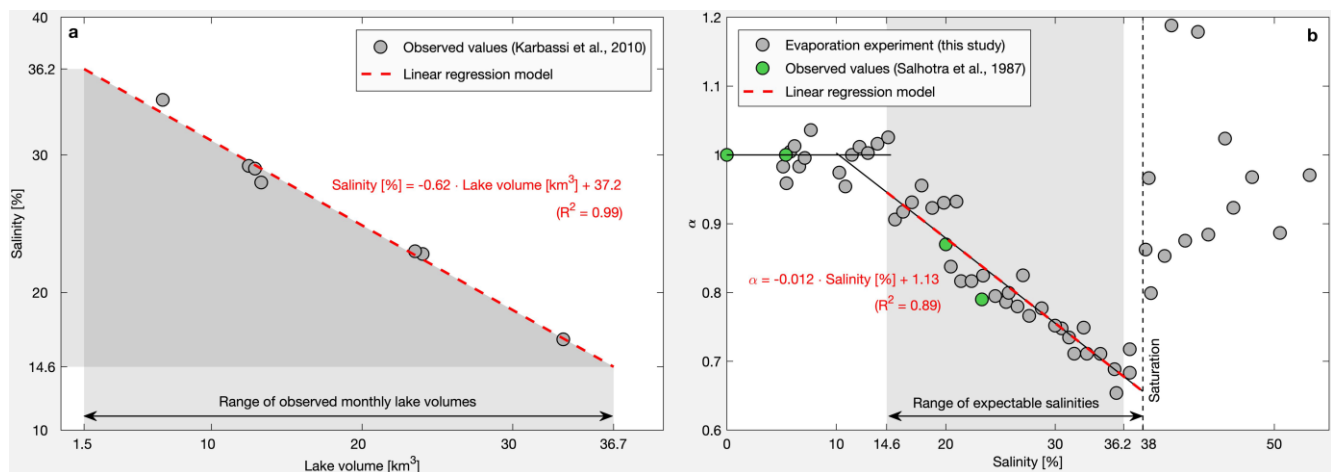


Fig. 2-2. Impact of lake volume on evaporation. (a) Relationship of salinity and lake volume (Karbassi *et al.*, 2010). (b) Relationship of the empirical ratio α and salinity; error bars for α from the evaporation experiment of Salhotra *et al.*, (1985, 1987) show the standard deviations for a range (n = 24) of different temperatures (16–35°C) and humidities (29–62%). (Plots are generated using MATLAB R2019b, www.mathworks.com).

Resulting values for α showed an average standard deviation of 0.06, which could be seen as a first approximation for the uncertainty of the presented approach. Being aware of the existence of more accurate concepts, we still consider the applied approach appropriate as it does not require additional

and, in our case, not continuously available data such as water temperature and humidity directly above the lake surface.

2.3.4 Statistics

The 12-months standardized precipitation evaporation index (SPEI) (Vicente-Serrano *et al.*, 2010) and the 12-months standardized runoff index (SRI) (Shukla and Wood, 2008) are calculated individually for all 132 runoff stations (AghaKouchak, 2015). Here, for the SPEI the closest available weather station, based on Thiessen polygons, is used. Subsequently, for each month during the test period from 1965 to 2016, the runoff-weighted averages for the indices are calculated (Fig. 2-4a). In order to investigate the temporal development of both time series, they are split into the six periods, which characterize the general trends in lake volume evolution (Fig. 2-3.). For each of these periods and for both indices a seasonal Mann-Kendall test is performed and the Sens slope is calculated (Hirsch and Slack, 1984; Burkey, 2012). The significance level for the seasonal Mann-Kendall test is 0.01 and the starting month for the 12-months interval is October (start of the hydrological year). Bootstrap sampling of the slope of the simple linear regression model of the SRI-SPEI relationship for the six periods is performed with a number of 1000 data samples (Fig. 2-4c).

2.4 Results and discussion

2.4.1 Lake Urmia's water balance.

Lake Urmia is the limnic end member of an endorheic (closed) basin, which means that its only relevant outflow component is the evaporation (E) from the lake surface. Inflow into the lake results from several rivers (Q) and from direct precipitation (P). Also, a certain groundwater component in the water balance cannot be precluded, especially if one considers the groundwater extraction through tens of thousands of legal and illegal wells in the Lake Urmia catchment (JICA, 2016). To the best of our knowledge, however, the vast majority of studies assume that a direct groundwater component is relatively small compared to the previously mentioned ones. For instance, hydrochemical investigations at the western shore indicated almost no direct hydraulic interaction between groundwater and lake water (Amiri *et al.*, 2016), another study considered a direct component to be less than 3% of total inflow (Shadkam *et al.*, 2016), and some studies provide even quantitative estimates ranging from about $60 \times 10^6 \text{ m}^3\text{a}^{-1}$ to $210 \times 10^6 \text{ m}^3\text{a}^{-1}$ (UNDP & DoE., 2008; HASHEMI, 2012; JICA, 2016). The reason for these rather low rates is the fact that the main receiving water bodies for the groundwater are the perennial rivers discharging into the lake (UNDP & DoE., 2008; Stone, 2015; Shadkam *et al.*, 2016; Vaheddoost and Aksoy, 2018). Therefore, a direct groundwater component is neglected in the water balance of the lake, Eq. (1).

$$\frac{dS}{dt} = \frac{P+Q-E}{dt} \quad \text{Eq. (1)}$$

where dS is the change of water storage in the lake over the time period dt . Available data sets allowed the computation of the water balance from October 1953 to September 2017 with hydrological seasons extending from October to September in the following year (Fig. 2-3.).

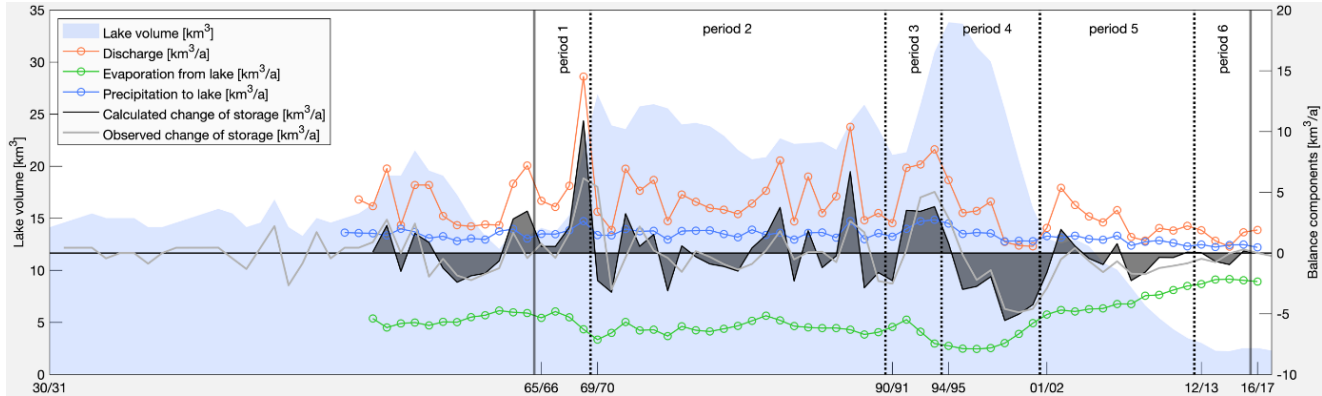


Fig. 2-3. Water balance of Lake Urmia. Temporal evolution of Lake Urmia's water balance components (seasonal sums) and observed lake volume (seasonal average). A hydrological season in the Lake Urmia basin extends from October to September of the following year. (Plot is generated using MATLAB R2019b, www.mathworks.com).

Between 1965 and 1995 the lake received an annual average of 4.9 km^3 water from its tributaries. Despite strong interannual variations, after 1995 a decline in river water inflow is evident, i.e., the mean annual discharge rate dropped by 50% to about $2.4 \text{ km}^3\text{a}^{-1}$ (1995 to 2017). The lowest annual surface discharge to the lake of only 0.5 km^3 was recorded in 2015 (Fig. 2-3.). The total volume of precipitation input and evaporation loss depend on the extent of the lake. Moreover, the actual evaporation rate depends on the salt concentration, which increases by reduction in lake volume. As a consequence of both, there has been a large evaporation rate in 1990s and the previous decades (up to $8.8 \text{ km}^3\text{a}^{-1}$). Thus, the decreasing evaporation loss to some extent buffers the lower inflow rates and leads to an almost equilibrated water balance since 2013. The calculated changes in the lake volume by considering the water balance components and the observed changes in lake volume agree quite well (Fig. 2-3.), indicating the validity of the proposed water balance.

For statistical analysis, which is the subject of the next section, we distinguished six periods between 1965 and 2017 that are characterized by their general trends in the lake volume evolution. Although, the available data set allowed us to draw the water balance for the lake since 1953, the number of operating hydrometric stations is rather limited before 1965, i.e., they have more than doubled from 1963 ($n = 18$) to 1965 ($n = 42$, Fig. 2-1c), which likewise improves the robustness of the data set. Besides, the separation of the periods bases on a visual analysis of storage change patterns, i.e. steep increase in lake volume during periods 1 and 3 with an observed change of storage (dS) of $3.2 \text{ km}^3\text{a}^{-1}$ in both cases, a quite stable lake volume during periods 2 and 6 with $dS = -0.3 \text{ km}^3\text{a}^{-1}$ and 0.1

km^3a^{-1} , respectively, a steep decrease in lake volume during period 4 ($dS = -3.0 \text{ km}^3\text{a}^{-1}$), and a moderate decrease during period 5 ($dS = -0.9 \text{ km}^3\text{a}^{-1}$, Fig. 2-3.).

2.4.2 Changing climate vs. irrigation water consumption

Precipitation and evaporation are the principal natural boundary conditions and drivers for streamflow. Here, we compare the temporal patterns of precipitation and evaporation with the discharge volumes of the rivers. To allow for a direct comparison, we applied the 12-months Standardized Precipitation Evaporation Index (SPEI), which is a multi-scalar measure accounting for precipitation and potential evaporation (Vicente-Serrano *et al.*, 2010). In analogy to the SPEI, we used the Standardized Runoff Index (SRI) (Shukla and Wood, 2008) representing the river flows. Both indices have the same scale and positive values indicating wetness, while negative values indicate dryness. For the SRI two different time series are used: one, which is based on the discharge weighted mean of all discharge stations and another one, which only bases on those stations that are the closest for each main river to the river mouth (Fig. 2-4a). The latter SRI series represents the inflow reaching the lake and is more relevant for the lake water budget. In analogy to the six periods, defined earlier for the evolution of the lake volume, we have also subdivided these time series into six periods. In addition to the six periods, we also show statistical parameters for a period from 1954 to 1965. Here it should be noted, however, that the corresponding data set might be less robust due to less operating hydrometric stations described above.

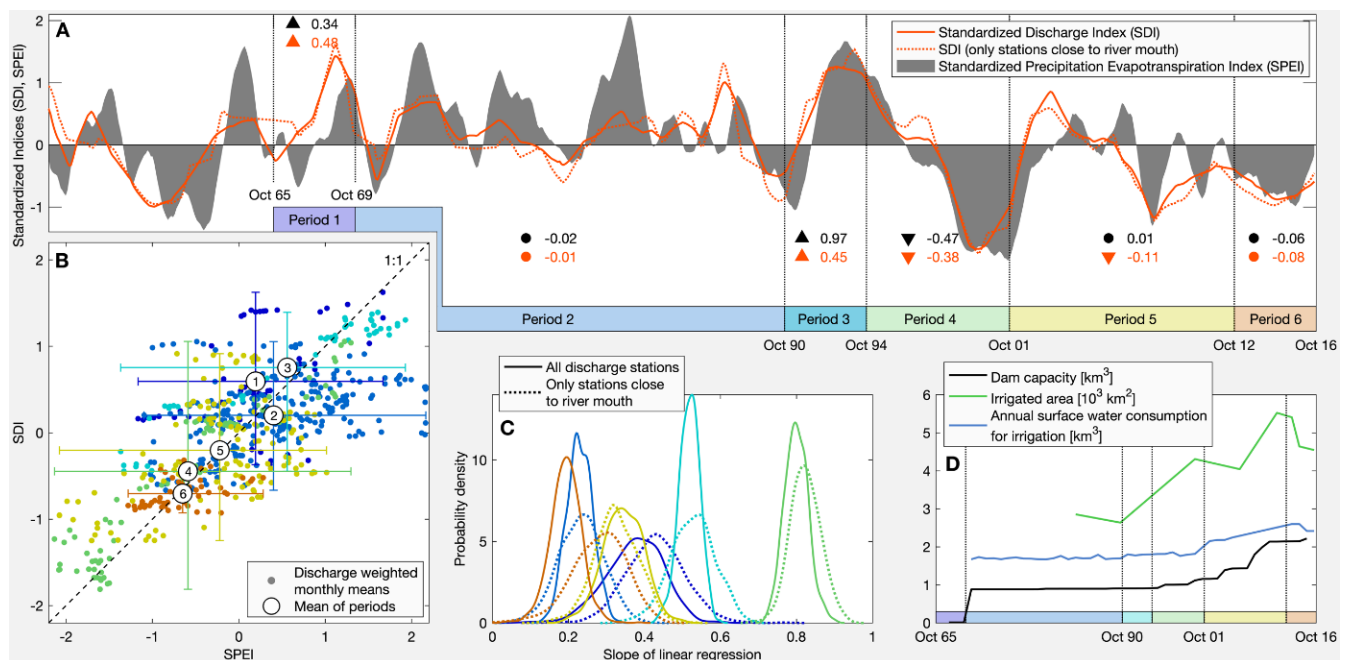


Fig. 2-4. Statistical analysis of runoff and weather time series. (a) Temporal evolution of 12-months SPEI and SRI (moving average filter with a kernel size of 12 months). A pointing up and down triangle shows a significant positive and negative Mann-Kendall trend, respectively. A dot means no significant trend ($p = 0.05$). (b) Relationship between discharge weighted monthly

mean SPEI and SRI values. (c) Probability density plot of the linear regression slope of the SRI-SPEI relationship based on bootstrap sampling. (d) Temporal evolution of anthropogenic influences affecting Lake Urmia's water budget. (a–d) The colour code used refers to the periods defined in Figs. 2-3 and 2-4a and grey coloured lines or dots representing the period 1954–1965. (Plots are generated using MATLAB R2019b, www.mathworks.com).

The SRI seems to follow the SPEI with a good approximation, which is also illustrated by the Mann-Kendall trends. Only in period 5 the trends differ significantly, with no significant trend for SPEI and a negative trend for SRI (Fig. 2-4a). Interestingly, this period is also characterized by a strongly increasing capacity of reservoirs in the catchment, i.e., it almost doubled from 1.2 km³ to 2.1 km³, and an increasing surface water consumption for irrigated agriculture (Fig. 2-4d). To further analyse the relationship between SPEI and SRI, their individual monthly values are compared (Fig. 2-4b). As expected, during periods which show a significant decline in lake volume (periods 4 and 5) or a very low volume (period 6), mean SRI and SPEI values are negative. During periods 1 and 3, Lake Urmia experienced an increase in water level, which is reflected by positive values of mean SRI and SPEI. Moreover, it can be observed that during period 1, the mean SRI is higher than the SPEI, which indicates more favourable discharge conditions. The lowest mean SRI in relation to the corresponding SPEI can be found in period 2. Other mean SRI and SPEI differ less, i.e., they plot quite close to the 1:1 line, including in periods 4 and 5 during which the severe lake level drop happened (Fig. 2-4b). We also analyse the slope of the linear regression of the monthly SPEIs and the responding SRIs. For this purpose, we not only analyse a single slope, but perform a bootstrap sampling with 1,000 data samples per period. The result of the bootstrapping analysis is displayed by a probability density function of the slopes for each period (Fig. 2-4c). Generally, higher slope values indicate stronger responses of river flow to changes in weather. Interestingly, anthropogenic alteration can cause both a weakened and an amplified response. A weakened response is usually expected due to damming, while an amplified response often results from water extraction for irrigation. This amplification commonly results from an exceptionally high irrigation water withdrawal during dry seasons and a reduced extraction during wet seasons (Döll *et al.*, 2009).

In our case, the strongest response appears for period 4, during which the most rapid lake level decline happened (Figs. 2-3 and 2-4c). Based on the previous discussions, this might be a consequence of increased extraction of irrigation water to mitigate the impact of drought. However, this explanation seems not very likely as the majority of the very dry months (very low SRI and SPEI) plotting well above the 1:1 line (Fig. 2-4b), i.e., they don't show exceptionally low discharge rates related to the weather conditions. In contrast, the weakest response (lowest slopes) of SRI to SPEI occurred during periods 2 and 6 followed by period 1 and 5 (Fig. 2-4c). In this case, too, the explanation that the dams could be the cause seems rather unlikely. Since the number and likewise the cumulative volume of dams has steadily increased over time (Fig. 2-4d), a steady increase in influence (i.e., weakening of response) could have been expected.

Results show that the temporal pattern of river flow rates can be well explained by weather changes, while an anthropogenic impact is not so obvious. However, in our analyses we have so far focused on an explanation for the temporal variability of the river runoff, which could imply the risk of a systematic influence being ignored. And indeed, a look at the temporal evolution of surface water consumption for irrigation reveals such a systematic influence (Fig. 2-4d). Since about 1970 irrigation was promoted for agricultural development and first large-scale water management was introduced with the construction the reservoirs Bukan and Mahabad (Fig. 2-1a) (Modares, 2018).

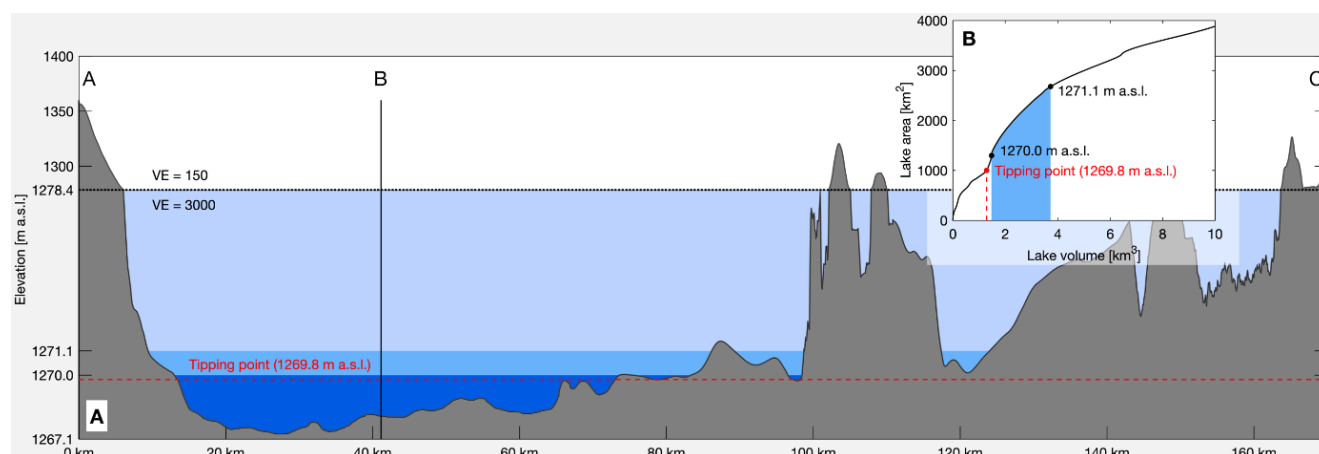


Fig. 2-5. Morphology of Lake Urmia. (a) Cross section of Lake Urmia with a vertical exaggeration (VE) of 150 and 3000 above and below 1278.4 m a.s.l., respectively. The location of the cross section is displayed in Fig. 2-1. (b) Volume-area relationship; the blue area shows the range of monthly values between 2013 and 2018. (Plots are generated using MATLAB R2019b, www.mathworks.com).

Since then, records of surface water extraction for irrigation show high, but relatively constant rates. The only remarkable change occurred during the period 5 with an increase from 2.1 to 2.6 km³a⁻¹. During the extreme lake level drop in period 4, the increase of irrigation water extraction was only about 0.2 km³a⁻¹, while the inflow to the lake decreased by 90% from 6.0 to 0.6 km³a⁻¹ (Figs. 2-3 and 2-4d). However, it is important to note that the withdrawal rates are generally on a quite high level and often (especially in the recent years) exceed the remaining inflow into the lake. On the basis of this perception and previous results, it can be concluded that although the massive irrigation withdrawal of surface water does not seem to directly cause the significant decline in the lake level over the last two decades, it has greatly weakened the lake's resilience, making it vulnerable to climate change.

This hypothesis is also supported by a parsimonious modeling experiment (Supplementary Information 1). Here it could be shown that even under more or less natural inflow conditions (irrigation water extraction added to the inflow), the simulated lake volume also decreased significantly over the last two decades. Its temporal variability does not differ too much from the observed lake volume either. However, under these natural inflow conditions, the simulated lake volume is constantly well above the simulated one, which takes irrigation water abstraction into

account. Hence, the volume decrease of the lake under natural inflow conditions is much less pronounced, i.e., for the year 2017 the simulated lake volume without irrigation water extraction (8.3 km³) is more than four times larger than the volume with irrigation water extraction (1.9 km³, Supplementary Fig. S1-1).

2.4.3 Reservoirs and discharge

From 1967 to 2015, 57 reservoirs with total capacity of 2.2 km³ were built in the Lake Urmia catchment to ensure a stable water supply for irrigated agriculture. An analysis of the impact of these reservoirs on the river runoff (Supplementary Information 1) revealed that runoff time series from downstream hydrometric stations do not show negative runoff trends more frequently than those that are not influenced, i.e., before reservoir construction or upstream of a reservoir (Appendix 3, Supplementary Fig. S1-2). After the construction of the reservoirs, on the other hand, the discharge is reduced on average by about 10%. Here, however, it is difficult to say whether this is a direct consequence of reservoir construction or merely a consequence of the generally declining runoff of recent decades. A clear difference between the runoff time series before and after reservoir construction is the interannual variability. After reservoir construction, the interannual variability is more balanced, i.e., runoff is relatively higher during dry months and relatively lower during wet months compared to the temporal runoff pattern before reservoir construction (Supplementary Fig. S1-3). This shows quite clearly the intended water retention to support the irrigation water supply in the dry months.

2.4.4 Implications on future perspectives

Evaporation from the lake strongly depends on the lake surface area and its salt concentration and thus counteracts low inflow rates. However, this only works effectively as long as there is a strong reduction of the lake area as a feedback to a decreasing volume. To analyse this, we need to take a look at the lake morphology. Lake Urmia is generally shallow and has a maximum depth of only about 10 meters. This shallowness is also reflected by a quite high average area-volume ratio of about 900 km⁻¹ (considering a lake level range of 1267.2–1278.4 m a.s.l.). In comparison, the Great Lakes in the US having an average area-volume ratio of about 10 km⁻¹ (Tilzer and Serruya, 1990). In particular in the south, the lake bottom's marginal planes are flat and have extremely gentle slopes. On the other hand, the northern part of the lake is slightly deeper (Fig. 2-5a). This morphology leads to a very non-linear volume- area relationship. A strong reaction of the lake area on a reduced volume can be observed for a lake volume between 1.3 and about 4 km³, while above and below this volume the reaction is weaker (Fig. 2-5b). The lower tipping point at about 1.3 km³ (sharp change in slope, Fig. 2-5b) is reached when the shallow southern part of the lake falls completely dry. The lake volume has fluctuated just above this tipping point since 2013, where the strongest reaction of the lake area on

volume changes can be observed. This may have contributed to the relatively stable lake volume of recent years, although the SPEI index was negative and despite the growing significance of agricultural water extraction. However, it should be noted that exceeding this tipping point leads to a reduced buffer effect and thus to a loss in resilience to climatic changes and agricultural water use.

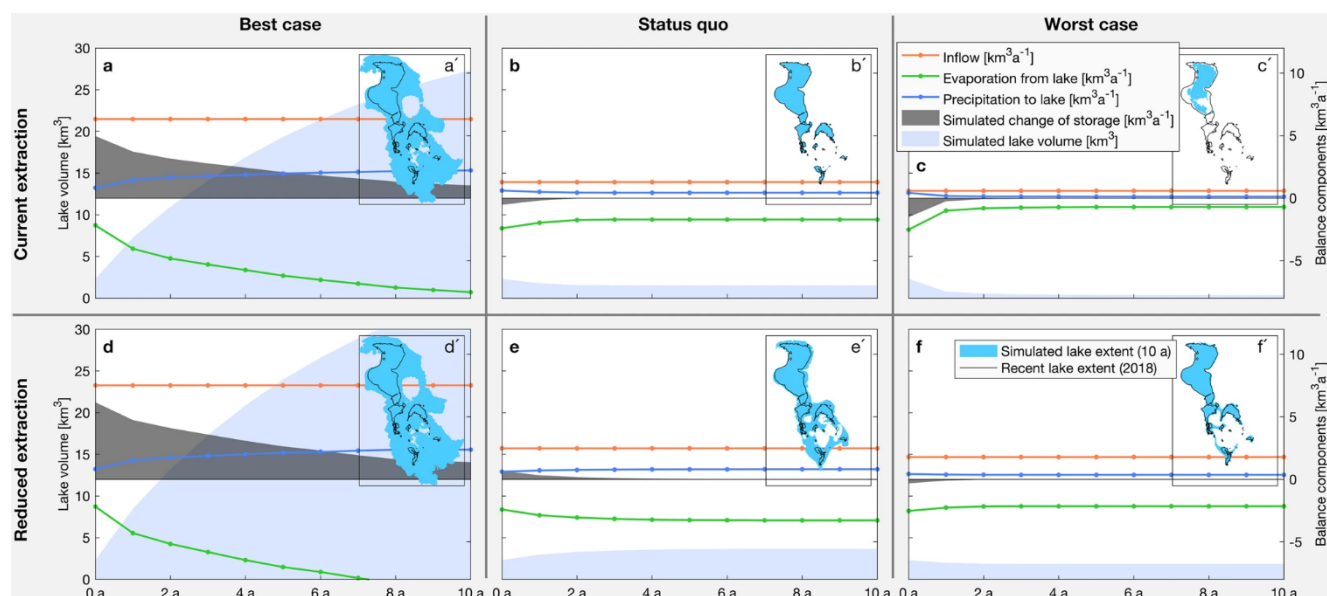


Fig. 2-6. Development scenarios for Lake Urmia. Climatic best-case (mean precipitation, potential evaporation and inflow of period 3), status quo (mean of period 6) and worst-case (mean of seasons 1999/00 to 2000/01) scenarios. (a–c) Scenarios assuming current irrigation water extraction. (d–f) Scenarios assuming a reduced irrigation water extraction by $1.2 \text{ km}^3\text{a}^{-1}$ (50% of current surface water extraction for irrigation). (Plots and maps are generated using MATLAB R2019b, www.mathworks.com).

Table 2.1. Climatic boundary conditions. Climatic boundary conditions for the simulations of development

| Scenario Related | Precipitation time period | Precipitation [mma^{-1}] | Potential evaporation [mma^{-1}] | Inflow [km^3a^{-1}] |
|---|---------------------------|-------------------------------------|---|---------------------------------------|
| Best-case | Period 3 | 414 | 1606 | 6.3 |
| Status quo (Current conditions) | Period 6 | 303 | 1776 | 1.3 |
| Worst-case | Oct 1999 – Sep 2001 | 213 | 1860 | 0.6 |

To draw some conclusions for Lake Urmia's future development, we run a series of forward simulations based on the lake water balance. The forecasting period of these simulations is ten years and six different scenarios are analysed. First, we distinguish between a best-case, status quo, and worst-case scenario for the climatic boundary conditions (Fig. 2-6a–c). These scenarios base on

observed mean precipitation, potential evaporation and inflow rates, for the period 3, period 6 and the two hydrological years from October 1999 to September 2001, respectively (Table 2-1). Here, the latter one was chosen due to exceptionally low inflow rates and the most severe drop in lake volume (Fig. 2-3). In addition, for these three climatic scenarios, we assumed an increased inflow of $1.2 \text{ km}^3\text{a}^{-1}$ into the lake, due to water savings in the agriculture sector (Fig. 2-6d–f). This corresponds to 50% of the surface water extraction for irrigation in 2016, savings that are considered possible in related studies (Stone, 2015; Mostafa *et al.*, 2017).

Our analysis show that for the climatic best-case scenario, the lake could reach a volume of 15 km^3 , which corresponds to an area of 4400 km^2 , already after about three years, even if agricultural withdrawal is not reduced (Fig. 2-6a,d). The gain in volume is significantly higher compared to observations in the best-case climatic reference period, due to the initially much smaller lake area, resulting in lower evaporation. However, the climatic status quo and also the worst-case scenarios are more likely, based on regional climate projections (Ashraf *et al.*, 2019; IPCC, 2014).

Here, agricultural water savings would have a significant impact on the lake volume. While without water savings the lake volume would further shrink (status quo scenario, Fig. 2-6b) or even dramatically shrink (worst-case scenario, Fig. 2-6c), a 50% reduction in withdrawal would lead to a 60% increase in lake volume after four years in the status quo scenario (Fig. 2-6e), and at least to a more or less constant lake volume, compared to today, even for the worst-case scenario (Fig. 2-6f).

2.5 Conclusion

We could show that in the last decades variation in the volume of Lake Urmia was mainly triggered by changes in climatic conditions, and even without agricultural water extraction the general trend of the lake volume variations would have been the same. However, this conclusion does not mean that human influence on the hydrological system in the Lake Urmia catchment is negligible. Using a parsimonious modeling experiment, we were also able to show that agricultural extraction has a massive influence on the resilience of the lake, as it exaggerates the general trend of declining lake volume, especially in the last two decades. This means, that without agricultural extraction the lake volume would also have decreased significantly in the last two decades, but would still have ended up at a much higher volume. Interestingly, the specific morphology of the lake could, to some extent buffer reduced inflows. However, the current climatic conditions together with the retraction of the lake to its northern and slightly deeper parts brought it into a very critical and labile state, close to the tipping point where it loses its ability to buffer reduced inflows by a reduced surface area. As agricultural water withdrawals are under the current climatic conditions comparable to the remaining surface water inflow volumes, or even higher, any changes in water withdrawal would have a significant impact on the lake volume. This is a risk, as well as an opportunity. Maintaining or even increasing the current extraction rates could result in a complete collapse of the lake, especially if

climate would further get dryer. However, substantial but realistic agricultural water savings could stabilize the lake by keeping the lake volume above the crucial tipping point, bringing therefore back its ability to buffer, even if climate would get dryer. Considering the current climatic conditions, it could as well lead to a significant volume and surface area increase of the lake, thus regaining its role as a very precious and special ecosystem.

2.8 Supplementary data

Data availability

All data used in this study is available from the corresponding author upon reasonable request.

Code availability

Matlab codes are archived at: <https://github.com/stephan-schulz-1/urmia.git>.

Supplementary information is available for this paper at <https://doi.org/10.1038/s41598-019-57150-y>. and in Appendix 3.

2.9 References

Agh, N., Van Stappen, G., Bossier, P., Sepehri, H., Lotfi, V., Rouhani, S.M.R., Sorgeloos, P., 2008. Effects of salinity on survival, growth, reproductive and life span characteristics of *Artemia* populations from Urmia Lake and neighboring lagoons. *Pakistan J. Biol. Sci. PJBS* 11, 164–172.

AghaKouchak, A. (2015). Standardized Drought Analysis Toolbox (SDAT) (<https://www.mathworks.com/matlabcentral/fileexchange/51081-standardized-drought-analysis-toolbox-sdat>), MATLAB Central File Exchange. Retrieved March 16, 2023.

Aghakouchak, A., Norouzi, H., Madani, K., Mirchi, A., Azarderakhsh, M., Nazemi, A., Nasrollahi, N., Farahmand, A., Mehran, A., Hasanzadeh, E., 2015. Aral Sea syndrome desiccates Lake Urmia: Call for action. *J. Great Lakes Res.* <https://doi.org/10.1016/j.jglr.2014.12.007>

Alborzi, A., Mirchi, A., Moftakhari, H., Mallakpour, I., Alian, S., Nazemi, A., Hassanzadeh, E., Mazdiyasn, O., Ashraf, S., Madani, K., Norouzi, H., Azarderakhsh, M., Mehran, A., Sadegh, M., Castelletti, A., AghaKouchak, A., 2018. Climate-informed environmental inflows to revive a drying lake facing meteorological and anthropogenic droughts. *Environ. Res. Lett.* <https://doi.org/10.1088/1748-9326/aad246>

Alizade Govarchin Ghale, Y., Altunkaynak, A., Unal, A., 2018. Investigation Anthropogenic Impacts and Climate Factors on Drying up of Urmia Lake using Water Budget and Drought Analysis. *Water Resour. Manag.* 32, 325–337. <https://doi.org/10.1007/s11269-017-1812-5>

Alizadeh-Choobari, O., Ahmadi-givi, F., Mirzaei, N., Owlad, E., 2016. Climate change and anthropogenic impacts on the rapid shrinkage of Lake Urmia. *Int. J. Climatol.* 4286, 4276–4286. <https://doi.org/10.1002/joc.4630>

Amiri, V., Nakhaei, M., Lak, R., 2016. Investigating the salinization and freshening processes of coastal groundwater resources in Urmia aquifer , NW Iran. *Environ. Monit. Assess.* <https://doi.org/10.1007/s10661-016-5231-5>

Arkian, F., Nicholson, S.E., Ziaie, B., 2016. Meteorological factors affecting the sudden decline in Lake Urmia's water level. *Theor. Appl. Climatol.* 1–11. <https://doi.org/10.1007/s00704-016-1992-6>

Asem, A., Eimanifar, A., Djamali, M., Rios, P.D.L., Wink, M., 2014. Biodiversity of the Hypersaline Urmia Lake National Park (NW Iran) 102–132. <https://doi.org/10.3390/d6020102>

Ashraf, S., AghaKouchak, A., Nazemi, A., Mirchi, A., Sadegh, M., Moftakhari, H.R., Hassanzadeh, E., Miao, C.-Y., Madani, K., Mousavi Baygi, M., Anjileli, H., Arab, D.R., Norouzi, H., Mazdiyasni, O., Azarderakhsh, M., Alborzi, A., Tourian, M.J., Mehran, A., Farahmand, A., Mallakpour, I., 2019. Compounding effects of human activities and climatic changes on surface water availability in Iran. *Clim. Change* 152, 379–391. <https://doi.org/10.1007/s10584-018-2336-6>

Burkey, J. (2012). Seasonal Kendall Test with Slope for Serial Dependent Data (<https://www.mathworks.com/matlabcentral/fileexchange/22389-seasonal-kendall-test-with-slope-for-serial-dependent-data>), MATLAB Central File Exchange. Retrieved March 16, 2023.

Chaudhari, S., Felfelani, F., Shin, S., Pokhrel, Y., 2018. Climate and anthropogenic contributions to the desiccation of the second largest saline lake in the twentieth century. *J. Hydrol.* 560, 342–353. <https://doi.org/https://doi.org/10.1016/j.jhydrol.2018.03.034>

Delju, A.H., Ceylan, A., Piguet, E., Rebetez, M., 2013. Observed climate variability and change in Urmia Lake Basin, Iran. *Theor. Appl. Climatol.* 111, 285–296. <https://doi.org/10.1007/s00704-012-0651-9>

Döll, P., Fiedler, K., Zhang, J., 2009. Global-scale analysis of river flow alterations due to water withdrawals and reservoirs. *Hydrol. Earth Syst. Sci.* 13, 2413–2432. <https://doi.org/10.5194/hess-13-2413-2009>

Eimanifar, A., Mohebbi, F., 2007. Urmia Lake (Northwest Iran): a brief review. *Saline Systems* 3, 5. <https://doi.org/10.1186/1746-1448-3-5>

Fathian, F., Morid, S., Kahya, E., 2015. Identification of trends in hydrological and climatic variables in Urmia Lake basin, Iran. *Theor. Appl. Climatol.* 119, 443–464. <https://doi.org/10.1007/s00704-014-1120-4>

Golabian, H., 2011. Urumia Lake: Hydro-Ecological Stabilization and Permanence, in: Badescu, V., Cathcart, R.B. (Eds.), *Macro-Engineering Seawater in Unique Environments: Arid Lowlands and Water Bodies Rehabilitation*. Springer Berlin Heidelberg, Berlin, Heidelberg, pp. 365–397. https://doi.org/10.1007/978-3-642-14779-1_18

Goossens, D., Gross, J., Spaan, W.I.M., 2001. AEOLIAN DUST DYNAMICS IN AGRICULTURAL LAND AREAS IN LOWER SAXONY , GERMANY 720, 701–720. <https://doi.org/10.1002/esp.216>

HASHEMI, M., 2012. A SOCIO-TECHNICAL ASSESSMENT FRAMEWORK FOR INTEGRATED WATER RESOURCES MANAGEMENT (IWRM) IN LAKE URMIA BASIN, IRAN 5, 13–15. <https://core.ac.uk/download/pdf/40007855.pdf>

Hassanzadeh, E., Zarghami, M., Hassanzadeh, Y., 2012. Determining the Main Factors in Declining the Urmia Lake Level by Using System Dynamics Modeling. *Water Resour. Manag.* 26, 129–145. <https://doi.org/10.1007/s11269-011-9909-8>

Hesami, A., Amini, A., 2016. Changes in irrigated land and agricultural water use in the Lake Urmia basin. *Lake Reserv. Manag.* 32, 288–296. <https://doi.org/10.1080/10402381.2016.1211202>

Hirsch, R.M., Slack, J.R., 1984. Nonparametric Trend Test for Seasonal Data With Serial Dependence. *Water Resour. Res.* 20, 727–732. <https://doi.org/10.1029/WR020i006p00727>

IPCC. Climate Change 2014: Synthesis Report. Contribution of Working Groups I, II and III to the Fifth Assessment Report of the Intergovernmental Panel on Climate Change. (2014)

Jalili, S., Hamidi, S.A., Namdar Ghanbari, R., 2016. Climate variability and anthropogenic effects on Lake Urmia water level fluctuations, northwestern Iran. *Hydrol. Sci. J.* 61, 1759–1769. <https://doi.org/10.1080/02626667.2015.1036757>

JICA, 2016. Japan international cooperation agency, data collection survey on hydrological cycle of lake Urmia basin in the Islamic Republic of Iran final report hydrological cycle of lake. 268.

Kabiri, K., Science, A., Pradhan, B., Sharifi, A., 2012. Manifestation of Remotely Sensed Data Coupled With Field Measured Meteorological Data for an Assessment of Degradation of Urmia Lake, Iran. *Adv. Biomed. Eng.* 5–12.

Karbassi, A., Bidhendi, G.N., Pejman, A., Bidhendi, M.E., 2010. Environmental impacts of desalination on the ecology of Lake Urmia. *J. Great Lakes Res.* 36, 419–424. <https://doi.org/10.1016/j.jglr.2010.06.004>

Khazaei, B., Khatami, S., Alemohammad, S.H., Rashidi, L., Wu, C., Madani, K., Kalantari, Z., Destouni, G., Aghakouchak, A., 2019. Climatic or regionally induced by humans? Tracing hydro-climatic and land-use changes to better understand the Lake Urmia tragedy. *J. Hydrol.* 569, 203–217. <https://doi.org/10.1016/j.jhydrol.2018.12.004>

Malekian, A., Kazemzadeh, M., 2016. Spatio-temporal analysis of regional trends and shift changes of autocorrelated temperature series in Urmia Lake basin. *Water Resour. Manag.* 30, 785–803. <https://doi.org/10.1007/s11269-015-1190-9>

Modares, F., 2018. The role of climate and land use change in Lake Urmia desiccation. <http://jultika.oulu.fi/files/isbn9789526221021.pdf>

Mostafa, H., El-Nady, R., Awad, M., El-Ansary, M., 2017. Drip irrigation management for wheat under clay soil in arid conditions. *Ecol. Eng.* 0–1. <https://doi.org/10.1016/j.ecoleng.2017.09.003>

Nouri, H., Mason, R.J., Moradi, N., 2017. Land suitability evaluation for changing spatial organization in Urmia County towards conservation of Urmia Lake. *Appl. Geogr.* 81, 1–12. <https://doi.org/10.1016/j.apgeog.2017.02.006>

Salhotra, A.M., Adams, E.E., Harleman, D.R.F., 1985. Effect of Salinity and Ionic Composition on Evaporation: Analysis of Dead Sea Evaporation Pans. *Water Resour. Res.* 21, 1336–1344. <https://doi.org/10.1029/WR021i009p01336>

Salhotra, A.M., Adams, E.E., Harleman, D.R.F., 1987. The alpha, beta, gamma of evaporation from saline water bodies. *Water Resour. Res.* 23, 1769–1774. <https://doi.org/10.1029/WR023i009p01769>

Shadkam, S., Ludwig, F., van Oel, P., Kiritmit, Ç., Kabat, P., 2016. Impacts of climate change

and water resources development on the declining inflow into Iran's Urmia Lake. *J. Great Lakes Res.* 42, 942–952. <https://doi.org/10.1016/j.jglr.2016.07.033>

Sharifi, A., Shah-Hosseini, M., Pourmand, A., Esfahaninejad, M., Haeri-Ardakani, O., n.d. *The Vanishing of Urmia Lake: A Geolimnological Perspective on the Hydrological Imbalance of the World's Second Largest Hypersaline Lake*. Springer Berlin Heidelberg, Berlin, Heidelberg, pp. 1–38. https://doi.org/10.1007/978-3-642-84077-7_1

Shukla, S., Wood, A.W., 2008. Use of a standardized runoff index for characterizing hydrologic drought. *Geophys. Res. Lett.* 35. <https://doi.org/10.1029/2007GL032487>

Simonovic, S. P. *Managing Water Resources - Methods and Tools for a Systems Approach*. (UNESCO, 2009)

Stone, R., 2015. Saving Iran's great salt lake. *Science* (80-.). 349. <https://doi.org/10.1126/science.1265210>

Tilzer, M. M. & Serruya, C. *Large Lakes - Ecological Structure and Function.*, (Springer Berlin Heidelberg, 1990). <https://doi.org/10.1007/978-3-642-84077-7>

Tourian, M.J., Elmi, O., Chen, Q., Devaraju, B., Roohi, S., Sneeuw, N., 2015. A spaceborne multisensor approach to monitor the desiccation of Lake Urmia in Iran. *Remote Sens. Environ.* 156, 349–360. <https://doi.org/10.1016/j.rse.2014.10.006>

UNDP & DoE., 2008. *An Independent Review: The Status of Water Resources in the Lake Urmia Basin*.

Vaheddoost, B., Aksoy, H., 2018. Interaction of groundwater with Lake Urmia in Iran. *Hydrol. Process.* 32, 3283–3295. <https://doi.org/10.1002/hyp.13263>

Valiantzas, J.D., 2006. Simplified versions for the Penman evaporation equation using routine weather data. *J. Hydrol.* 331, 690–702. <https://doi.org/10.1016/j.jhydrol.2006.06.012>

Vicente-Serrano, S.M., Beguer?a, S., Lopez-Moreno, J.I., 2010. A Multiscalar Drought Index Sensitive to Global Warming: The Standardized Precipitation Evapotranspiration Index. *J. Clim.* 23, 1696–1718. <https://doi.org/10.1175/2009JCLI2909.1>

Wurtsbaugh, W.A., Miller, C., Null, S.E., Justin De Rose, R., Wilcock, P., Hahnenberger, M., Howe, F., Moore, J., 2017. Decline of the world's saline lakes. *Nat. Geosci.* 10, 816–821. <https://doi.org/10.1038/NGEO3052>

Zoljoodi, M., Didevarasl, A., 2014. Water-Level Fluctuations of Urmia Lake : Relationship with the Long-Term Changes of Meteorological Variables (Solutions for Water-Crisis Management in Urmia Lake Basin). *Atmos. Clim. Sci.* 4, 358-368 358–368. <https://doi.org/10.4236/acs.2014.43036>

Competing interests

The authors declare no competing interests.

Additional information

Supplementary information is available for this paper at <https://doi.org/10.1038/s41598-019-57150-y>.

Correspondence and requests for materials should be addressed to S.S.

Reprints and permissions information is available at www.nature.com/reprints.

Publisher's note Springer Nature remains neutral with regard to jurisdictional claims in published maps and institutional affiliations.

3 A Low-cost Environmental Chamber to simulate warm Climatic Conditions

Sahand Darehshouri ^a, Nils Michelsen ^a, Christoph Schüth ^a, Stephan Schulz ^{a*}

^a Technische Universität Darmstadt, Institute of Applied Geosciences, Schnittspahnstr. 9, 64287 Darmstadt, Germany

*Corresponding author: Stephan Schulz, schulz@geo.tu-darmstadt.de

Published in *Vadose Zone Journal*, 2020, Vol. 19, Issue1, <https://doi.org/10.1002/vzj2.20023>

3.1 Abstract

Environmental chambers are utilized for a variety of experiments in multiple disciplines, but are often prohibitively expensive. In this study, we developed an environmental chamber that allows a reliable regulation of temperature and relative humidity in a range typical for warm climatic conditions. As we have only used consumer products, which are readily available off-the-shelf, the device is affordable (< 900 €) and easy to replicate. The presented chamber has inner dimensions of 1,790 x 970 x 520 mm (height x width x depth). It is heated with two infrared lamps and for moistening an ultrasonic mister is used. Air dehumidification and cooling down to ambient temperature are realized with inflowing compressed laboratory air. Additionally, we installed a Peltier element cooling system to enable temperatures below ambient laboratory temperature. The chamber works in a temperature and humidity range of 15-50 °C and 10-95%, respectively.

3.2 Introduction

Environmental chambers (also termed climate or climatic chambers) enabling temperature and relative humidity regulation during laboratory experiments, are required in a range of disciplines, including ecology, geology, and hydrology. They are, for example, used to study salt weathering of rocks (Goudie and Parker, 1998), nutrient leaching in soils (Grant et al., 2019), water repellency of soils (Jiménez-Pinilla et al., 2016), or in evaporation studies (Huang et al., 2013; Song et al., 2014; Shokri-Kuehni et al., 2017; Merz et al., 2018; Qazi et al., 2018). Moreover, environmental chambers serve to test monitoring equipment (Windhorst et al., 2013; Prechsl et al., 2014; Papapostolou et al., 2017). Yet, commercial devices are often prohibitively expensive (Greenspan et al., 2016), particularly for labs that do not use them on a routine basis. Consequently, scientists tend to improvise (Schulz et al., 2015; Michelsen et al., 2018) and although improvisation helped in these cases, a fully functional but affordable environmental chamber would be a useful addition to the researcher's toolbox.

Some researchers have designed affordable environmental chambers, but often only propose solutions for the control of temperature (Song et al., 2014; Greenspan et al., 2016). Others have constructed working models for the control of both, temperature and humidity, yet they mostly focused on plant growth chambers simulating moderate environmental conditions (Katagiri et al., 2015; Bernard et al., 2015). Katagiri et al. (2015), for instance, aimed at a temperature of 22 °C and a relative humidity of 75%, and generally assumed that the temperature in their chamber would be within 8 °C of the ambient temperature.

In view of much harsher conditions prevailing in nature, we developed a robust climate chamber that can mimic a relatively wide range of warm environmental conditions, in terms of temperature and humidity. We describe a simple, affordable (< 900 €) do-it-yourself (DIY) chamber that mainly consists of off-the-shelf equipment. After providing an overview of the design, we present the results of a rigorous multi-week test of the device. A bill of materials, including suppliers and prices, a construction manual, and a comparison to commercially available environmental chambers is given in the Supplemental Material 2, in Supplemental Table S2-1.1. and Supplemental Material 2-S3:, respectively.

3.3 Design

Aiming at a versatile tool for multiple applications such as larger column experiments (Schulz et al., 2015) or tests of equipment (Michelsen et al., 2018), we designed an environmental chamber with an inner dimensions of 1,790 x 970 x 520 mm (height x width x depth). Although we generally acknowledge the usefulness of microcontrollers, we deliberately avoided this tool (and the associated coding) and entirely relied on readily available consumer products to allow for easy replication and operation.

The chamber itself consists of 16 mm polycarbonate twin-wall sheets framed by a heavy-duty shelf. The front has an opening of about 900 x 400 mm, which is covered by a transparent acrylic glass panel (Fig. 3-1A). To guarantee a homogeneous temperature and humidity distribution, an air circulation system with a fan ensures a gentle, but constant air flow through the chamber (Fig. 3-1B).

The temperature is controlled by a dual relay thermostat. If the temperature in the chamber falls below a defined threshold, two infrared-lamps (2 x 150 W or 2 x 300 W) are switched on. If the temperature exceeds a threshold, the lamps are switched off and a valve opens so that cool and dry air, provided by the compressed air system in the laboratory, flows into the chamber. Here, a pressure reducing valve, set to 0.5 bar, maintains a constant flow rate of 0.14 l/s. Our compressed laboratory air is dehumidified and has a constant temperature of 21-22°C, which in turn constitutes the minimum temperature that can be reached in this set-up. For most experiments targeting warm arid conditions, this would be cold enough. Nevertheless, we installed an additional cooling system, which replaces the previously described one, if temperatures below the compressed air temperature have to be reached. This system is based on eight 60 W Peltier elements that are installed into the back wall of the chamber. On top of the cooling side of the Peltier elements (inside of the chamber), a fan is mounted for the cold air distribution. On the warming side (outside of the chamber), a water-cooling block is attached. Nonetheless, for the simulation of warm arid conditions, the cooling system using compressed laboratory air should be sufficient. Hence, the cooling method based on Peltier elements can be considered as an optional add-on.

Simultaneously to temperature, relative humidity is controlled by a dual relay hygrostat. When the relative humidity falls below or exceeds a threshold, the air inside the chamber will be moistened or dehumidified, respectively. Air moistening is realized with a fan-driven air circuit passing an external humidifier (Fig. 3-1A). This humidifier consists of a polypropylene container with deionized water and an ultrasonic mister (Hannusch, 1995; Katagiri et al., 2015). Air dehumidification works the same way as the firstly described cooling method, i.e., via inflow of cool and dry compressed air. For both, cooling and drying, the compressed air flows into the internal air tubing system for quick distribution.

The thermostat and the hygrostat are simple plug and play devices, which allow intuitive programming and in case of the thermostat even for different time windows per day. To avoid a permanent on and off switching of the cooling/heating or moistening/drying systems, a buffer can be applied to the target values for temperature and humidity.

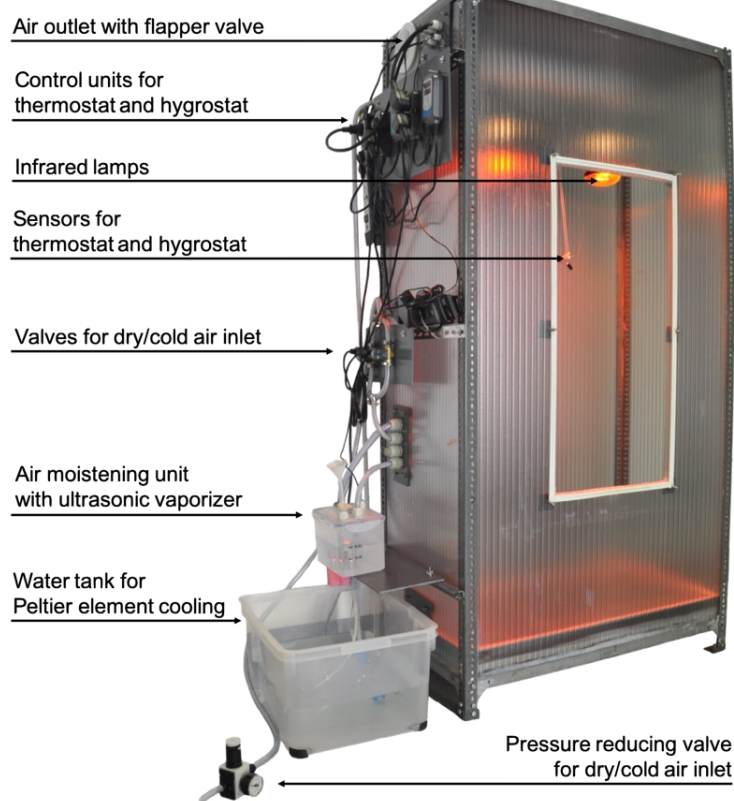
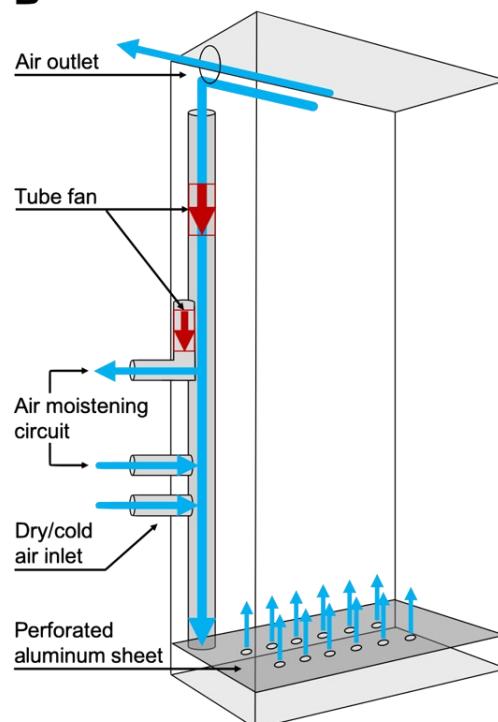
A**B**

Fig. 3-1. (A) Operating environmental chamber with activated infrared lamps; opening can be closed with a transparent acrylic glass panel (for bill of materials and construction manual, see Supplementary information 2); (B) Schematic sketch of the air circulation.

3.4 Test

To explore the chamber's capabilities and limits, it was tested with various temperature and relative humidity settings for several weeks. For monitoring purposes during this test, we additionally installed a CS215 temperature and relative humidity probe (Campbell Scientific) next to the sensors of the thermostat and the hygostat, which are located in the center of the chamber about 60 cm below the infrared lamps. Measurements were recorded with a CR800 datalogger (Campbell Scientific) with a one-minute logging interval. The laboratory, in which the test was performed, has an ambient temperature of 21-22°C and a relative humidity between 50% and 60%. These conditions correspond approximately to the test standard, i.e., most commercial chambers are tested at 23°C ambient temperature and about 65% relative humidity (ESPEC CORP, 2019a; b; Memmert GmbH, 2019; Russells, 2019).

In a series of pre-tests, we figured out that depending on the target temperature, different hardware configurations of the environmental chamber are required. For target temperatures of 25-35°C, two 150 W infrared lamps are suitable. For higher target temperatures of up to 50°C, the 150 W lamps should be replaced by two 300 W bulbs. For both temperature ranges, the cooling is realized with

inflowing compressed laboratory air. In case of lower desired temperatures, ranging from ambient laboratory temperature down to 15°C, the compressed air-cooling system has to be replaced by the Peltier element cooling system (see above).

The test was conducted with target temperatures of 15, 20, 25, 30, 35, 40, 45, and 50°C. For each temperature setting, the relative humidity was initially set to 5% and subsequently increased to 10, 30, 50% etc. until a temperature-dependent limit was reached. As soon as the feasible relative humidity setting was exceeded (indicated by unstable relative humidity records and condensed water at the acrylic glass), we gradually lowered the target humidity until the values stabilized (Fig. 3-2). The buffers for the thermostat and the hygostat (see previous section) were set to $\pm 0.5^\circ\text{C}$ and $\pm 1\%$, respectively. Each selected temperature-humidity combination was tested for 24 hours, resulting in a total test period of 48 days.

The test yielded several findings. First, it showed how long it takes to reach a given target value (lag time). Generally, temperature increases by 5°C are associated with lag times of less than 10 minutes. In case of relative humidity, lag times are not that constant. For the increases from 10 to 30%, 30 to 50%, and 50 to 70%, lag times of about 30, 60, and 120 minutes were noted, respectively. The strong decrease in relative humidity at the start of a new temperature setting lasted even longer. In case of the transition from 90 to 5% (at 25-30°C), it took about 8 hours. This is caused by the condensation of water drops and the rather long time required for their evaporation.

As soon as a target setting was reached, temperature and relative humidity records were rather stable. Small fluctuations are usually within the buffer range of the thermostat and hygostat. An exception is the period, in which the Peltier elements were used for cooling. Here, stronger fluctuations were noticed (Fig. 3-2).

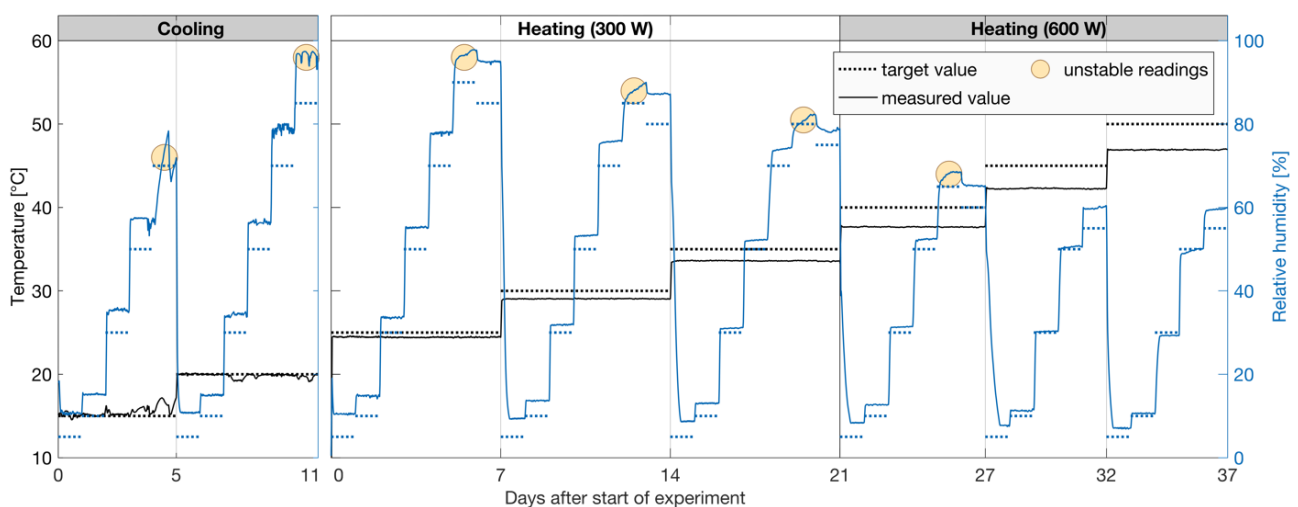


Fig. 3-2. Target and measured temperature (left axis) and relative humidity (right axis) over the 48 days testing period.

The test of the environmental chamber showed that temperature as well as humidity measurements of the thermostat and hygostat differ from those recorded by the independent CS215 probe (Fig. 3-2). The latter is a tested device with a temperature accuracy of $\pm 0.4^{\circ}\text{C}$ (5-40 $^{\circ}\text{C}$), a relative humidity accuracy of $\pm 2\%$ (10-90%), and a temperature dependency of $\pm 2\%$ (-20-60%) for the relative humidity sensor (CampbellScientific, 2016). For our purposes, these are very satisfying accuracies. Hence, we consider the measurements of the CS215 probe as true reference values. For future applications of the environmental chamber, we would like to have the possibility to omit the somewhat expensive reference probe and datalogger. Therefore, we developed correction functions for the measurements of the thermostat and the hygostat.

The temperature sensor deviation is independent from humidity and only depends on the temperature itself. The relation between true temperature and target temperature can be described by a simple linear regression model (Equation 1).

$$\vartheta = 0.901 \cdot \vartheta_{tar} + 1.843 \quad \text{with } n = 8 \text{ and } R^2 = 1.00 \quad (1)$$

where ϑ is the true temperature [$^{\circ}\text{C}$] and ϑ_{tar} is the target temperature [$^{\circ}\text{C}$].

The relative humidity sensor drift depends on both, temperature and relative humidity. The relation between true relative humidity and target temperature and target relative humidity can be described by a multivariate linear regression model (Equation 2).

$$\varphi = 1.008 \cdot \varphi_{tar} - 0.175 \cdot \vartheta_{tar} + 8.957 \quad \text{with } n = 42 \text{ and } R^2 = 0.99 \quad (2)$$

where φ is the true relative humidity [%], φ_{tar} is the target relative humidity [%] and ϑ_{tar} is the target temperature [$^{\circ}\text{C}$].

Finally, this test shows the range of feasible temperature and relative humidity settings. While the temperature range seems to be independent from the relative humidity, the range of the relative humidity is very sensitive to the temperature. The presented environmental chamber can simulate a temperature window from 15°C to about 50°C. A low relative humidity of 10-60% is possible over the entire temperature range. However, a higher relative humidity of up to 95% is only feasible with moderate temperatures around 25°C. From this optimum, the maximum possible relative humidity continuously decreases to 60% towards the minimum and maximum temperature limits (Fig. 3-3). For high temperatures, this can be explained by increasing gradients to the ambient laboratory temperature. The higher the gradient, the lower the relative humidity, which leads to condensation, i.e. reaching of the dew point, at the inner walls.

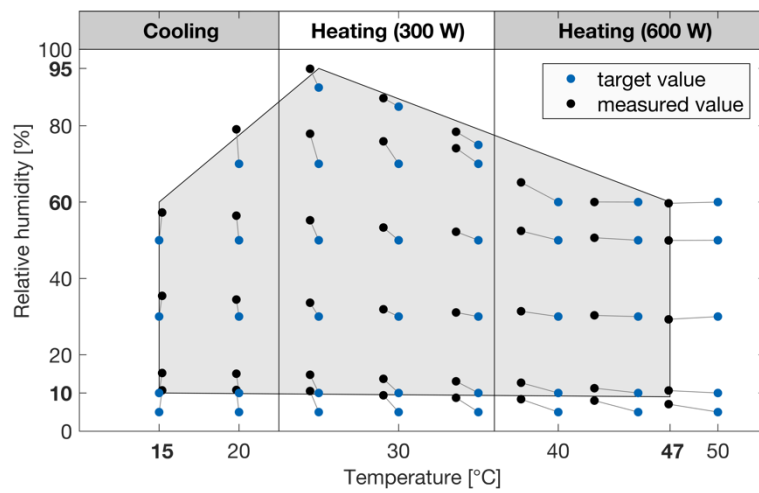


Fig. 3-3. Temperature and relative humidity ranges that can be simulated with the environmental chamber (grey box).

In addition, we performed a second series of tests to analyse the homogeneity of the temperature distribution within the chamber for the target temperatures of 25, 30, 35, 40, 45, and 50°C. To analyse the vertical temperature distribution, we installed eight temperature sensors in two arrays below the infrared lamps at different levels. It is not surprising that the upper sensors, which were closest to the lamps, showed the highest temperatures, while the lowest sensors showed the lowest temperatures. Here, the largest difference (4.3°C) was recorded for the target temperature of 50°C (Supplementary information 2, Fig. S2-2.2). We then repeated the test with the same target temperatures, but positioned 21 sensors aligned on a horizontal plane 80 cm above the bottom of the chamber to map out the lateral homogeneity. In general, the recorded temperatures differ less with this sensor arrangement. Again, the largest difference (1.7°C) was recorded for the highest temperature setting of 50°C (Supplementary information 2, Supplemental Fig. S2-2.4). A more detailed description of this test can be found in the Supplementary information 2.

We also point out to the reader that there might be a difference between air temperature and sample temperature (caused by the infrared radiation emitted by the heating system), which implies that researchers would have to decide where to place the sensors of the thermostat and hygrometer. Using the example of a soil column experiment, one has to consider which temperature is relevant: air or soil temperature. Accordingly, one has to place the sensor in the air or on the soil surface. For a simple test case, we observed a surface of a soil column (fine quartz sand, 10 cm diameter, 20 cm height) about 1°C warmer than the air temperature (shielded sensor, 40°C).

3.5 Concluding remarks

The presented environmental chamber has proven to be a reliable and affordable tool to mimic warm arid conditions. All necessary parts are consumer products and readily available off-the-shelf. Moreover, the set-up does not require microcontroller coding or difficult wiring, enabling replication with reasonable effort.

Nevertheless, the test of the chamber also revealed some limitations. The simulation of temperatures below ambient laboratory temperature requires a hardware modification, i.e., Peltier elements have to be used for cooling instead of compressed air. In our case, this enables only a minor temperature decrease of 6-7°C below ambient temperature. Moreover, higher relative humidities are only possible for moderate temperatures. For example, 80% are only possible in the range of 20-35°C. In most of the tested cases, the target settings are relatively quickly reached, which allows to simulate diurnal cycles. However, a strong decrease of relative humidity from its temperature-dependent maximum down to the minimum takes several hours. For some applications (e.g., short-term humidity fluctuation during the simulation of diurnal cycles), these long equilibrium times might be not acceptable. In those cases, the total possible humidity range cannot be used, i.e., one must stay below the upper humidity limit to prevent condensation at the inner chamber walls. A further limitation is the slightly

inhomogeneous temperature distribution, which is due to the small number of lamps, acting as a point heat source.

Given these limitations, commercial environmental chambers may still be the better choice for some applications. For example, various commercial chambers can simulate temperatures that exceed our 50 °C limit while maintaining relative humidity of up to almost 100%. However, many of these are unable to simulate low temperatures (< 30°C) and low relative humidities (< 20%; Appendix 2, Supplemental Fig. S2-3.1). Others cover a wide temperature and humidity range, but may not provide sufficient space for the planned experiment (Supplementary information 2, Supplemental Table S2-3.1). Eventually, the right choice depends on individual and demand-specific needs. To check whether our DIY chamber is suitable for one's purpose or which commercial chamber would be an alternative, we provide a comparison of selected environmental chambers in the Supplementary information 2.

In view of the simulation of warm arid conditions, the presented environmental chamber shows a very satisfying performance. Moreover, its design leaves margin for demand-specific adaptations, e.g., in terms of (i) chamber size, (ii) number, distribution and power of cooling/heating units, or (iii) improved insulation. Such an improved insulation could potentially remedy some limitations and enhance cooling capabilities or increase relative humidity limits for higher temperatures, if necessary.

3.6 Acknowledgments

The first author acknowledges the support from the German Academic Exchange Service (DAAD) programme "Sustainable Water Management (NaWaM) Study Scholarships and Research Grants 2015" (57156376) funded by the German Federal Ministry of Education and Research (BMBF).

3.7 Supplementary data

Supplementary data to this article can be found online at <https://access.onlinelibrary.wiley.com/doi/10.1002/vzj2.20023> and in Appendix 2. The Supplemental Material comprises (i) a bill of materials and a construction manual, (ii) results of temperature homogeneity mapping experiments, and (iii) a comparison with commercial environmental chambers.

3.8 References

Bernard, M.J., S.L. Pitz, C.-H. Chang, and K. Szlavecz. 2015. Continuous ¹³C and ¹⁵N Labeling of Tree Litter using a Climate-Controlled Chamber. *Commun. Soil Sci. Plant Anal.* 46(21): 2721–2733. <https://doi.org/10.1080/00103624.2015.1089273>.

CampbellScientific. 2016. User Guide: CS215 Temperature and Relative Humidity Probe. <https://www.campbellsci.eu>.

ESPEC CORP. 2019a. Platinous J Series Brings New Value to the World of Test Equipment.

ESPEC CORP. 2019b. Bench-Top Type Temperature and Humidity Chamber.

Goudie, A.S., and A.G. Parker. 1998. Experimental simulation of rapid rock block disintegration by sodium chloride in a foggy coastal desert. *J. Arid Environ.* 40(4): 347–355. <https://doi.org/10.1006/jare.1998.0465>.

Grant, K.N., M.L. Macrae, F. Rezanezhad, and W.V. Lam. 2019. Nutrient Leaching in Soil Affected by Fertilizer Application and Frozen Ground. *Vadose Zo. J.* 18:180150. <https://doi.org/10.2136/vzj2018.08.0150>.

Greenspan, S.E., W. Morris, R. Warburton, L. Edwards, R. Duffy, et al. 2016. Low-cost fluctuating-temperature chamber for experimental ecology. *Methods Ecol. Evol.* 7(12): 1567–1574. <https://doi.org/10.1111/2041-210X.12619>.

Hannusch, D. 1995. A simple and inexpensive control of relative humidity in a flow-through environmental chamber. *Environ. Exp. Bot.* 35(3): 411–415. [https://doi.org/10.1016/0098-8472\(95\)00002-5](https://doi.org/10.1016/0098-8472(95)00002-5).

Huang, M., P.G. Bruch, and S.L. Barbour. 2013. Evaporation and Water Redistribution in Layered Unsaturated Soil Profiles. *Vadose Zo. J.* 12:120108. <https://doi.org/10.2136/vzj2012.0108>.

Jiménez-Pinilla, P., S.H. Doerr, S. Ahn, E. Lozano, J. Mataix-Solera, et al. 2016. Effects of relative humidity on the water repellency of fire-affected soils. *Catena* 138: 68–76. <https://doi.org/10.1016/j.catena.2015.11.012>.

Katagiri, F., D. Canelon-Suarez, K. Griffin, J. Petersen, R.K. Meyer, et al. 2015. Design and Construction of an Inexpensive Homemade Plant Growth Chamber. *PLoS One* 10(5): e0126826. <https://doi.org/10.1371/journal.pone.0126826>.

Memmert GmbH. 2019. Climate chambers. Schwabach.

Merz, S., B.J. Balcom, R. Enjilela, J. Vanderborght, Y. Rothfuss, et al. 2018. 1H-Magnetic Resonance Monitoring and Numerical Modeling of Soil Moisture during Evaporation. *Vadose Zo. J.* 17:160099. <https://doi.org/10.2136/vzj2016.10.0099>.

Michelsen, N., R. van Geldern, Y. Roßmann, I. Bauer, S. Schulz, et al. 2018. Comparison of precipitation collectors used in isotope hydrology. *Chem. Geol.* 488: 171–179. <https://doi.org/10.1016/j.chemgeo.2018.04.032>.

Papapostolou, V., H. Zhang, B.J. Feenstra, and A. Polidori. 2017. Development of an environmental chamber for evaluating the performance of low-cost air quality sensors under controlled conditions. *Atmos. Environ.* 171: 82–90. <https://doi.org/10.1016/j.atmosenv.2017.10.003>.

Prechsl, U.E., A.K. Gilgen, A. Kahmen, and N. Buchmann. 2014. Reliability and quality of water isotope data collected with a low-budget rain collector. *Rapid Commun. Mass Spectrom.* 28(8): 879–885. <https://doi.org/10.1002/rcm.6852>.

Qazi, M.J., D. Bonn, and N. Shahidzadeh. 2018. Drying of Salt Solutions from Porous Media: Effect of Surfactants. *Transp. Porous Media.* <https://doi.org/10.1007/s11242-018-1164-5>.

Russells. 2019. Russells G - 64 Specifications. Michigan.

Schulz, S., M. Horowitz, R. Rausch, N. Michelsen, U. Mallast, et al. 2015. Groundwater evaporation from salt pans: Examples from the eastern Arabian Peninsula. *J. Hydrol.* 531: 792–801. <https://doi.org/10.1016/j.jhydrol.2015.10.048>.

Shokri-Kuehni, S.M.S., M. Norouzi Rad, C. Webb, and N. Shokri. 2017. Impact of type of salt and ambient conditions on saline water evaporation from porous media. *Adv. Water Resour.* 105: 154–161. <https://doi.org/10.1016/j.advwatres.2017.05.004>.

Song, W.-K., Y.-J. Cui, A.M. Tang, W.-Q. Ding, and T.D. Tran. 2014. Experimental study on water evaporation from sand using environmental chamber. *Can. Geotech. J.* 51(2): 115–128. <https://doi.org/10.1139/cgj-2013-0155>.

Windhorst, D., T. Waltz, E. Timbe, H.-G. Frede, and L. Breuer. 2013. Impact of elevation and weather patterns on the isotopic composition of precipitation in a tropical montane rainforest. *Hydrol. Earth Syst. Sci.* 17(1): 409–419. <https://doi.org/10.5194/hess-17-409-2013>.

4 Evaporation from the dried-up lake bed of Lake Urmia, Iran

Sahand Darehshouri ^{a,*}, Nils Michelsen ^a, Christoph Schüth ^a, Massoud Tajrishy ^b, Stephan Schulz ^a

^a Technische Universität Darmstadt, Institute of Applied Geosciences, Schnittspahnstr.9, 64287 Darmstadt, Germany

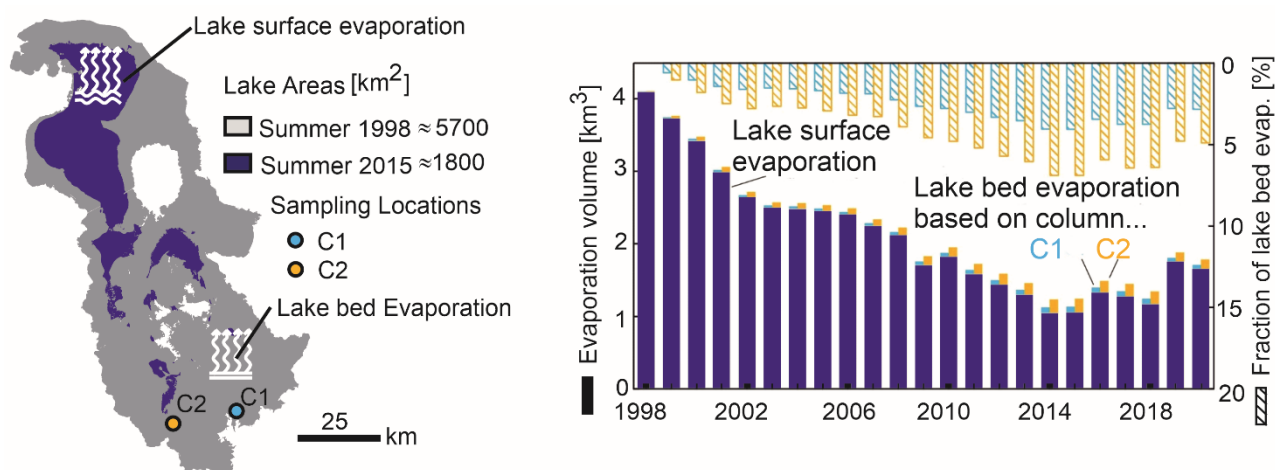
^b Sharif University of Technology, Department of Civil Engineering, Azadi Ave, 11365-11155 Tehran, Iran

* Corresponding author: Sahand Darehshouri, sahand64@yahoo.com

Published in Science of The Total Environment, 2022, Vol. 858, Article number: 159960 (2023),

<https://doi.org/10.1016/j.scitotenv.2022.159960>

Graphical abstract



4.1 Abstract

Lake Urmia in north-western Iran was once one of the world's largest hyper-saline lakes and represented a unique ecosystem for a number of endangered species. The lake's shrinking over the past decades has attracted considerable attention and several studies have addressed its water balance. Yet, evaporation of shallow groundwater from the dried-up lake bed has not been fully quantified – despite the appreciable size of these areas (approx. 4000 km² in summer 2015).

Here, we target this water cycle component by combining column experiments with upscaling and regionalisation techniques. In the experiments, we studied evaporation from two undisturbed soil cores from the exposed lake bed in a climate chamber, mimicking diurnal temperature and humidity variations in the three summer months of the study area. Despite the dropping water levels in the

columns and the formation of salt crusts, evaporation rates remained remarkably constant (0.12 and 0.20 mm d⁻¹). This suggests that the system is not driven by slow vapour diffusion, but controlled by capillary rise in the fine-grained sediments, ensuring steady water supply to the column surface. Thus, evaporation from the dried-up lake bed can be assumed to be largely independent from the unsaturated zone thickness (within the observed water level range) and evaporation rates can be simply upscaled and regionalised by considering the satellite-derived development of dried-up lake bed areas (1998–2020).

In this time-period, estimated summer evaporation from the exposed lake bed reached maximum values of 0.04 and 0.07 km³ (summer 2015). While these absolute numbers are significant (comparable to the catchment's annual urban drinking water consumption), they correspond to only 4 and 7 % of the evaporation from the open lake surface (1.06 km³).

4.2 Introduction

The Lake Urmia catchment is an endorheic basin in the northwest of the Iranian Plateau (Fig. 4-1). The hyper-saline Lake Urmia is considered as a “Wetland of International Importance” by the Ramsar Convention, and is listed in UNESCO's world network of biosphere reserves (UNESCO, 2019). The lake is vital for a wide range of biota, including various endangered migratory bird species (Asem et al., 2014). The most important aquatic lake species is the brine shrimp *Artemia Urmiana*, which serves as a food source for birds and hence plays a crucial role for the habitat (Agh et al., 2008).

In 1995, Lake Urmia had an area of about 5700 km² (Alesheikh et al., 2007) and a volume of approx. 33 km³ (Schulz et al., 2020; Sima and Tajrishy, 2013) and was one of the world's largest hyper-saline lakes. Since then its water level has been declining (Alipour, 2006; Abbaspour and Nazaridoust, 2007; Eimanifar and Mohebbi, 2007) and until 2015 the lake had lost about 90 % of its volume and 60 % of its area (Schulz et al., 2020). A system dynamics model of the Lake Urmia catchment by Hassanzadeh et al. (2012) and similarly a land transformation model by Rahimi and Breuste (2021) showed that the increase in anthropogenic activities, i.e., the increase in agricultural land, over extraction of surface water resources, and the construction of dams, has accelerated the decline in lake volume. Another recent study by Schulz et al. (2020) quantified the overall water balance components of Lake Urmia (precipitation, inflow, evaporation, and change in storage) and analysed their temporal evolution over the last five decades. They concluded that, in addition to anthropogenic activities, the lake's decline is also highly affected by climatic changes.

In addition to the loss of habitat area, the decrease in lake volume led to an increase in salinity from 160 g l⁻¹ in 1995 to about 340 g l⁻¹ in 2008 (Ahmadi et al., 2007; Karbassi et al., 2010). This increase has drastically affected the ecology of Lake Urmia. It has, for instance, led to a decline of the reproductive rate of *Artemia Urmiana*, which only tolerates a certain salinity range (Agh et al., 2008), and this, in turn, has caused a decline in the number of migratory birds in the area (Sima et al., 2021). Lake Urmia is an endorheic lake and thus evaporation from the open lake surface constitutes the

main natural water loss term of its water balance. Evaporation from the large dried-up area around the lake is typically not considered to be relevant in the lake water budget (Ahmadzadeh Kokya and Ahmadzadeh Kokya, 2008; Bhattacharjee et al., 2021; Hassanzadeh et al., 2012; Schulz et al., 2020). However, considering the size of the dried-up areas, evaporation from these surfaces may play a non-negligible role for the catchment water balance.

There are several studies on evaporation of shallow groundwater in arid areas, harnessing a broad range of methods, including tracer analyses (chloride, isotopes; Allison and Barnes, 1985), monitoring of water table fluctuations (Patterson and Kinsman, 1981), or deployment of microlysimeters (Tyler et al., 1997) or portable chambers for evaporation measurements (e.g., Johnson et al., 2010; Reicosky and Peters, 1977). From such studies, two general findings can be derived: (i) evaporation rates decrease with increasing depth to the (ground)water (e.g., Allison and Barnes, 1985; Johnson et al., 2010), and (ii) evaporation rates from salt-covered surfaces are lower than those from bare dried-up lake bed surfaces (Allison and Barnes, 1985; Tyler et al., 1997; Ullman, 1985). Consequently, reported evaporation rates range from 88 to 104 of mm a^{-1} (Tyler et al., 1997; Ullman, 1985) to about 250 mm a^{-1} or, on a daily basis, to up to 1.6 mm d^{-1} (Allison and Barnes, 1985), depending on the study area setting.

The high variability in measured evaporation rates indicates the influence of site-specific conditions on results, like variations in temperature, depth to groundwater, precipitation, or temporary surface water flooding (Tyler et al., 1997). In addition, chloride profiles have been shown to be highly sensitive to thermal and density-driven fluxes near the surface and hence their analysis appears to underestimate annual groundwater evaporation (Allison and Barnes, 1985). This limits transferability of results to other areas and hampers estimation of average values over longer time periods.

An alternative promising approach is to estimate evaporation in the laboratory, using climate chambers and weighable columns containing undisturbed soil cores from a target area (Schulz et al., 2015). Columns should represent typical conditions in the respective region so that results can be transferred to larger areas. Therefore, in this study two undisturbed soil columns from the large dried-up area of Lake Urmia were taken in the flat, uniformly salt-covered southern part of the former lake bed. These columns were placed in a climate chamber, which mimicked diurnal temperature and relative humidity cycles of the three summer months in the study area. Results are used to estimate the contribution of evaporation from such dried-up areas to the overall evaporation from the lake area.

4.3 Study area

The Lake Urmia catchment covers an area of about 52,000 km^2 on the Iranian Plateau in the northwest of Iran (Fig. 4-1). It is bound by mountain ridges in the east, south, and west, with heights well above 3000 m a.s.l. The lake itself lies in the flatter north-western part of the catchment, on an

elevation of about 1270 m a.s.l.. In recent decades, the lake surface area peaked at about 5700 km² in the mid-1990s (Alesheikh et al., 2007). On the contrary, in 2014 and 2015 the lake area reached a minimum of less than 1800 km² with a dried-up area of about 4000 km² (Fig. 4-1a). These variations are most likely due to a combination of a long-lasting meteorological drought and agricultural water demand, limiting surface water inflow into the lake (Schulz et al., 2020). Mean annual precipitation in the Lake Urmia Basin is 401mm and more than 90 % of the annual precipitation occurs between October and May (JICA, 2016; WRMC, 2021). Together with the elevation of the basin, this results in a relatively cold and humid rainy season with a mean temperature of 7.6 °C. In the dry and warmer summer season between June and September, the mean summer temperature is about 20.7 °C. This pronounced seasonality indicates that substantial evaporative losses from the catchment, and therefore also from the dried-up lake area, mainly occur during the summer season.

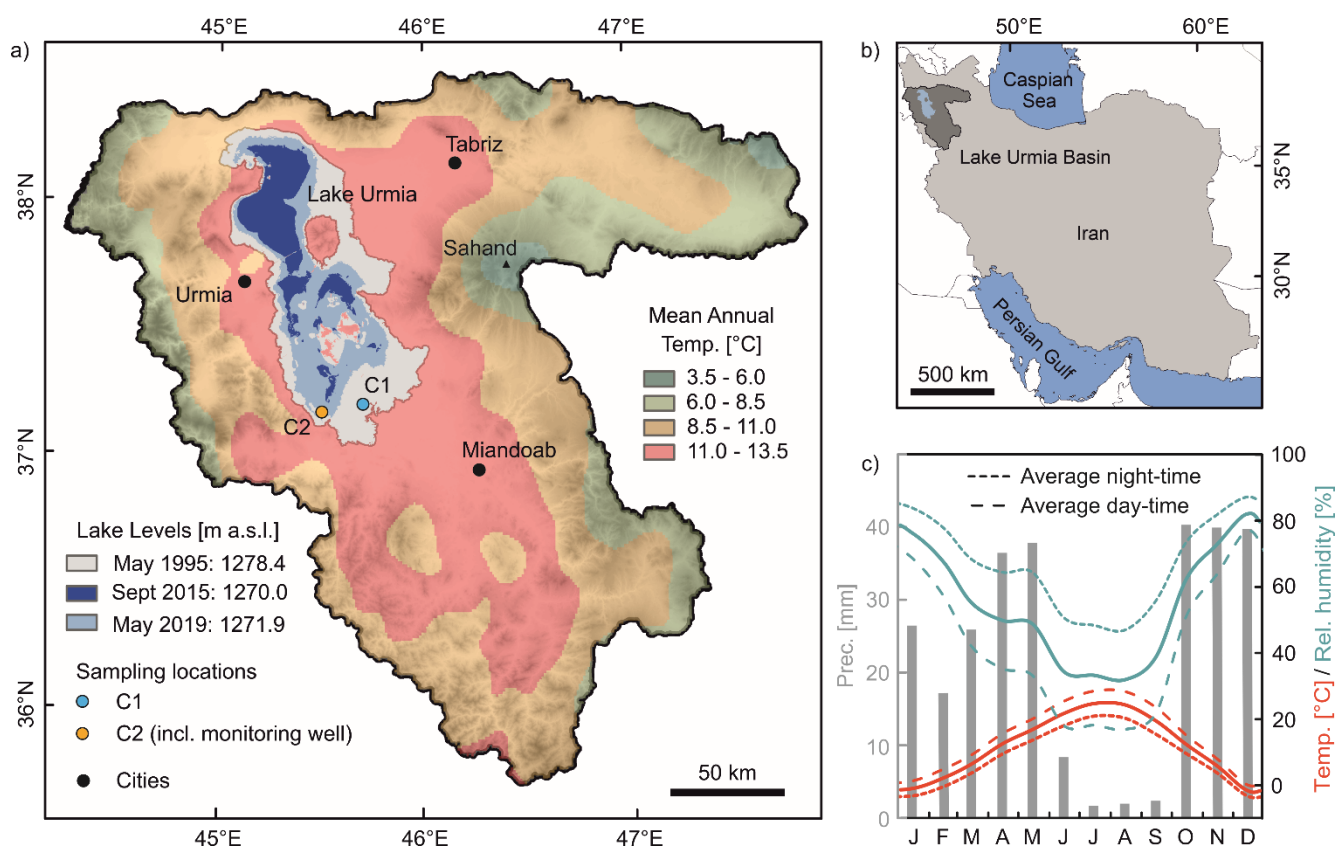


Fig. 4-1. a) Overview of the study area, with location of monitoring well and sampling sites, and distribution of annual average temperature (Data source: WRMC, 2021). Moreover, selected lake extents are shown, at initial (May 1995), lowest (Sept 2015), and recent (May 2019) lake levels between 1995 and 2020 (Data source: ULRP, 2021). b) Regional geographic overview. c) Climatic data for Urmia, incl. Mean temperature and relative humidity data and monthly precipitation sums (2012–2017; Data source: WRMC, 2021).

Lake Urmia is hyper-saline with higher salinities in the northern part of the lake than in the southern part (Zeinoddini et al., 2014). The average salinity ranges from 160 g l⁻¹ to 340 g l⁻¹ (Ahmadi et al., 2007; Karbassi et al., 2010). The prevailing cations are Na⁺, Mg²⁺, Ca²⁺, and K⁺ and the main anions are Cl⁻, SO₄²⁻, and HCO₃⁻ (Alipour, 2006; Supplementary material 3, Table S3-1.). As streams transport fine-grained materials into the lake, the upper ten meters of the lake bed (apart from the lake's estuary areas) are silty and/or clayey, especially in the southern and central part of the lake (Amiri et al., 2016). In the dried-up areas, the upper part of these fine-grained sediments also contain precipitated salt, partly forming a solid salt crust at the top with a very low hydraulic conductivity (Sheibani et al., 2020).

4.4 Materials and methods

4.4.1 Water level monitoring and soil core sampling

In a field campaign in October 2016, at the beginning of the rainy season, a 2 m deep observation well was installed for groundwater level monitoring. The well was located in the south-western part of the dried-up lake area, in some accessible distance to the lake shore (37.114°N, 45.458°E; Fig. 4-1a). Due to the lack of a topographic reference point for our monitoring well, the elevation of the well head was determined by classifying a series of Landsat satellite images using the Normalized Difference Water Index (NDWI) method (McFeeters, 1996) to identify the image with the closest shoreline to our monitoring well. The result of this analysis was a Landsat-5 image with the acquisition date 2006-10-02. On that day, the lake level was at 1272.80 m a.s.l. (ULRP, 2021; Supplementary material 3, Fig. S3-1).

The monitoring well was equipped with a pressure transducer with automatic compensation of barometric pressure changes (DCX-22AA, KELLER Druckmesstechnik AG) to measure the piezometric head. The recorded data were collected a year later and converted to water levels, considering the density of the water. In addition, a groundwater sample was obtained from the well and analysed for its major ion composition (Supplementary material 3, Table S3-1).

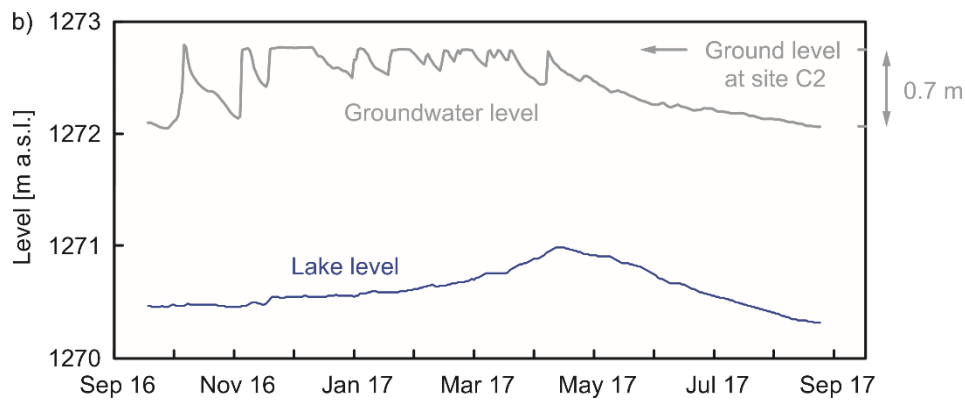


Fig. 4-2. Groundwater levels (daily mean) in the monitoring well during the 2016 rainy season and the 2017 dry season. For comparison, also the Lake Urmia water level is shown.

The operating time of the monitoring well was chosen to observe the water table fluctuations over a full rainy and dry season (Fig. 4-2). The gathered data show groundwater levels at or close to the surface in the rainy season (until April 2017). In the following dry season, the level drops due to evaporation and finally reaches about 70 cm below the surface. This indicates the approximate range of unsaturated zone thicknesses that has to be related to evaporation rates. Next to the monitoring well, an undisturbed soil core was taken (C1–37.128°N, 45.760°E). A second soil core was collected in the dried-up lake area about 15 km to the east (C2–37.114°N, 45.458°E). The sites were located in large and quite uniform dried-up areas to represent typical conditions. For sampling, a custom-made soil corer (Schulz et al., 2015) was utilized. The device consists of a sharp-edged steel pipe containing a thick-walled (1 cm) PVC liner. The latter is 50 cm long and has an inner diameter of 16 cm. To acquire a quasi-undisturbed sample, the corer is hammered into the ground and then excavated (Supplementary material 3, Fig. S3-2). The soil cores were sealed and transported to the laboratory for the column experiment. The collected sediment mainly consisted of clayey silt (C1) and fine sandy, clayey silt (C2), as indicated by grain size analyses (Supplementary material 3, Fig. S3-3).

4.4.2 Column experiment

The experiment in a climate chamber intended to measure (water level dependent) evaporation rates from the columns by simulating the mean diurnal temperature and humidity fluctuations during the dry summer season from June to September at Lake Urmia (Fig. 4-1c). In this season the mean day-time temperature is 27.3 °C, with a mean relative humidity of 18 %. At night-time, the mean temperature is 19.6 °C and the mean relative humidity accounts for 48 % (WRMC, 2021; Fig. 4-1c). To simulate these conditions, a modified climate chamber (Darehshouri et al., 2020) was used. While the climate chamber can simulate environmental conditions such as temperature and humidity, it does not

simulate wind. Wind affects evaporation. In the case of bare soil evaporation, however, this is mainly due to the fact that moist air layers are removed from the soil surface (Davarzani et al., 2014). In our experiment, this removal is guaranteed by a tube fan driven circulation system (Fig. 4-3) and temperature-induced convection ensuring slow continuous circulation in the chamber.

Initially, the columns were gradually saturated from bottom to top with saline water with a chemical composition similar to that of the groundwater from our monitoring well (Supplementary material 3, Table S3-1). The saturated columns were then exposed to the diurnal temperature and humidity cycles (Fig. 4-3).

A vented pressure transducer (Dipper-PT, SEBA Hydrometrie) was mounted to the bottom of each column, separated from the sediments in the columns by stainless-steel mesh and a layer of glass beads. The pressure heads were recorded at 2 min intervals and later converted to saturated water level (considering water density).

Evaporation-induced mass changes were gravimetrically measured by placing the columns on two scales (GAB 30 K0.2N, KERN). To avoid signal drift due to the permanent dynamic loading, the columns were not permanently placed on the scales. Instead, an automated lifting gear system was programmed to lower the columns onto the scales at 1-h intervals for a 5-min period. Data from the scales were recorded using the Data Acquisition Systems Laboratory software (DASYLab 10). The obtained evaporation induced mass losses were later converted to evaporation rates, considering the cross-sectional area of the columns.

The column experiment was conducted for 37 days. After this time period, the water levels had reached the bottom of the columns. The corresponding water level drop of about 50 cm hence covers a large part of the fluctuation range observed in the field over a one-year period (approx. 70 cm; see Section 3.1).

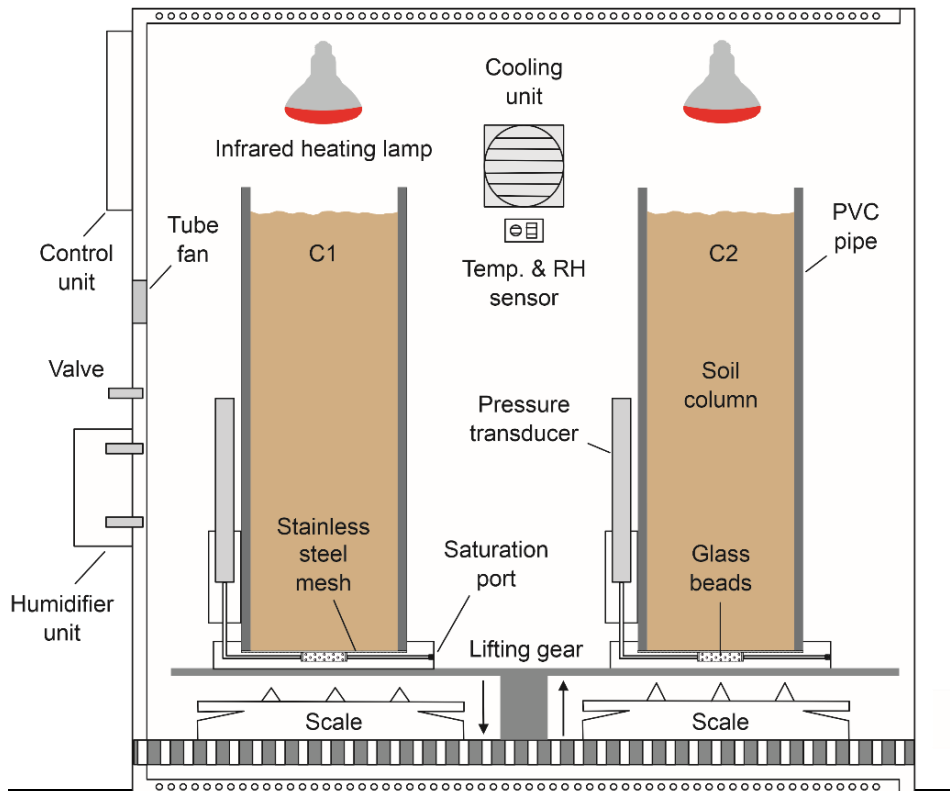


Fig. 4-3. Climate chamber and column experiment setup.

4.4.3 Upscaling and regionalization of evaporation data

To determine the total amount of water evaporating from the dried-up lake bed, the lab-derived evaporation rates (Section 3.2) were multiplied with the dried-up lake areas. These areas were estimated based on the latest available bathymetry (Schröder et al., 2022; ULRP, 2017) and lake water level data (ULRP, 2021). To assess the relevance of this evaporation amount, we also examined how much water evaporates from the lake surface. To calculate evaporation from the open lake surface, we followed the approach of Schulz et al. (2020), which we present in Supplementary Information 3.

4.5 Results and Interpretation

4.5.1 Column experiment

The results of the evaporation experiment are summarized in Fig. 4-4. The temperatures and relative humidities recorded in the climate chamber during the evaporation experiment are shown in Fig. 4-4a. These conditions have caused significant water level drops (Fig. 4-4b) and mass losses (Fig. 4-4c). The pressure transducer-derived water level records exhibit slightly irregular and partly differing curve shapes, but show somewhat similar values towards the end of the experiment (Fig. 4-4b; roughly 40

cm drop within one month, comparable to the initial decline rate observed in the field in April/May 2017, Fig. 4-2). The cumulative mass loss developments are rather linear over the bulk of the experiment (smoothed lines in Fig. 4-4c). The final cumulative losses amount to approx. 90 g (C1) and 150 g (C2) and the corresponding rates are 2.4 g d^{-1} and 4.1 g d^{-1} , respectively.

It is also noteworthy that the hourly water level and mass loss data (dashed lines in Fig. 4-4b and c) show pronounced diurnal fluctuations. In principle, temperature changes could influence capillary rise and hence water levels (mainly due to changed water viscosity), and the column mass may be affected by recondensation during cooling. Yet, the possibility of artefacts has to be considered as well, particularly in view of reported issues with temperature compensation of pressure transducers (Rau et al., 2019, Cain et al., 2004, Sorensen and Butcher, 2011). Hence, we conducted a short (8 d) dedicated experiment with sealed, i.e., evaporation-protected, columns exposed to similar climatic fluctuations (Supplementary material 3). The encountered daily fluctuations of about 4 cm and 5 g indeed suggest that the observed short-term fluctuations largely represent artefacts. We hence focus on the smoothed data (moving 12 h median filters) and the overall trends.

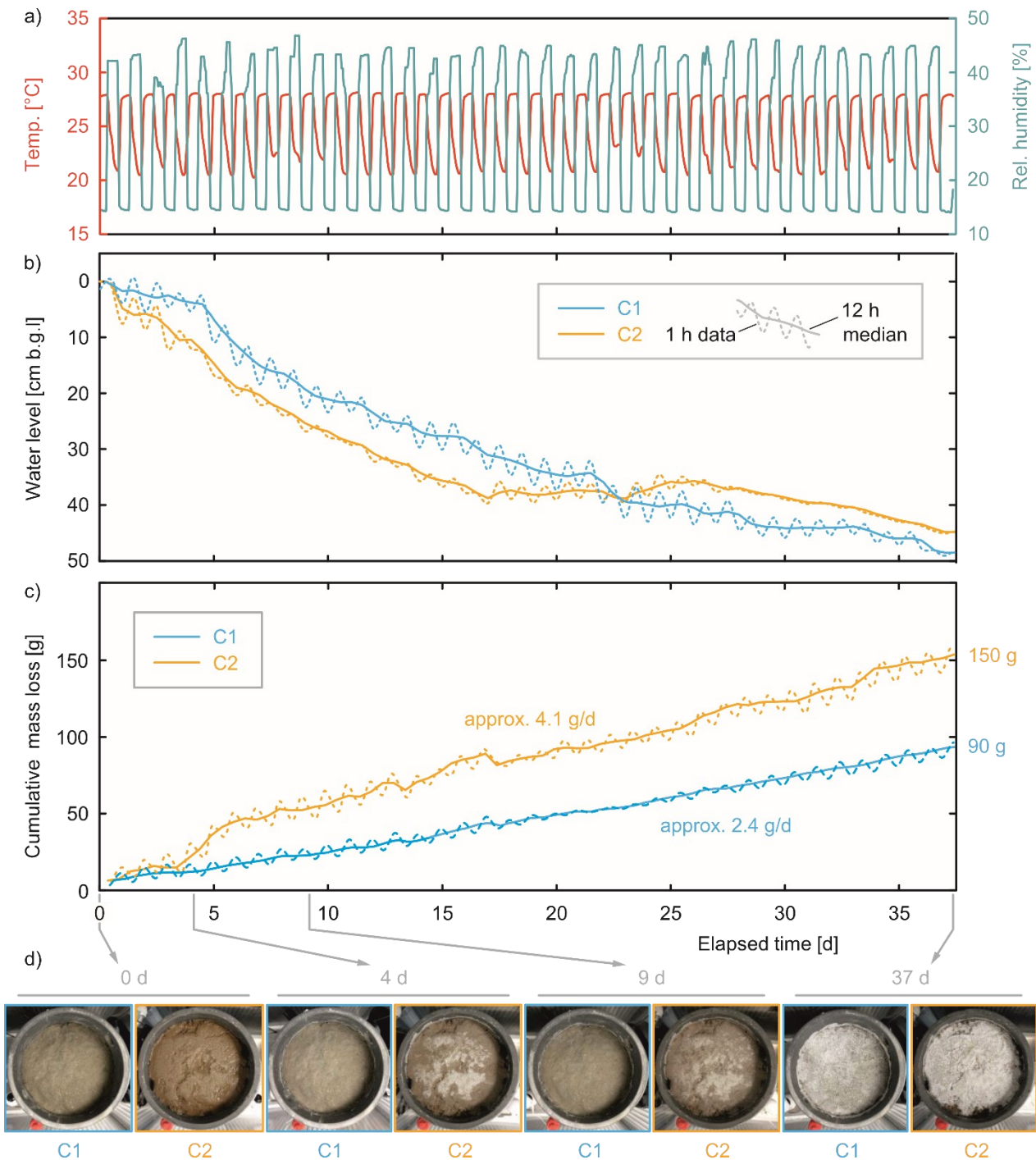


Fig. 4-4. a) Temperature and relative humidity in the climate chamber. b) Water level development in the two columns C1 and C2. c) Cumulative mass loss (12 h median). d) Photo documentation of column tops (after 0, 4, 9, and 37 d) showing increasing salt precipitation on the soil surfaces.

Although the water level curves are irregular (possibly due to smallscale stratigraphic heterogeneities in grain size), the evaporative mass losses from C1 and C2 are largely constant. This means that the evaporation rates did not decrease with increasing thickness of the unsaturated zone, as one may

expect. Hence, the evaporative system does not seem to be driven by vapour diffusion, but is apparently controlled by capillary action, which ensures sufficient water supply to the surface. This dominant role of capillary rise is in line with the fine-grained nature of the sediments (see Section 3.1).

It is also noted that the evaporation was accompanied by increasing precipitation of salt on the column surfaces, indicated by the progressing white colour coverage (Fig. 4-4d). However, this process does not appear to be an evaporation-limiting factor either. Under the given conditions – very shallow groundwater and thin salt crusts – the evaporative mass losses from columns C1 and C2 of 2.4 and 4.1 g d⁻¹ (i.e., 0.12 and 0.20 mm d⁻¹) may hence be used for upscaling, i.e., to estimate evaporation from the dried-up lake bed during the three summer months June, July, and August.

4.5.2 Implications for water balance calculations

The constant evaporation rates observed in our columns, independent from the unsaturated zone thickness, allow for a straight forward regionalisation of our results, although the water level drop was limited to the column length, i.e., 50 cm, compared to the maximum unsaturated zone thickness of 70 cm, measured in our monitoring well (Fig. 4-2). However, we assume a similar evaporation rate for the entire dried-up area as in our column experiments, as the location of the monitoring well in the south was far away from the present open lake surface. Approaching the lake would be associated with a thinner unsaturated zone, due to the flat lake bed with a gentle slope to its centre part.

For calculating the temporal evolution of the overall evaporation from the dried-up lake bed in comparison to evaporation from the open lake surface, the change of the respective areas over time has to be considered. Due to the shallow water depth of the lake (maximum depth of 10 m; Schulz et al., 2020) and the flat morphology with an extremely gentle lake bed gradient, especially in the southern part of the lake bed (Sima et al., 2021), each metre of lake water level change results on average in opposed changes of about 580 km² in the dried-up lake bed area (Fig. 4-5) and the open lake surface (Supplementary material 3, Fig. S3-4), respectively.

Based on data on the lake levels between 1998 and 2020, the lake level was at a maximum of 1277.6 m a.s.l. in 1998, and at a minimum of 1270.1 m a.s.l. in the summers of 2014 and 2015 (Fig. 4-5; ULRP, 2021). This resulted in a maximum lake surface area of 5150 km² in summer 1998 that decreased to only 1800 km² in the summer seasons of 2014 and 2015. During the same time, the dried-up lake bed area increased to about 4000 km² in the summer seasons of 2014 and 2015. On average, the decline in lake levels between 1998 and 2015 led to the formation of 260 km² a⁻¹ of dried-up lake bed (Fig. 4-5). Between 2016 and 2020, the lake surface area increased by a similar area per year.

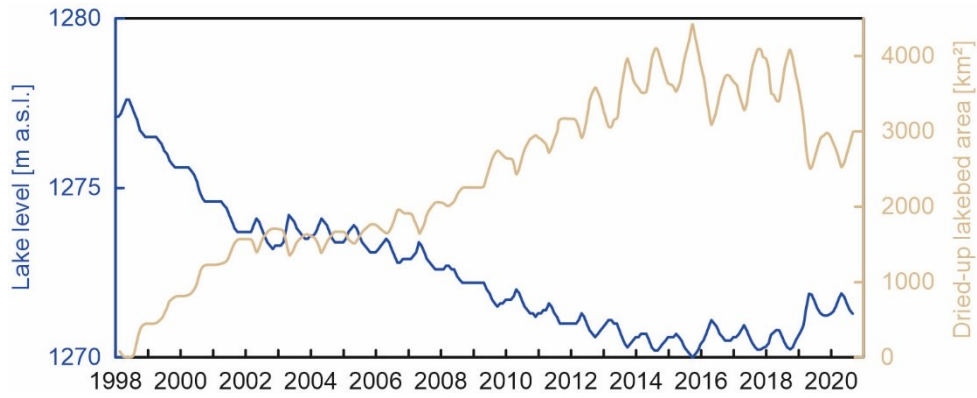


Fig. 4-5. Lake Urmia level compared to dried lake bed area (monthly mean) from 1998 to 2020.

With the evaporation rates measured in the two columns, and the calculated dried-up lake bed areas for the period 1998–2020, the evaporation from the dried-up lake bed area in the three summer months of this period can be estimated. It can be then compared to the corresponding evaporation from the open lake surface, as calculated by Schulz et al. (2020), based on climatic data and considering the salinity of the lake water (Fig. 4-6).

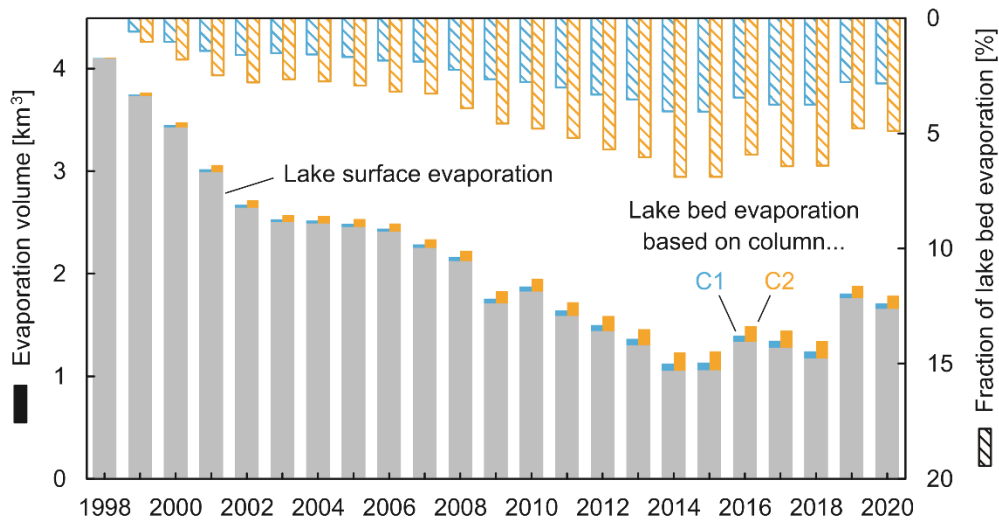


Fig. 4-6. Evaporation from the dried-up lake bed area (blue, orange) and open lake surface (grey) for the three summer months in the period 1998–2020. For better overview, also corresponding fractions are displayed (hatched areas; right axis).

Evaporation from the dried-up lake bed area reached maximum values of 0.04 km³ and 0.07 km³ in the summer months of 2015, based on the results of the two columns. Compared to 1.06 km³

evaporation from the open lake surface in this year's summer months, these volumes make up about 4 % and 7 % of the open lake surface evaporation.

Schulz et al. (2020) also calculated yearly evaporation from the open lake surface (Supplementary material 3, Fig. S3-6). Depending on the year, the three summer months roughly account for 40 % to 50 % of the yearly open lake surface evaporation. It is uncertain whether this ratio also holds for the dried-up lake area, but it can be assumed that it is not significantly different.

4.6 Conclusion

Our results show that the relation between evaporation from the dried-up lake bed area and the open lake surface is highly dependent on the water level of the lake, as the resulting areas are complementary. At the lowest water level in 2015, associated with an open lake surface area of 1800 km² and a dried-up lake bed area of about 4000 km², evaporation from the latter was, at the most, only about 7 % of the open lake surface evaporation (maximum value; often only 3–5 %). Overall, this seems to be a low number for the total water balance of the Lake Urmia basin. However, in absolute numbers for the year 2015 this exceeds the average annual urban drinking water consumption (0.064 km³ a⁻¹; JICA, 2016; WRMC, 2021) and is more than three times the average annual industrial water consumption (0.022 km³ a⁻¹; JICA, 2016; WRMC, 2021) in the entire Lake Urmia catchment.

It must be noted that our estimations are based on the results of column experiments with only two undisturbed soil cores from the dried-up lake bed area and that evaporation rates for these two columns differ by about 40 %. Whether these values represent rates at the upper and lower range of what can be expected for the whole area is uncertain. Nevertheless, our data provide a first indication of the (comparatively small) relevance of this component of the local hydrological cycle.

4.7 Authorship contribution statement

S.D. and S.S. designed the research; S.D. and M.T. gathered the data; S.D. performed the evaporation experiment; S.S., S.D., N.M., performed the data analysis; S.S., S.D., N.M., and C.S. wrote the paper. All authors reviewed the manuscript.

4.8 Data availability

All data used in this study are available for research purposes upon request from the corresponding author and the Urmia Lake Restoration Program (ULRP) office.

4.9 Acknowledgments

The first author gratefully acknowledges the support from the German Academic Exchange Service (DAAD) programme “Sustainable Water Management (NaWaM) Study Scholarships and Research Grants 2015” (57156376) funded by the German Federal Ministry of Education and Research (BMBF).

4.10 Supplementary data

All data used in this study is available from the corresponding author upon request.

Supplementary information is available for this paper in Appendix 4.

4.11 References

Song, W.-K., Y.-J. Cui, A.M. Tang, W.-Q. Ding, and T.D. Tran. 2014. Experimental study on water evaporation from sand using environmental chamber. *Can. Geotech. J.* 51(2): 115–128. <https://doi.org/10.1139/cgj-2013-0155>.

Windhorst, D., T. Waltz, E. Timbe, H.-G. Frede, and L. Breuer. 2013. Impact of elevation and weather patterns on the isotopic composition of precipitation in a tropical montane rainforest. *Hydrol. Earth Syst. Sci.* 17(1): 409–419. <https://doi.org/10.5194/hess-17-409-2013>.

Abbaspour, M., Nazaridoust, A., 2007. Determination of environmental water requirements of Lake Urmia, Iran: an ecological approach. *Int. J. Environ. Stud.* 64, 161–169. <https://doi.org/10.1080/00207230701238416>

Agh, N., Van Stappen, G., Bossier, P., Yari, A.M., Rahimian, H., Sorgeloos, P., 2008. Life cycle characteristics of six *Artemia* populations from Iran. *Pak. J. Biol. Sci.* 11, 854–861. <https://doi.org/10.3923/pjbs.2008.854.861>.

Ahmadi, R., Negarestan, H., Peikaranmana, N., Esmailly, L., Hosseinpour, R., Shoahasany, A., Ganji, S., Mehrannejad, R., Mostfazadeh, B., 2007. *Artemia* population changes on Orumieh Lake. Available at: Iran Ministry of Agriculture, Fisheries Science Research Institute. <https://aquadocs.org/handle/1834/12957>

Ahmadzadeh Kokya, B., Ahmadzadeh Kokya, T., 2008. Proposing a formula for evaporation measurement from salt water. *Hydrol. Process.* 22, 2005–2012. <https://doi.org/10.1002/hyp.6785>.

Alesheikh, A.A., Ghorbanali, A., Nouri, N., 2007. Coastline change detection using remote sensing. *Int. J. Environ. Sci. Technol.* 4 (1), 61–66. <https://doi.org/10.1007/BF03325962>.

Alipour, S., 2006. Hydrogeochemistry of seasonal variation of Urmia Salt Lake, Iran. *Saline Syst.* 2, 9. <https://doi.org/10.1186/1746-1448-2-9>. Allison, G.B., Barnes, C.J., 1985. Estimation of evaporation from the normally “dry” Lake Frome in South Australia. *J. Hydrol.* 78, 229–242. [https://doi.org/10.1016/0022-1694\(85\)90103-9](https://doi.org/10.1016/0022-1694(85)90103-9).

Amiri, V., Nakhaei, M., Lak, R., Kholghi, M., 2016. Geophysical, isotopic, and hydrogeochemical tools to identify potential impacts on coastal groundwater resources from Urmia hypersaline Lake, NW Iran. *Environ. Sci. Pollut. Res.* 23, 18952. <https://doi.org/10.1007/s11356-016->

[7380-z](#).

Asem, A., Eimanifar, A., Djamali, M., De los Rios, P., Wink, M., 2014. Biodiversity of the hypersaline Urmia lake national park (NW Iran). *Diversity* 6 (1), 102–132. <https://doi.org/10.3390/d6010102>.

Bhattacharjee, J., Rabbil, M., Fazel, N., Darabi, H., Choubin, B., Khan, M.M.R., Marttila, H., Haghghi, A.T., 2021. Accuracy assessment of remotely sensed data to analyze lake water balance in semi-arid region. *Sci. Total Environ.* 797, 149034. <https://doi.org/10.1016/j.scitotenv.2021.149034>.

Cain, S.F., Davis, G.A., Loheide, S.P., Butler, J.J., 2004. Noise in pressure transducer readings produced by variations in solar radiation. *Ground Water* 42, 939–944. <https://doi.org/10.1111/j.1745-6584.2004.t01-12-x>.

Darehshouri, S., Michelsen, N., Schüth, C., Schulz, S., 2020. A low-cost environmental chamber to simulate warm climatic conditions. *Vadose Zone J.* 19 (1), e20023. <https://doi.org/10.1002/vzj2.20023>.

Davarzani, H., Smits, K., Tolene, R.M., Illangasekare, T., 2014. Study of the effect of wind speed on evaporation from soil through integrated modeling of the atmospheric boundary layer and shallow subsurface. *Water Resour. Res.* 50, 661–680. <https://doi.org/10.1002/2013WR013952>.

Eimanifar, A., Mohebbi, F., 2007. Urmia Lake (Northwest Iran): a brief review. *Saline Syst.* 3,5. <https://doi.org/10.1186/1746-1448-3-5>.

Hassanzadeh, E., Zarghami, M., Hassanzadeh, Y., 2012. Determining the main factors in declining the Urmia Lake level by using system dynamics modeling. *Water Resources Managment.* 26, 129–145. <https://doi.org/10.1007/s11269-011-9909-8>.

JICA, 2016. Japan International Cooperation Agency, data collection survey on hydrological cycle of lake Urmia basin in the Islamic Republic of Iran final report hydrological cycle of lake. 268. Available at: http://open_jicareport.jica.go.jp/. (Accessed 5 January 2021).

Johnson, E., Yáñez, J., Ortiz, C., Muñoz, J., 2010. Evaporation from shallow groundwater in closed basins in the Chilean Altiplano. *Hydrol. Sci. J.* 55, 624–635. <https://doi.org/10.1080/02626661003780458>.

Karbassi, A., Bidhendi, G.N., Pejman, A., Bidhendi, M.E., 2010. Environmental impacts of desalination on the ecology of Lake Urmia. *J. Great Lakes Res.* 36, 419–424. <https://doi.org/10.1016/j.jglr.2010.06.004>.

McFeeters, S.K., 1996. The use of the normalized difference water index (NDWI) in the delineation of open water features. *Int. J. Remote Sens.* 17 (7), 1425–1432. <https://doi.org/10.1080/01431169608948714>.

Patterson, R.J., Kinsman, D.J.J., 1981. Hydrologic framework of a sabkha along Arabian Gulf. *Am. Assoc. Pet. Geol. Bull.* 65, 1457–1475. <https://doi.org/10.1306/03b5956c-16d1-11d7-8645000102c1865d>.

Rahimi, A., Breuste, J., 2021. Why is Lake Urmia drying up? Prognostic Modeling With Land-Use Data and Artificial Neural Network. 9, pp. 1–11. <https://doi.org/10.3389/fenvs.2021.603916>.

Rau, G.C., Post, V.E.A., Shanafield, M., Krekeler, T., Banks, E.W., Blum, P., 2019. Error in hydraulic head and gradient time-series measurements: a quantitative appraisal. *Hydrol. Earth Syst. Sci.* 23, 3603–3629. <https://doi.org/10.5194/hess-23-3603-2019>.

Reicosky, D.C., Peters, D.B., 1977. A portable chamber for rapid evapotranspiration measurements on field plots. *Agron. J.* 69 (4), 729–732. <https://doi.org/10.2134/agronj1977.00021962006900040051x>.

Schröder, T., Hassanzadeh, E., Darehshouri, S., Tajrishy, M., Schulz, S., 2022. Satellite based lake bed elevation model of Lake Urmia using time series of Landsat imagery. *J. Great Lakes Res.* <https://doi.org/10.1016/j.jglr.2022.08.016>

Schulz, S., Horovitz, M., Rausch, R., Michelsen, N., Mallast, U., Köhne, M., Siebert, C., Schüth, C., Al-Saud, M., Merz, R., 2015. Groundwater evaporation from salt pans: examples from the eastern Arabian Peninsula. *J. Hydrol.* 531, 792–801. <https://doi.org/10.1016/j.jhydrol.2015.10.048>.

Schulz, S., Darehshouri, S., Hassanzadeh, E., Tajrishy, M., Schüth, C., 2020. Climate change or irrigated agriculture – what drives the water level decline of Lake Urmia. *Sci. Rep.* 10, 236. <https://doi.org/10.1038/s41598-019-57150-y>.

Sheibani, S., Ataie-Ashtiani, B., Safaie, A., Simmons, C.T., 2020. Influence of lake bed sediment deposit on the interaction of hypersaline lake and groundwater: a simplified case of Lake Urmia, Iran. *J. Hydrol.* 588, 125110. <https://doi.org/10.1016/j.jhydrol.2020.125110>.

Sima, S., Tajrishy, M., 2013. Using satellite data to extract volume-area-elevation relationships for Urmia Lake, Iran. *J. Great Lakes Res.* 39, 90–99. <https://doi.org/10.1016/j.jglr.2012.12.013>.

Sima, S., Rosenberg, D.E., Wurtsbaugh, W.A., Null, S.E., Kettenring, K.M., 2021. Managing Lake Urmia, Iran for diverse restoration objectives: moving beyond a uniform target lake level. *J. Hydrol. Reg. Stud.* 35, 100812. <https://doi.org/10.1016/j.ejrh.2021.100812>.

Sorensen, J.P.R., Butcher, A.S., 2011. Water level monitoring pressure transducers—a need for industry-wide standards. *Groundw. Monit. Remediat.* 31, 56–62. <https://doi.org/10.1111/j.1745-6592.2011.01346.x>.

Tyler, S.W., Kranz, S., Parlange, M.B., Albertson, J., Katul, G.G., Cochran, G.F., Lyles, B.A., Holder, G., 1997. Estimation of groundwater evaporation and salt flux from Owens Lake, California, USA. *J. Hydrol.* 200 (1–4), 110–135. [https://doi.org/10.1016/S0022-1694\(97\)00007-3](https://doi.org/10.1016/S0022-1694(97)00007-3).

Ullman, W.J., 1985. Evaporation rate from a salt pan: estimates from chemical profiles in near-surface groundwaters. *J. Hydrol.* 79, 365–373. [https://doi.org/10.1016/0022-1694\(85\)90066-6](https://doi.org/10.1016/0022-1694(85)90066-6).

ULRP, 2017. Urmia Lake Restoration programme. Bathymetric data. Developed by Ministry of Energy's Water Research Institute in 2017, Data available upon request, more info: <https://www.ulrp.ir>.

ULRP, 2021. Urmia Lake Restoration programme. Daily Lake Urmia level data. Available at: https://www.ulrp.ir/fa/آرشیو_تراز_دریاچه_ارومیه/. (Accessed 26 November 2021).

UNESCO, 2019. Lake Oromeeh Biosphere Reserve, Islamic Republic of Iran. <https://en.unesco.org/biosphere/aspac/lake-oromeeh>. (Accessed 8 May 2022).

WRMC, 2021. Water Resources Management Company (WRMC) of Iran Ministry of Energy.

Zeinoddini, M., Tofghi, M.A., Bakhtiari, A., 2014. Assessment of 2DH and pseudo-3D modelling platforms in a large saline aquatic system: Lake Urmia, Iran. *Hydrol. Process.* 28, 4953–4970. <https://doi.org/10.1002/hyp.9923>.

Amiri, V., Nakhaei, M., Lak, R. & Kholghi, M. Investigating the salinization and freshening processes of coastal groundwater resources in Urmia aquifer, NW Iran. *Environ. Monit. Assess.* 188, 233 (2016).

5 Outlook

5.1 Climate Change and perspectives for lake development

Lake Urmia's future is influenced by the broader regional climate trends. West Central Asia (WCA), including the region where Lake Urmia is located, has already been experiencing various climate changes, such as an increase in the frequency of hot extremes, agricultural and ecological droughts, and heavy precipitation (Hu et al., 2016; Zhang et al., 2017; Sun et al., 2021). Comparing the global observed surface temperature record between 1850 and 2020 with the reconstructed temperatures for the past 2000 years using paleoclimate archives and Coupled Model Intercomparison Project (CMIP6), a remarkable warming trend of more than 2000 years is apparent (IPCC, 2021). The IPCC (2021) indicates that between 2010 and 2019, the global surface temperature was more than 1°C higher compared to the period between 1850 and 1900. The IPCC (2021) projections, based on five climate scenarios with different levels of CO₂ and greenhouse gas concentrations (Fig. 5-1), indicate that even if the most favourable scenario (SSP1-1.9) of achieving net-zero CO₂ emissions by 2050 and substantially reducing greenhouse gas emissions is reached, global surface temperatures will continue to rise until at least the middle of the century.

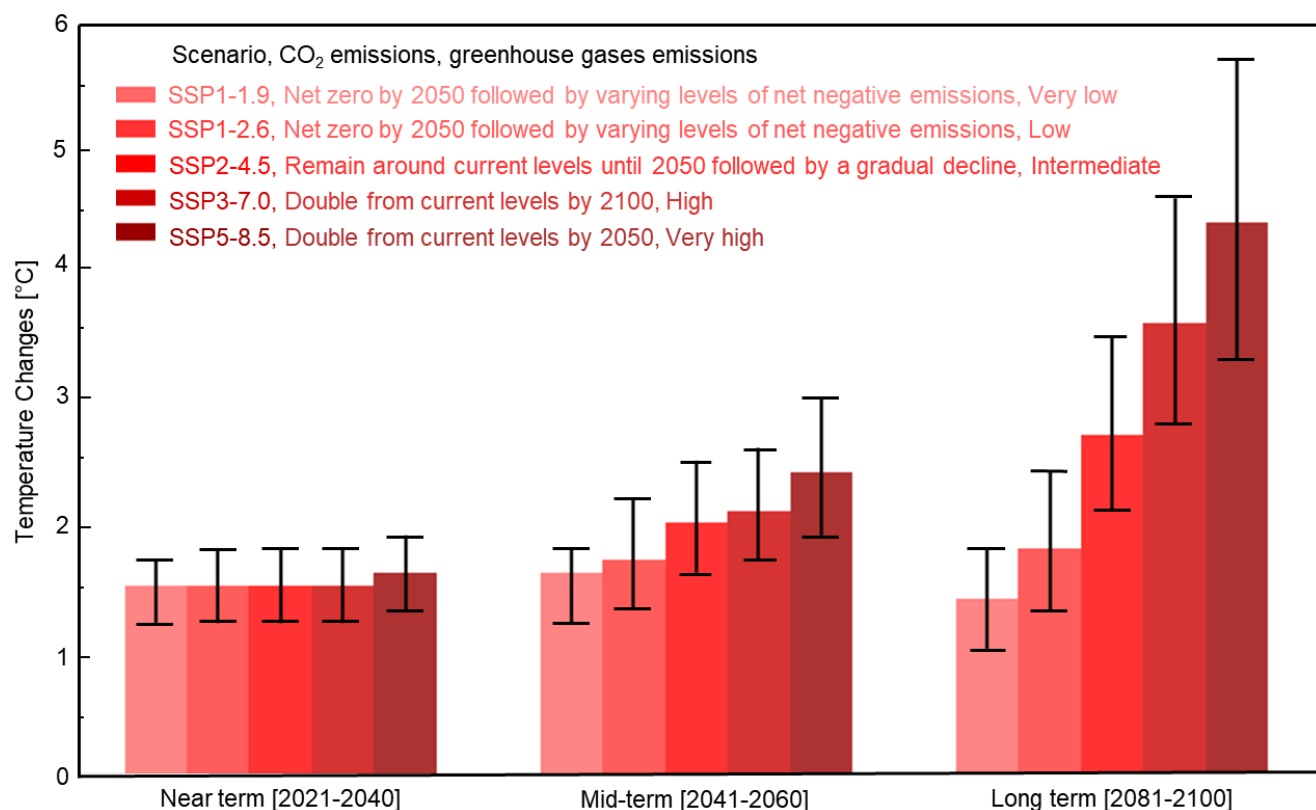


Fig 5-1. Temperature changes under five emission scenarios considering, different levels of CO₂ and greenhouse gas emissions (data: IPCC, 2021). Bar represent the best estimate of the projected temperature change and error bars represent estimate of the uncertainty associated with the projections. For example, range of temperature change in the near term (2021-2040) under the SSP1-1.9 scenario is 1.2 to 1.7°C. This means that there is a high degree of confidence that the temperature change will fall within this range. Best estimate represents the

value that is considered to have the highest probability. For example, the best estimate for the temperature change in the near term (2021-2040) under the SSP1-1.9 scenario is 1.5°C.

Climate change is expected to have significant impacts on the lake and its catchment area. Lake Urmia has been shown to be sensitive to changes in climatic conditions, with studies revealing periods of high-water levels (Djamali et al., 2008) and low lake levels, sometimes even drying out (Kong et al., 2022), as well as recent decreases in the lake's water volume because of changes in climatic conditions (Schulz et al., 2020).

Schulz et al. (2020) conducted series of forward simulations to forecast the development of Lake Urmia over 10-year periods. Even under current climatic boundary conditions similar to October 2012 to October 2016 and without water savings, Lake Urmia volume will continue to decrease (Schulz et al., 2020). Given the worsening climatic conditions, simulations based on lower precipitation, higher potential evaporation, and lower inflow into the lake, similar to observed climate conditions between October 1999 and September 2001, projects a dramatic decrease in the lake's volume.

5.2 Counter measures

The Urmia Lake Restoration Program (ULRP) was launched in 2015 with the aim of restoring the lake's water volume. The ULRP involves the cooperation of several government agencies, local communities, and universities. The program aims to address the issues through various measures, such as improving water management practices and promoting conservation and sustainable use of water resources. The program also seeks to improve the lake's ecosystem and promote sustainable agriculture. Although some achievements were made, most significantly completing the construction of a 36 km of artificial inflow channel connecting a dam in southern part to the lake and promising supply of 0.65 km³a⁻¹ inflow into the lake, the restoration remains challenging. According to Danesh-Yazdi and Ataie-Ashtiani (2019), the restoration initiative was not able to meet its schedule due to inaccurate estimation caused by data deficiencies. Despite these challenges, the ULRP remains an ongoing and significant effort to ensure the long-term sustainability of Urmia Lake and its catchment area.

6 Conclusions

Concluding remarks on Chapter 2

In conclusion, the variation in the volume of Lake Urmia over the last few decades has mainly been driven by changes in climatic conditions. However, human activities, particularly agricultural water extraction, have had a significant impact on the resilience of the lake. Without agricultural extraction, the lake volume would still have decreased, but it would have ended up at a much higher volume. The current climatic conditions and the lake's retraction to its northern and deeper parts have put it in a critical state, close to the tipping point where it loses its ability to buffer the reduced inflows into the lake. Therefore, any changes in water withdrawal could have a significant impact on the lake volume, presenting a risk but also an opportunity. Maintaining or increasing current extraction rates could result in a complete collapse of the lake, especially if climate continues to get dryer. However, substantial but realistic agricultural water savings could stabilize the lake and keep its volume above the crucial tipping point, thus bringing back its ability to buffer even if climate becomes dryer. In light of the current climatic conditions, such savings could also lead to a significant increase in the lake's volume and surface area, consequently restoring its role as a valuable and unique ecosystem.

Concluding remarks on Chapter 3

The DIY environmental chamber presented in this study provides a reliable and cost-effective means of simulating warm arid conditions. While some limitations were identified, such as a restricted temperature range for cooling and a slow equilibrium time for humidity, the set-up is easily replicable and adaptable to specific needs. The presented DIY chamber design allows for potential adaptations, such as improved insulation, which could potentially enhance the chamber's cooling capabilities and increase relative humidity limits for higher temperatures. However, commercial environmental chambers may be more suitable for certain applications that require specific temperature and humidity ranges or larger chamber sizes. Ultimately, the choice between a DIY or commercial chamber depends on individual needs and demands.

Concluding remarks on Chapter 4

The evaporation from the dried-up lake bed area and the open lake surface are dependent on the water level of the lake. At the lowest lake's water level observed in 2015, where the lake surface area was 1800 km² and the dried-up lake bed area was approximately 4000 km², the maximum evaporation from the dried-up area was estimated to only around 7% of the evaporation from the open lake surface, and often as low as 3-5%. Although this may appear to be a small component of the overall water balance of the Lake Urmia basin, it is important to note that this amount of evaporation exceeded the average annual urban drinking water consumption and was more than three times the average annual industrial water consumption for the entire Lake Urmia catchment in 2015.

Open research questions

Interaction between Lake Urmia and its groundwater

Understanding the complex interaction between Lake Urmia and its groundwater is critical to predicting how changes in groundwater extraction may impact the lake's water level and on the other hand the groundwater quality. While some studies have found significant groundwater inflow to the lake and thus a considerable hydraulic connection, some studies have estimated relatively low rates of direct groundwater inflow into the lake.

These studies investigate the influence of the lakebed layer, as well as lake level fluctuations, on groundwater-lake water interactions using a simple conceptual model, for a lakebed characterized by a thick sediment layer (e.g., Sheibani et al., 2022). And often because of factors, such as heterogeneity in the sediment layer, variations in water salinity and density, and oversimplification in conceptual models compared to the natural complexity of the system, this interaction has not been fully quantified. Further research is necessary to gain a better understanding of the dynamics involved in the interactions between the lake and groundwater.

Microclimate changes

Apart from predicted increase in the frequency of hot extremes, agricultural and ecological droughts, extreme precipitation events are also projected to increase in major mountainous regions, with the potential for floods, landslides, and lake outbursts (IPCC, 2021). For WCA projections based on CMIP6 models for the most favourable climate scenario, even under a 1.5°C warming level, it is predictable to see an increase in the intensity and frequency of heavy precipitation compared to the 1°C warming level. Although changes in climatic conditions are evident and will have a severe impact on the lake and surrounding area, it is not yet clear to what extent these anticipated changes will affect the local climate dynamics of Lake Urmia. Moreover, the potential ecological, agricultural, and socio-economic consequences of these changes remain uncertain.

Economic consequences

The IPCC (2021) shows that the risks associated with desertification, land degradation, and food insecurity are strongly influenced by socioeconomic conditions and extend beyond the scope of global temperature rise. In the Lake Urmia catchment area, where the economy relies heavily on agricultural activities, tourism, and factories, all of which have very high-water demand, understanding the economic consequences of drought is crucial. This understanding will help in planning a series of socioeconomic pathways to minimize negative impacts of drought in the region. To effectively address these consequences, it is important to consider the adverse effects of inequality, poverty, and the absence of international cooperation in achieving desired outcomes (O'Neill et al., 2020).

Acknowledgments

Special thanks to my dear colleagues Mrs. Gabriella Schubert, Mrs. Steffanie Smidt, and Mr. Rainer Seehaus for the support at the laboratory of the IAG at TU-Darmstadt. Many thanks to Mr. Mahdi Akbari and Mr. Amin Roozbahani at ULRP and thanks to Mr. Saber Faraji, M.Sc. student of Tabriz University, for the support during the field work. My deepest appreciation to my family and dear friends, whose love have been a constant source of inspiration and strength for me.

Supplementary information 1

Supplementary Information for:

Climate change or irrigated agriculture – what drives the water level decline of Lake Urmia

Stephan Schulz ^{a,*}, Sahand Darehshouri ^a, Elmira Hassanzadeh ^b, Massoud Tajrishy ^c,
Christoph Schüth ^a

^a Technische Universität Darmstadt, Institute of Applied Geosciences, Schnittspahnstr. 9, 64287, Darmstadt, Germany

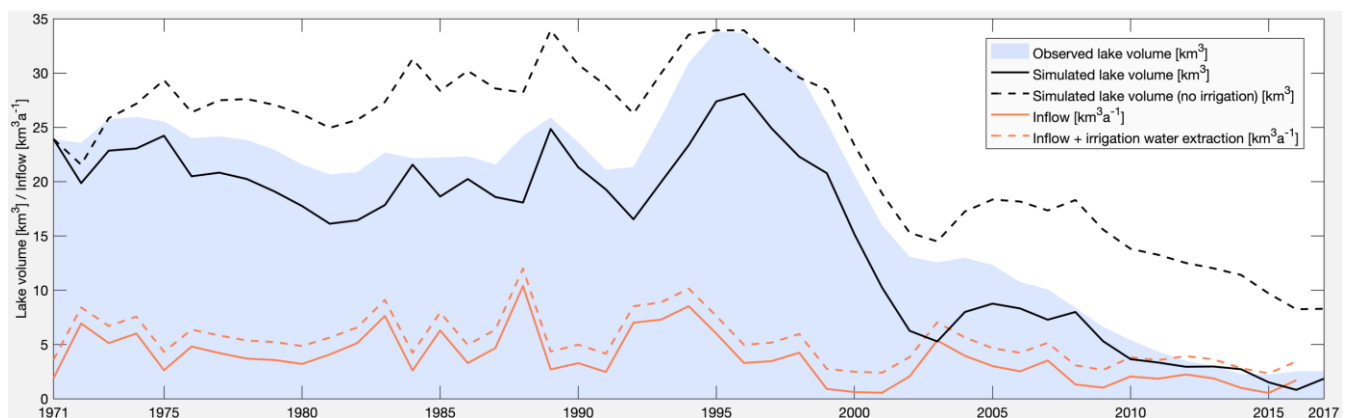
^b Polytechnique Montréal, Department of Civil, Geological and Mining Engineering, Montreal, Canada.

^c Sharif University of Technology, Urmia Lake Restoration Program, Department of Civil Engineering, Azadi Ave, P.O.Box: 11155, 9313, Tehran, Iran.

*Corresponding author: Stephan Schulz, schulz@geo.tu-darmstadt.de

Supplementary Information 1-S1

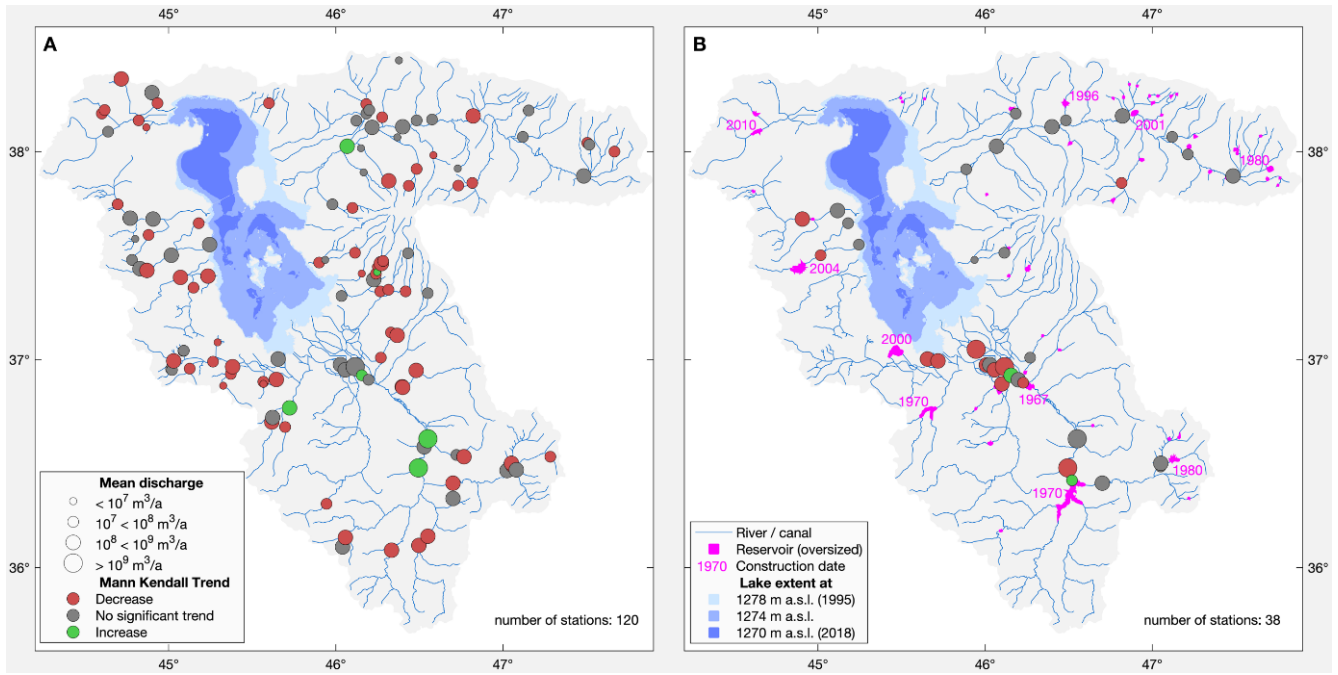
Based on the water balance and the computation of its individual components, we carried out two simulations to analyse the influence of surface water extraction for irrigation agriculture on the evolution of the lake volume. For the first scenario we simulated the change of the lake volume depending on the observed climatic boundary conditions and the observed inflow rates ("Simulated Lake volume", Fig. S3-1). For the second scenario we added the irrigation water extraction to the inflow to mimic natural runoff conditions ("Simulated Lake volume, no irrigation", Fig. S3-1). Limited by the availability of data on surface water extraction, the simulations were carried out for a period from 1971 to 2017. The common starting point for the lake volume is the observed volume of 23.9 km³ in 1971. For the year 2017 the simulated lake volume without irrigation water extraction (8.3 km³) is more than four times larger than the volume with irrigation water extraction (1.9 km³).



Supplemental **Fig. S1-1**. Simulated Lake volume evolution. Simulated lake volume evolution from 1971 to 2017 for observed inflow rates and natural inflow rates (inflow + irrigation water extraction). (Plot is generated using MATLAB R2019b, www.mathworks.com.)

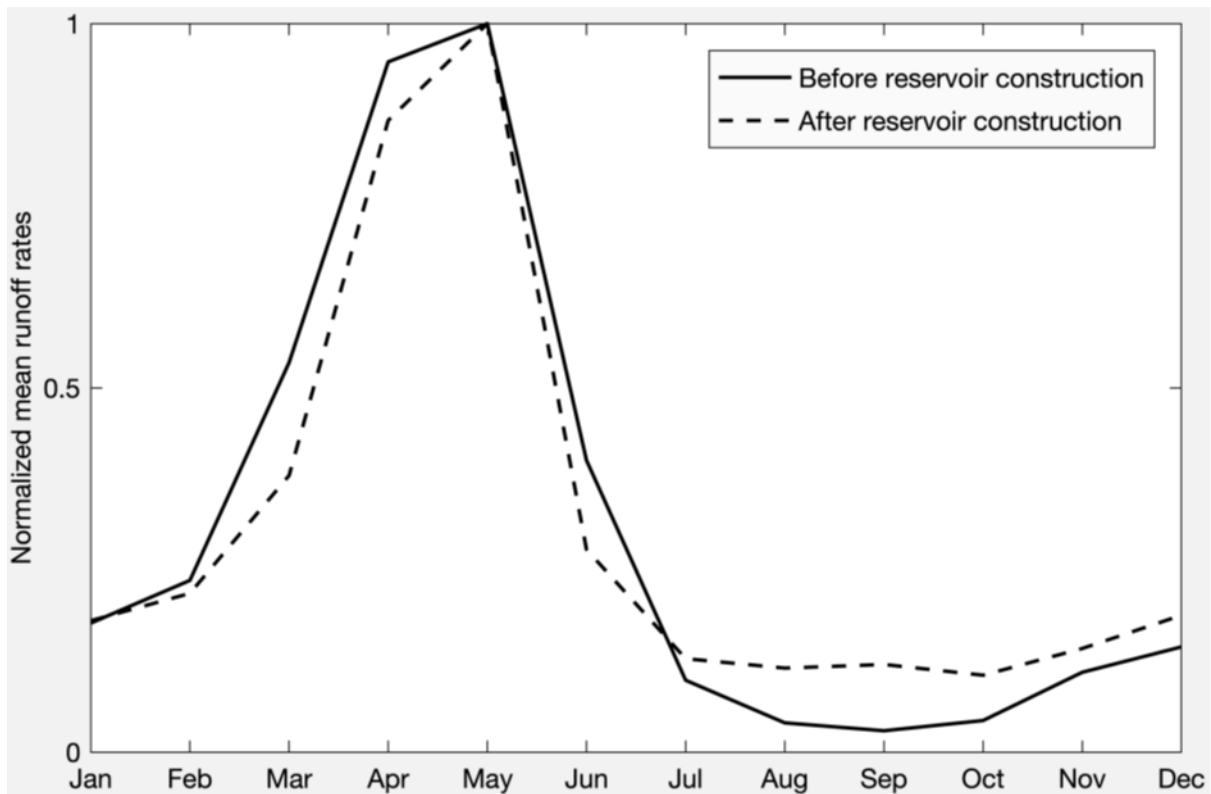
Supplementary Information 1-S2

To analyse the impact of the reservoirs on the temporal evolution of river discharge, we subdivided the discharge time series in those ones, which are not influenced by dams (i.e. before reservoir construction or upstream of a reservoir (Fig. S3-2a), and in those ones, originating from a station located downstream of a reservoir (Fig. S3-2b). Subsequently, we compared the Mann-Kendall trends and the mean discharge rates of both time series sets. The somehow surprising result is that there is not a big difference. Time series from stations located downstream of a reservoir show even less often negative trends (32%) compared to those, which are not influenced by dams (54%, Fig. S3-2). In order to compare the difference of the mean discharge rates, we could only use stations ($n = 30$), which are located downstream of a reservoir and have discharge records before as well as after construction. The runoff weighted mean discharge after storage construction is about 10% lower than before construction.



Supplemental Fig. S1-2. Mann-Kendall trends and mean annual flow rates for discharge stations. a, Upstream of reservoirs or before reservoir construction. b, Downstream of operating reservoirs. (Maps are generated using MATLAB R2019b, www.mathworks.com.)

The separation of the runoff time series into those influenced by reservoirs and those not influenced (see above) also served to analyse the interannual temporal runoff behaviour. Mean runoff time series are normalized to the maximum discharge occurring in May for both cases (Fig. S1-2.).



Supplemental **Fig. S1-3**. Interannual runoff variability. Interannual runoff variability of normalized mean runoff rates before and after dam construction. (Plot is generated using MATLAB R2019b, www.mathworks.com.)

Supplementary information 2

Supplemental Material for:

A low-cost environmental chamber to simulate warm climatic conditions

Sahand Darehshouri ^a, Nils Michelsen ^a, Christoph Schüth ^a, Stephan Schulz ^{a*}

^a Technische Universität Darmstadt, Institute of Applied Geosciences, Schnittspahnstr. 9,
64287 Darmstadt, German

*Corresponding author: Stephan Schulz, schulz@geo.tu-darmstadt.de

11 Pages:

13 Supplemental Figures

2 Supplemental Tables

Contents:

Supplemental Material 2-S1: Bill of materials and construction manual

Supplemental Material 2-S2: Homogeneity mapping experiments

Supplemental Material 2-S3: Comparison with commercial devices

Supplemental **Table S2-1.1**. Bill of materials, prices and suppliers.

| Name | Function | Number | Unit price [€] | Total price [€] | Supplier | Link |
|---|---|--------|----------------|-----------------|-----------------------|----------------------|
| Chamber framework | | | | | | - |
| Heavy-duty shelf | Chamber framework | 1 | 64,95 | 64,95 | Simonrack | Link |
| PC twin-wall sheet (2500 x 980 x 16 mm) | Climate chamber wall | 4 | 37,55 | 150,20 | Bauhaus | Link |
| PVC sheet (1000 x 495 x 5 mm) | Controlling board platform & access port | 2 | 17,00 | 34,00 | alt-intech PVC Platte | Link |
| Transparent acrylic glass panel | Access doorway | 1 | 11,80 | 11,80 | Bauhaus | Link |
| Window/door sealant | Sealant for access doorway | 1 | 11,99 | 11,99 | TESA | Link |
| Foam rubber sealing roll (10 m x 3 mm) | Sealant for door/access ports | 1 | 5,99 | 5,99 | CTA Dichtungen | Link |
| Cable glands (M16/M20/M25, 8 pieces) | Ports for cables/pipes | 1 | 15,99 | 15,99 | INIBUD | Link |
| Air circulation unit | | | | | | - |
| Pressure reducing valve | Reducing dry air pressure (10 bar to 0.5 bar) | 1 | 55,69 | 55,69 | Riegler | Link |
| PVC pipe (1 m, Ø 100 mm) | Air circulation | 2 | 4,59 | 9,18 | Awenta | Link |
| Inline fan (Ø 100 mm) | Air circulation | 1 | 18,09 | 18,09 | Vents | Link |
| PVC elbow pipe (90°, Ø 100 mm) | Air circulation | 1 | 4,06 | 4,06 | Awenta | Link |
| Tube fan (Ø 100) | Air circulation | 1 | 3,09 | 3,09 | Awenta | Link |

| | | | | | | |
|---|---|---|-------|-------|------------------------|----------------------|
| mm) | | | | | | |
| Connector flap for ventilation pipes | Connector flap for ventilation pipes | 1 | 2,56 | 2,56 | Lüftungssysteme Awenta | Link |
| Ventilation tube cap | Ventilation tube cap | 1 | 1,90 | 1,90 | MKK | Link |
| PVC non-return flap | Non-return flap | 1 | 2,64 | 2,64 | Awenta | Link |
| PVC air circulation pipe holder | Pipe holder | 3 | 2,51 | 7,53 | Awenta | Link |
| Cable plug | Cable plug | 4 | 3,49 | 13,96 | Kopp | Link |
| Aluminum sheet (1000 x 495 x 6 mm) | Bottom stabilization/air diffuser sheet | 1 | 72,66 | 72,66 | HLS tactical | Link |
| Flat plastic strip with rubber lip | Sealant for bottom plate | 1 | 11,30 | 11,30 | ROLLLA | Link |
| Pipe connector with male thread & grommet | Pipe connection | 2 | 7,99 | 15,98 | REKUBIK | Link |
| Heating unit | | | | | | - |
| Digital thermostat (dual relay) | Thermostat | 1 | 47,99 | 47,99 | INKBIRD | Link |
| Infrared heating lamp (150 W) | Heating | 2 | 8,69 | 17,38 | Philips | Link |
| Infrared heating lamp (300 W) | Heating | 2 | 9,43 | 18,86 | Sylvania | Link |
| Ceramic hanging lamp socket | Infrared lamp holder | 2 | 5,99 | 11,98 | TerraBasic | Link |
| Cable connector (water-proof) | Cable connectors for heating unit | 2 | 10,99 | 21,98 | LEBRIGHT | Link |
| Cooling unit | | | | | | - |
| Peltier element | Cooling device | 8 | 3,99 | 31,92 | HALJIA | Link |

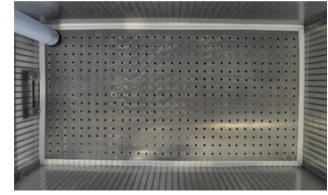
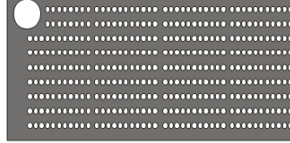
| | | | | | | |
|---|--|---|-------|-------|----------------------------|----------------------|
| (12 V, 60 W) | | | | | | |
| Aluminum heat sink (4 x 4 x 2 cm) | Heat exchanger | 8 | 1,39 | 11,12 | Ebay seller: heimwerker666 | Link |
| PC fan (Ø 6 cm) | Distribution of cold air from heat exchanger | 2 | 7,99 | 15,98 | Noiseblocker | Link |
| Water-cooling block (16 x 4 cm) | Cooling of Peltier elements | 2 | 9,39 | 18,78 | Kokiya | Link |
| Submersible water pump (12 V, 10 L/min) | Circulation of water through water block liquid cooler | 1 | 13,99 | 13,99 | COMET | Link |
| PC power supply (400 W, modified) | Power supply for Peltier element | 1 | 41,49 | 41,49 | Be quiet | Link |
| Humidifier unit | | | | | | |
| - | | | | | | |
| Digital humidity regulator (dual relay) | Air humidity controller | 1 | 44,99 | 44,99 | INKBIRD | Link |
| Ultrasonic humidifier | Humidifier | 1 | 9,99 | 9,99 | MagiDeal | Link |
| Air pump | Circulation of humid air from humidifier | 1 | 12,99 | 12,99 | POMISTY | Link |
| Plastic container (rectangular, 3.9 L) | Humidifier box | 1 | 7,99 | 7,99 | Lock & Lock | Link |
| Pipe connector with male thread & grommet | Pipe connection | 2 | 4,77 | 9,54 | sourcingmap | Link |
| Dry air injector | | | | | | |
| - | | | | | | |
| Pressure reducing valve | Reducing dry air pressure (10 bar to 0.5 bar) | 1 | 55,69 | 55,69 | Riegler | Link |
| Solenoid valve (G1/4 inch, NC) | Control of dry air flow | 2 | 34,90 | 69,80 | Magnetventile-shop | Link |
| Cable plug | Cable plug for solenoid | 2 | 7,29 | 14,58 | Kopp | Link |

| valve | | | | | | |
|--------------------------------------|--|---|-------|-------|-----------------|----------------------|
| Hose connector (T-shape, Ø 10 mm) | Connector for dry air hose | 1 | 1,99 | 1,99 | arbeitsbedarf24 | Link |
| Miscellaneous | | | | | | - |
| Cable (10 m, 1.5 mm ²) | Cable (e.g. for infrared lamps, solenoid valves, etc.) | 1 | 16,99 | 16,99 | Kopp | Link |
| PVC hose (reinforced, Ø 10 mm) | Hose (e.g. for dry air, humidified air, etc.) | 1 | 17,99 | 17,99 | Fittingstore | Link |

Construction manual

Polycarbonate twin-wall sheet
520×970 mm (Top)

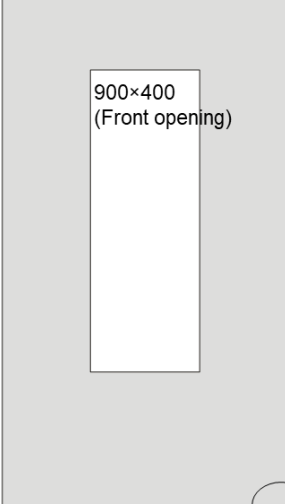
Perforated aluminium sheet
520×970 mm



1850×540 mm
(Left)



1850×980 mm
(Front)

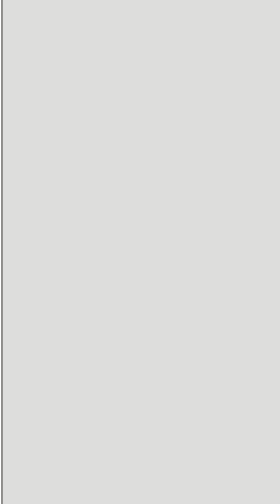


900×400
(Front opening)

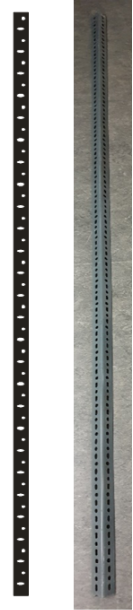
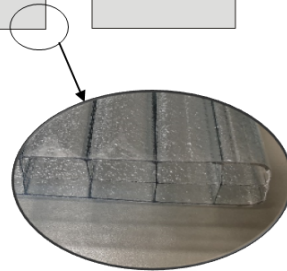
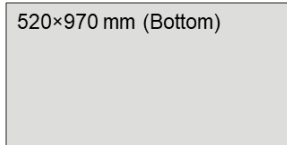
1850×540 mm
(Right)



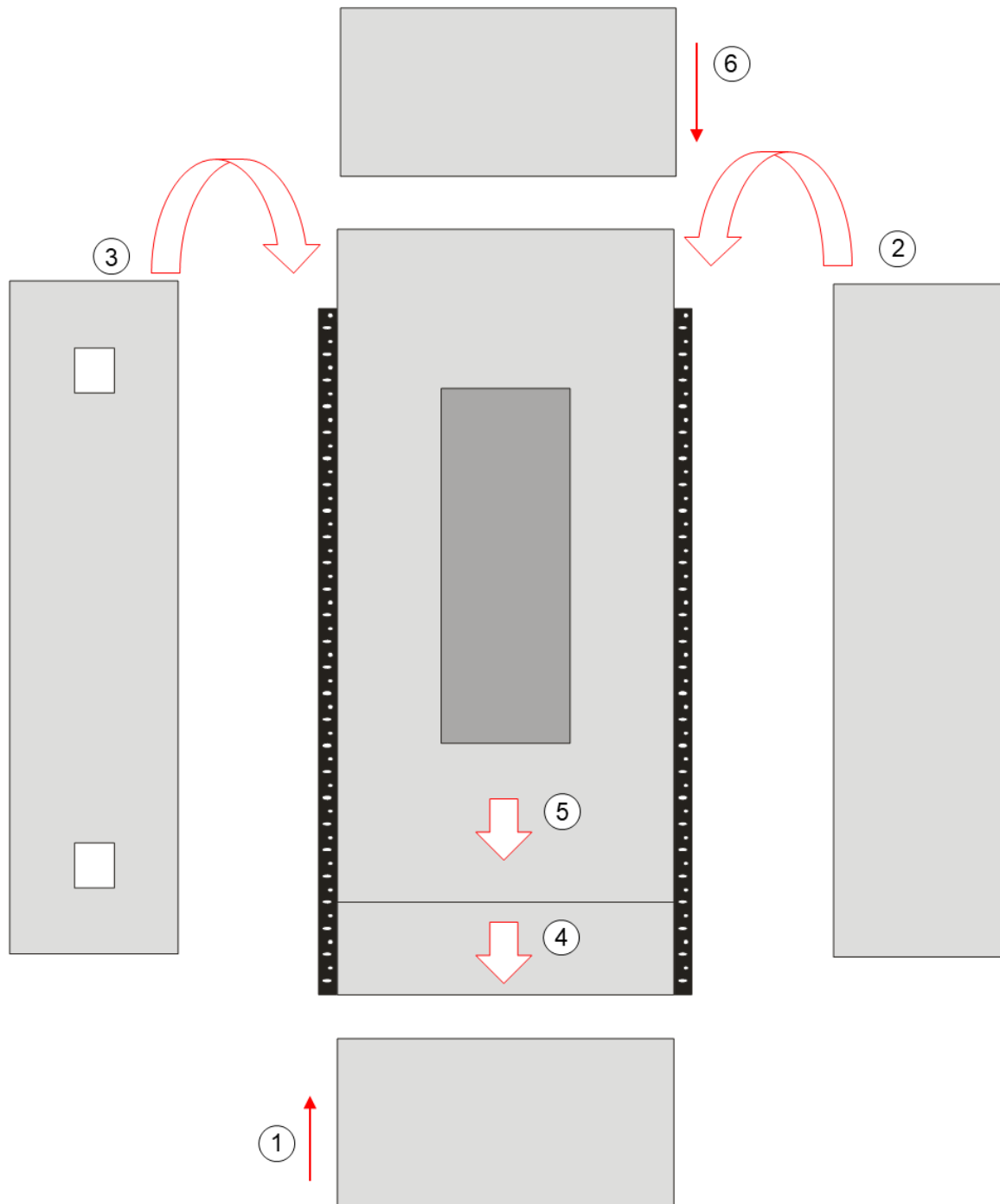
1850×980 mm
(Rear)



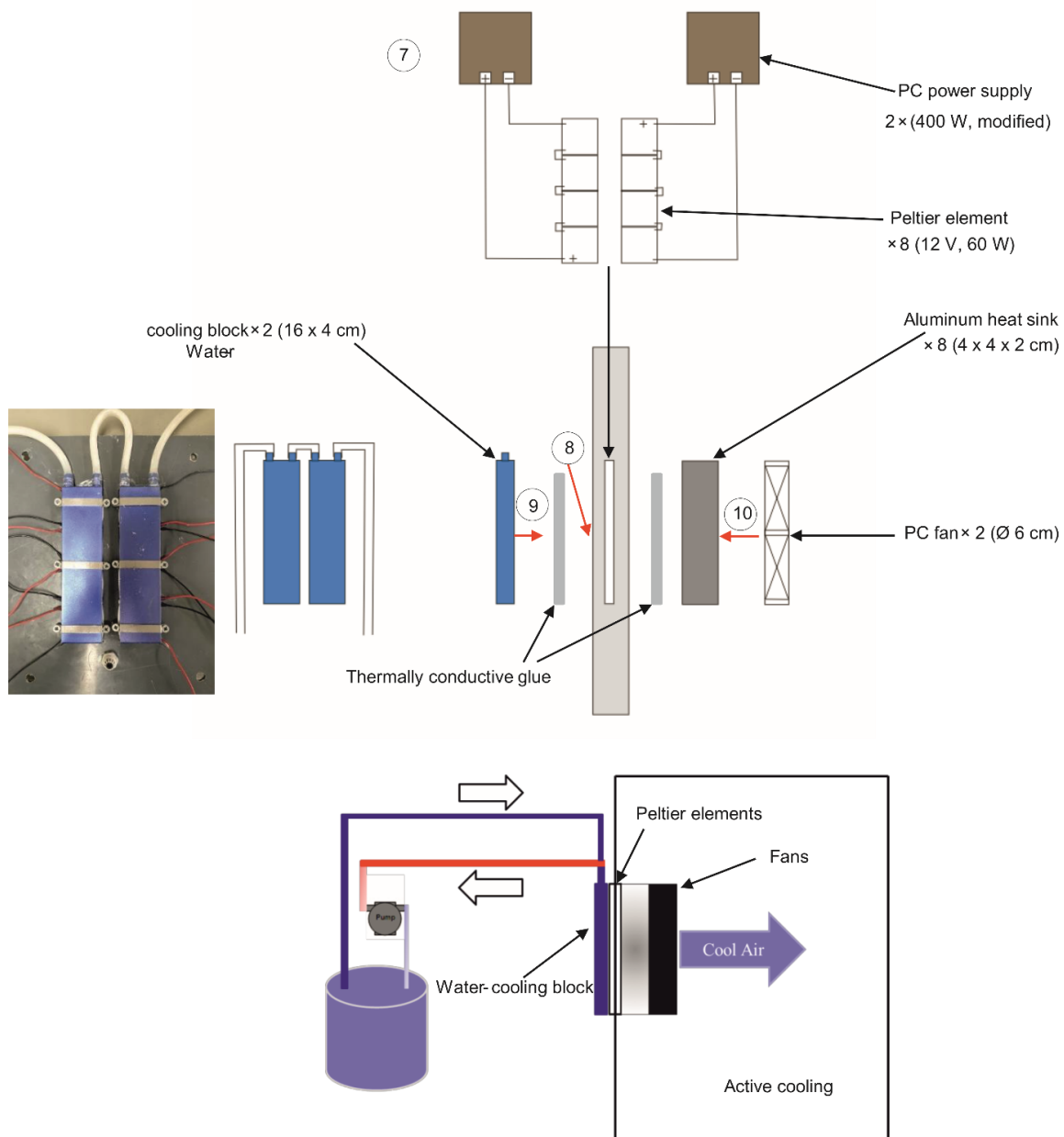
520×970 mm (Bottom)



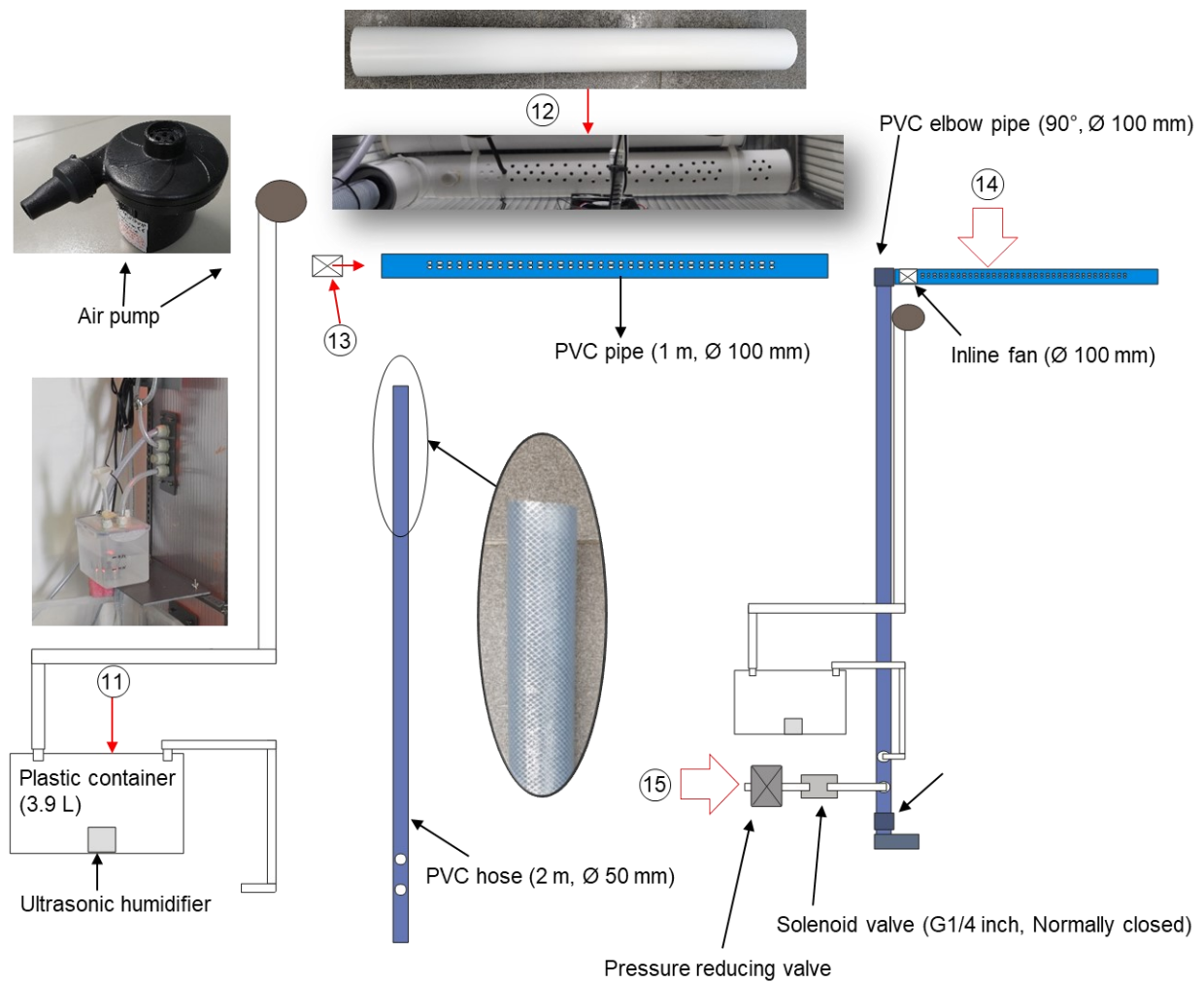
Supplemental **Fig. S2-1.1.** Cutting templates



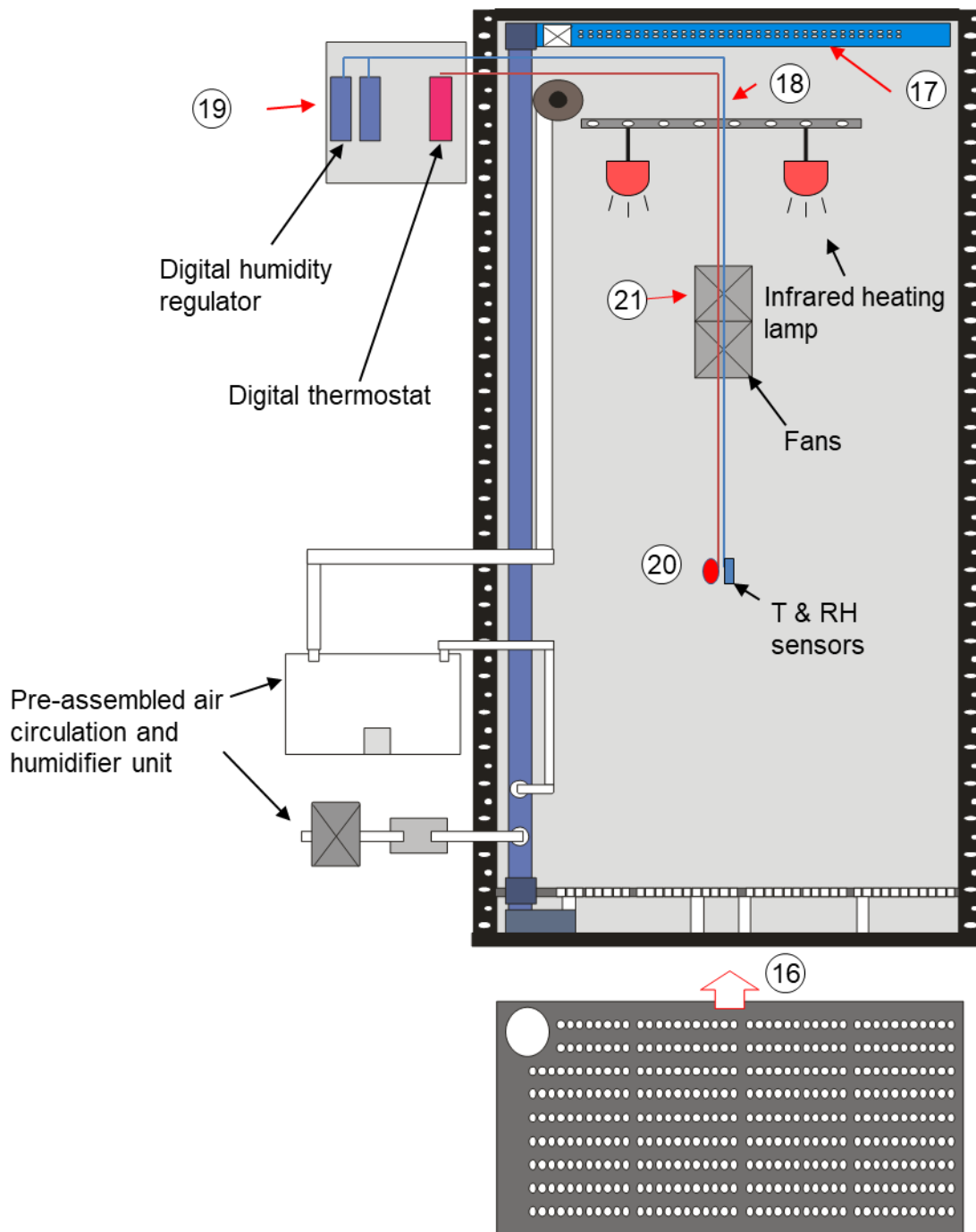
Supplemental **Fig. S2-1.2.** Assembly of the heavy-duty shelf, sliding in the climate chamber walls (1 to 6) and application of the sealing materials



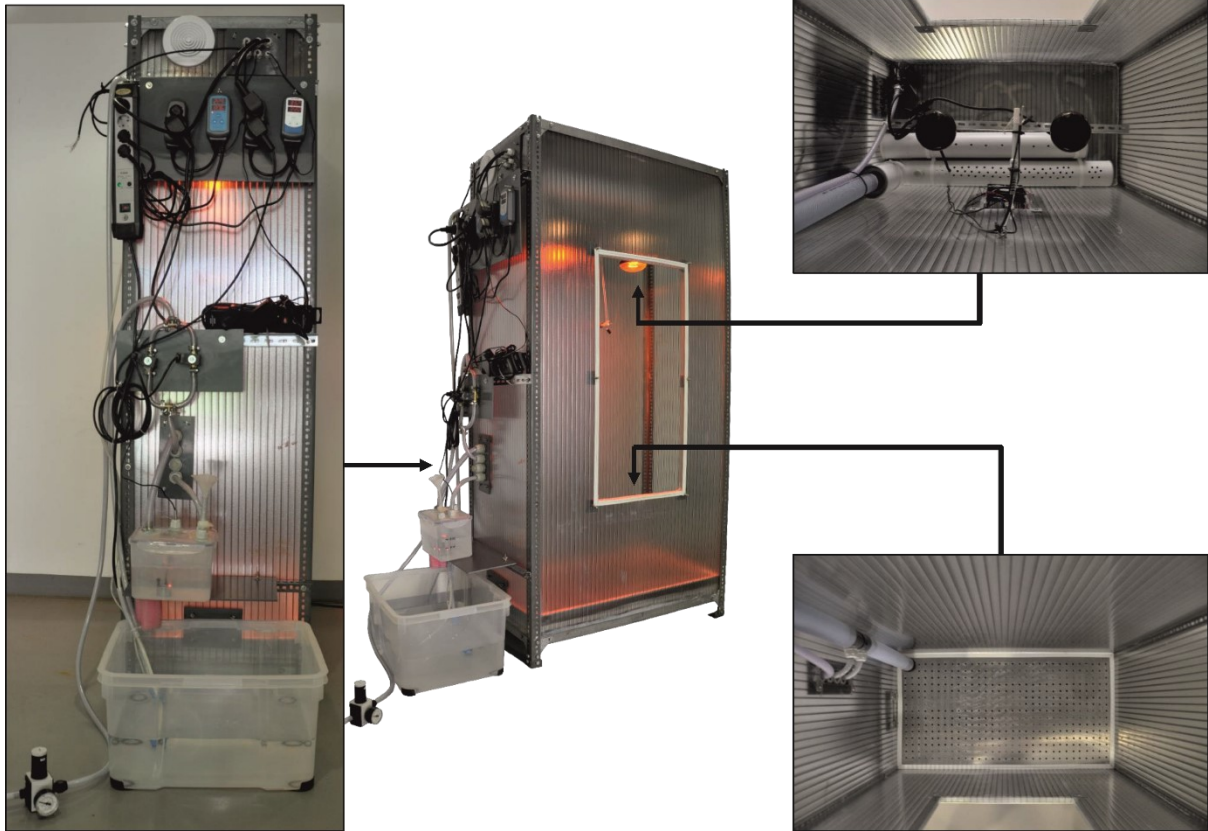
Supplemental **Fig. S2-1.3**. Cooling unit assembly: The wiring of the Peltier elements (7), application of the thermally conductive glue on the Peltier elements (8), mounting of the water-cooling blocks (9), mounting of the aluminium heat sinks and fans (10).



Supplemental **Fig. S2-1.4.** Air circulation and humidifier assembly: Construction of the moistening unit (11), perforation of the PVC pipe (12), installation of the inline fan (Ø 100 mm) (13), connection of PVC pipes with elbows and pipe connectors (14), installation of pressure reducing and solenoid valves (15).



Supplemental **Fig. S2-1.5**. Mounting of the pre-assembled units into the environmental chamber: Aluminium sheet installation (16), humidifier and air circulation unit installation (17), infrared heating lamps installation (18), controlling board platform & access port installation (19), temperature and relative humidity sensors installation (20), cooling unit installation (21)



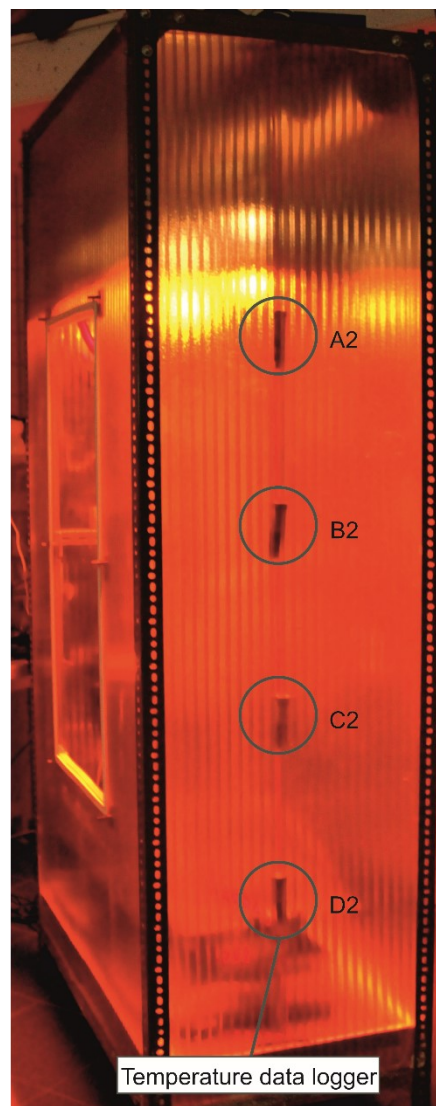
Supplemental Fig. S2-1.6. Detailed photographs

Supplemental Material 2-S2: Homogeneity mapping experiments

To detect deviations from the target temperature, USB temperature data loggers (EasyLog1, Lascar Electronics) were used. Eight loggers were tested against each other for a bias error in a preliminary experiment (pre-test 1). They were set to 1-minute measurement intervals and placed in an insulated box at a constant temperature for 24 hours. The average temperatures recorded by the individual loggers differed slightly and maximum negative and positive deviations accounted for -0.20°C and $+0.22^{\circ}\text{C}$, respectively. The encountered offsets were used to correct logger results in subsequent experiments (bias-correction). To map out vertical temperature deviations at different target temperatures, eight temperature data loggers (with 1-minute measurement intervals) were placed inside the climate chamber (two arrays; levels: 40, 70, 100, and 130 cm; Supplemental Fig. S2.1). Tests were conducted for six different temperatures, namely 25, 30, 35, 40, 45, and 50°C (24 hours each; Supplemental Fig. S2.2). To investigate lateral homogeneity, more sensors were needed, requiring an additional preliminary experiment (pre-test 2). Here, 21 loggers were set to 1-minute measurement intervals and placed in an insulated box at a constant temperature for

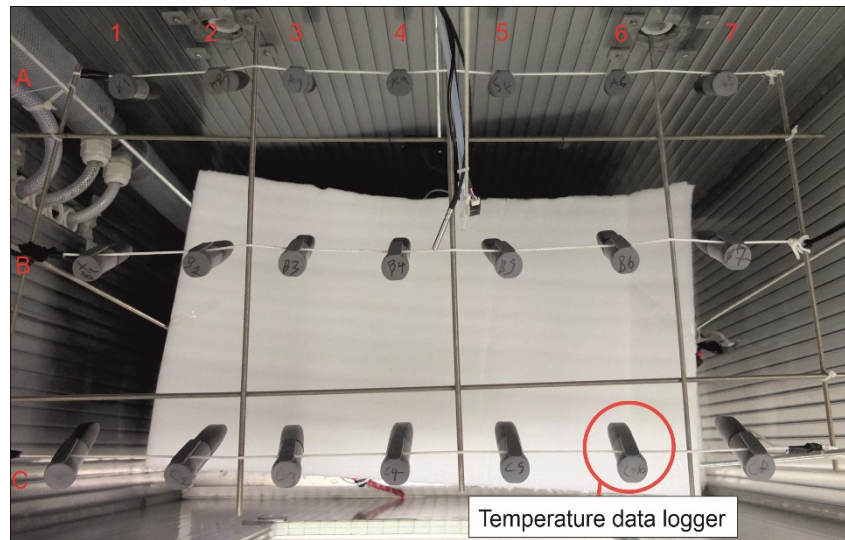
24 hours. The average temperatures recorded by the individual loggers again differed slightly and maximum negative and positive deviations accounted for -0.15°C and $+0.27^{\circ}\text{C}$, respectively. The encountered offsets were used to correct logger results in subsequent experiments (bias-correction). To map out horizontal temperature deviations at different target temperatures, the 21 temperature data loggers (with 1-minute measurement intervals) were placed inside the climate chamber (3 by 7 grid 80 cm above the perforated aluminium sheet; Supplemental Fig. S2.3). Tests were conducted for six different temperatures, namely 25, 30, 35, 40, 45, and 50°C (24 hours each; Supplemental Fig. S2.4).

Vertical temperature deviation from target temperature

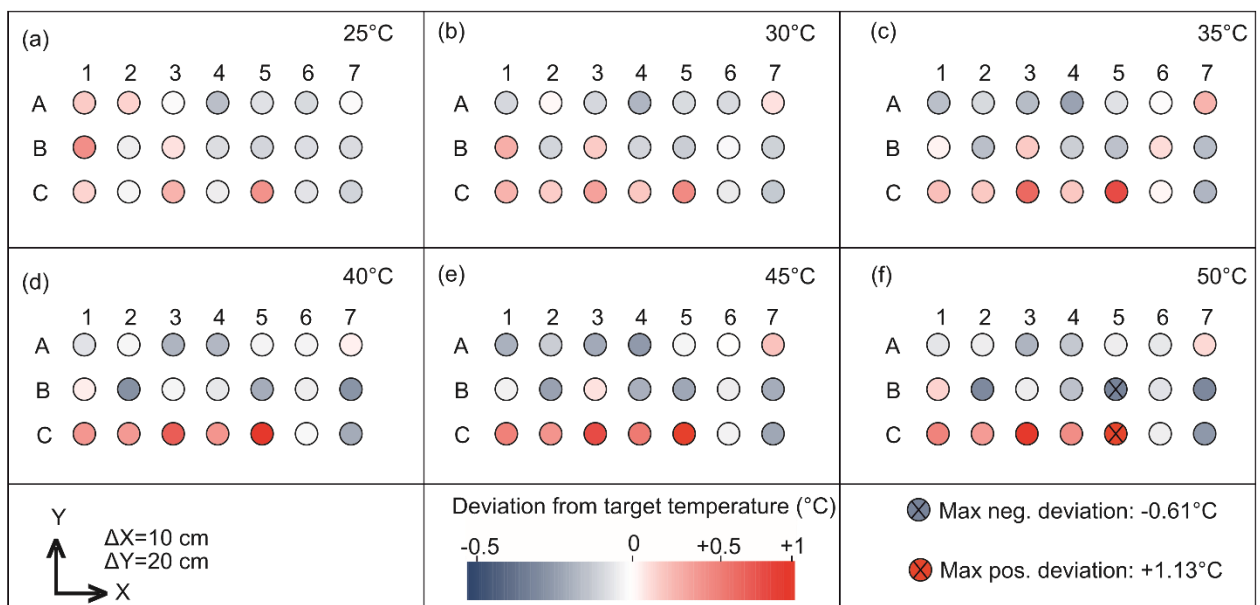


Supplemental **Fig. S2-2.1**. Vertical distribution of temperature data loggers.

Horizontal temperature deviation from target temperature



Supplemental Fig. S2-2.3. Horizontal distribution of temperature data loggers.

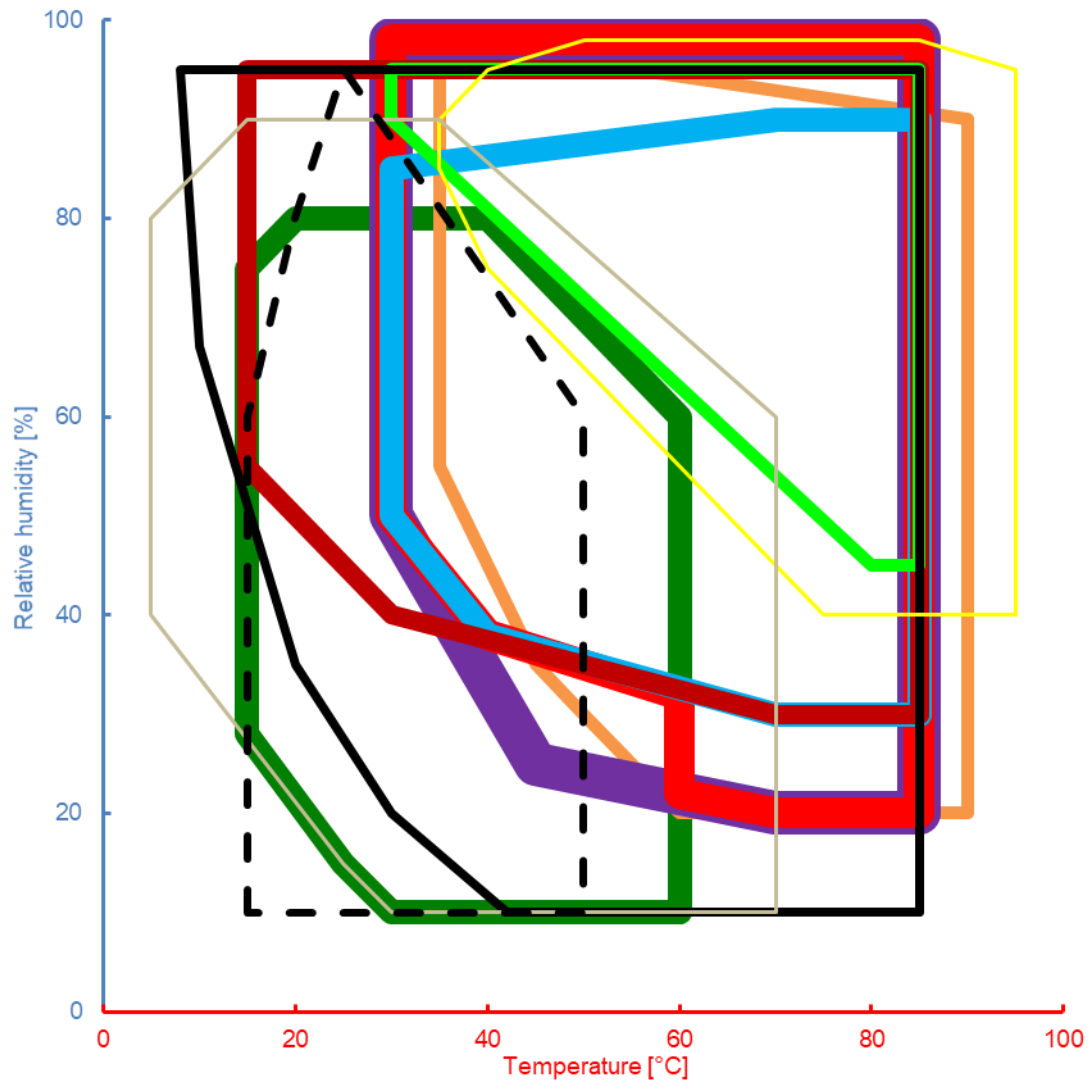


Supplemental Fig. S2-2.4. Horizontal temperature deviation from target temperature at 25°C (a), 30°C (b), 35°C (c), 40°C (d), 45°C (e), and 50°C (f).

Supplemental Material 2-S3: Comparison with commercial devices

Supplemental **Table S2-3.1**. Temperature and humidity control ranges for commercial environmental chambers and the DIY environmental chamber presented in this study. The colour code applies to Fig. S2-3.1.

| Colour Code | Brand | Model | Temperature range [°C] | Humidity range [%] | Inner dimensions w x h x d [mm] | Reference |
|--------------|---------------------------|------------------|------------------------|--------------------|---------------------------------|----------------------|
| Gold | Memmert | HPP110 | +5 to +70 | 10 to 90 | 560 x 480 x 400 | Memmert GmbH, (2019) |
| | Memmert | HPP260 (A) | +5 to +70 | 10 to 90 | 640 x 800 x 500 | Memmert GmbH, (2019) |
| | Memmert | HPP750 | +5 to +70 | 10 to 90 | 1040 x 1200 x 600 | Memmert GmbH, (2019) |
| Green | Memmert | HPP260 (B) | +15 to +60 | 10 to 80 | 640 x 800 x 500 | Memmert GmbH, (2019) |
| | Memmert | HPP1400 | +15 to +60 | 10 to 80 | 1250 x 1450 x 750 | Memmert GmbH, (2019) |
| | Memmert | HPP2200 | +15 to +60 | 10 to 80 | 1972 x 1450 x 750 | Memmert GmbH, (2019) |
| Orange | Memmert | HCP105 | +35 to +90 | 20 to 95 | 800 x 1030 x 800 | Memmert GmbH, (2019) |
| Purple | ESPEC | Platinus PSL-4J | +30 to +85 | 20 to 98 | 1000 x 1000 x 800 | ESPEC CORP, (2019a) |
| | ESPEC | Platinus PR-4J | +30 to +85 | 20 to 98 | 1000 x 1000 x 800 | ESPEC CORP, (2019a) |
| Yellow | ESPEC | Platinus PHP-4J | +35 to +95 | 40 to 98 | 1000 x 980 x 800 | ESPEC CORP, (2019a) |
| Red | ESPEC | Platinus PDL-4J | +30 to +85 | 20 to 98 | 1000 x 1000 x 800 | ESPEC CORP, (2019a) |
| Cyan | ESPEC | Platinus PCR-3J | +30 to +85 | 30 to 90 | 600 x 650 x 800 | ESPEC CORP, (2019a) |
| Dark Red | ESPEC | Bench top SH-642 | +15 to +85 | 30 to 95 | 400 x 400 x 400 | ESPEC CORP, (2019b) |
| Bright Green | ESPEC | Bench top LH-114 | +30 to +85 | 45 to 95 | 500×600×390 | ESPEC CORP, (2019b) |
| Black | Russells | G-64-5-5 | +8 to +85 | 10 to 95 | 1220 x 1220 x 1220 | Russells, (2019) |
| ----- | DIY environmental chamber | | +15 to 50 | 10 to 95 | 970 x 1790 x 520 | This study |



Supplemental **Fig. S2-3.1.** Temperature and relative humidity control ranges that can be simulated, for selected commercially available devices and for the DIY environmental chamber presented in this study. All commercial environmental chambers were tested at an ambient temperature of 23°C and the DIY environmental chamber was at an ambient temperature between 21 and 22°C.

References (Supplemental Material)

ESPEC CORP. 2019a. Platinous J Series Brings New Value to the World of Test Equipment. Available at: https://espec.com/images/uploads/files/e_platinum.pdf

ESPEC CORP. 2019b. Bench-Top Type Temperature and Humidity Chamber. Available at: <https://www.espec.co.jp/english/inquiry/catalog/sh.pdf>

Memmert GmbH. 2019. Climate chambers. Schwabach. Available at: <https://www.memmert.com/fileadmin/products/documents/categories/BR-ClimateChambers-english-USA.pdf>

Russells. 2019. Russells G - 64 specifications. Michigan. Available at: <https://www.russells-tech.com/g-64-elite-test-chambers.htm>

Supplementary information 3

Supplementary Information for:

Evaporation from the dried-up lake bed of Lake Urmia, Iran

Sahand Darehshouri ^{a,*}, Nils Michelsen ^a, Christoph Schüth ^a, Massoud Tajrishy ^b, Stephan Schulz ^a

^a Technische Universität Darmstadt, Institute of Applied Geosciences, Schnittspahnstr. 9, 64287 Darmstadt, Germany

^b Sharif University of Technology, Urmia Lake Restoration Program, Department of Civil Engineering, Azadi Ave, 11365-11155 Tehran, Iran

Corresponding author: Sahand Darehshouri, sahand64@yahoo.com

Hydrochemistry

Table S3-1. Chemical composition of the lake's water and the extracted groundwater sample from our monitoring well

| Samples Elements | Urmia Lake water | Groundwater ‡ |
|-------------------------------|------------------|-------------------|
| [mg l ⁻¹] | (Alipour, 2006) | (Monitoring well) |
| Mg ²⁺ | 6600 | 6240 |
| Ca ²⁺ | 1210 | 600 |
| K ⁺ | 1100 | 1270 |
| Na ⁺ | 88000 | 75250 |
| SO ₄ ²⁻ | 14200 | 15600 |
| Cl ⁻ | 153000 | 133800 |
| HCO ₃ ⁻ | 284 | 65 |

‡ Groundwater sample was extracted from our monitoring well (Fig. 1a). We analysed the major ion concentrations using ion chromatography (882 Compact IC plus from Metrohm, Herisau, Switzerland) at the Institute of Applied Geosciences, Technical University of Darmstadt, Germany.

Location and elevation of monitoring well

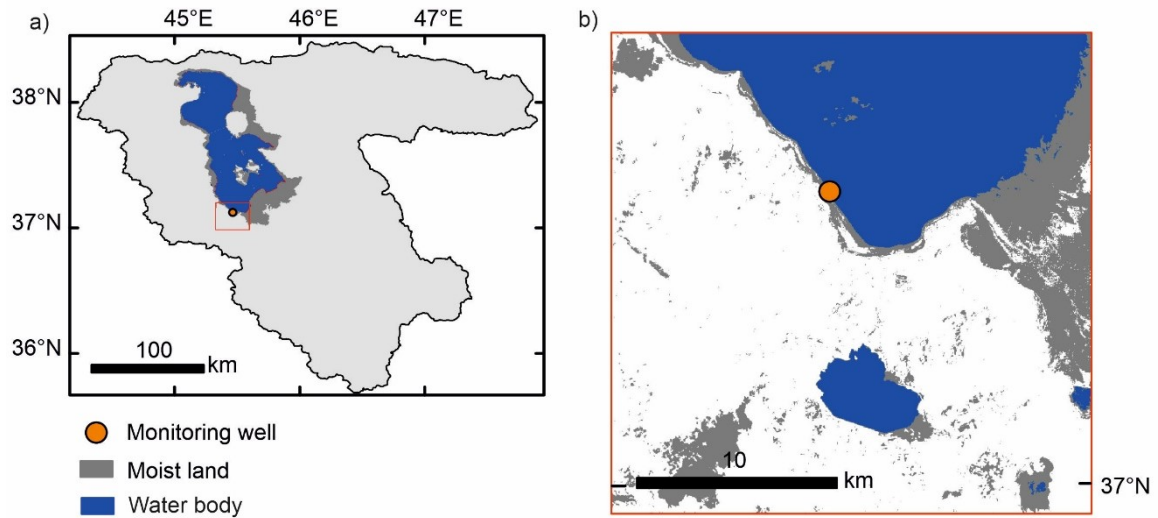


Fig. S3-1. Estimating the approximate elevation of monitoring well; (a) overview location of the monitoring well, (b) elevation estimation of the wellhead using classified Landsat-5 image (acquisition date: 2nd of October 2006) showing the closest lake shoreline to our monitoring well, and the lake level at that date was 1,272.80 m a.s.l. (data source; ULRP, 2021).

Sampling procedure



Fig. S3-2. Sampling procedure; (a) column 1 at 37.128°N, 45.760°E, and (b) column 2 at 37.114°N, 45.458°E were collected in October 2016 from the southwestern and southern part of the dried up lake bed, respectively. (c) the excavated lakebed, consisting of fine silty sediments that also contain clay.

Grain size distribution

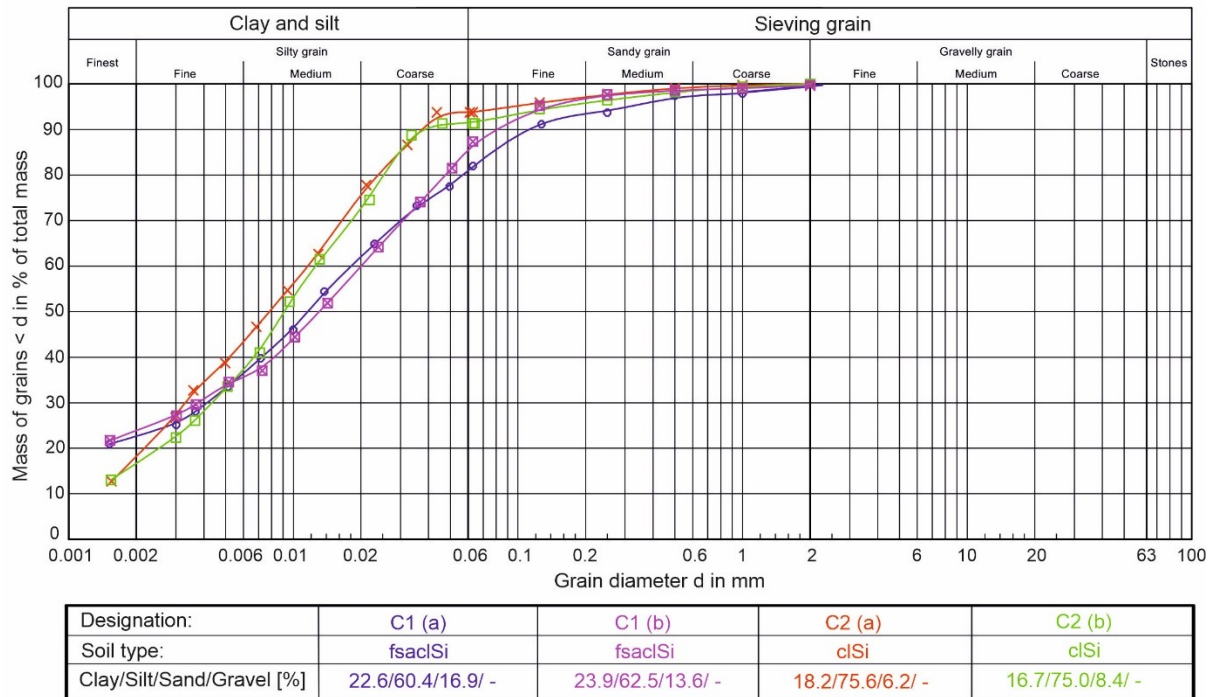


Fig. S3-3. Grain size distribution curve, Samples collected in October 2016 from the southern (C1) and southwestern (C2) part of Lake Urmia (Fig. 1) at 0 (a) to 0.5 m (b) depth. The sediments consist mainly of clayey silt (clSi) and fine sandy, clayey silt (fsacSi).

Lake surface evaporation and regionalization

Using a simplified versions of the standardised Penman equation (Eq. S1; Valiantzas, 2006), we first calculated potential evaporation for fresh water from the open water using daily meteorological data from the city of Urmia between 1998 and 2020 (WRMC, 2021) which is the closest weather station to the lake. To estimate the actual evaporation from the lake, the calculated potential evaporation was then multiplied by the corresponding lake area and the corresponding evaporation reduction coefficient (α) of Lake Urmia, which constitutes the ratio between fresh and saline water evaporation (Salhotra et al. 1985). Here, we used the salinity index (Eq. S5) and α coefficient of Lake Urmia (Eq. S6) following Schulz et al. (2020) for our time series.

$$E_{PEN} \approx 0.047R_S\sqrt{T + 9.5} - 2.4\left(\frac{R_S}{R_A}\right)^2 + 0.09(T + 20)\left(1 - \frac{RH}{100}\right) \quad \text{Eq. S1}$$

Where:

T: temperature [°C],

RH: relative humidity [%],

R_S : solar radiation calculated based on measured sunshine hours [$\text{MJ m}^{-2} \text{d}^{-1}$] using an empirical relationship (Eq. S2).

$$R_S \approx R_A \cdot \left(0.5 + 0.25 \cdot \frac{n}{N}\right) \quad \text{Eq. S2}$$

Where:

n: is the measured bright sunshine hours per day [h],

N: is the maximum possible daylight duration [h] calculated using the simplified empirical approximations of Shuttleworth (1993) and Allen & Pereira (1994), which is given by Valiantzas (2013) in Eq. S3.

$$N \approx 4\phi \sin(0.53i - 1.65) + 12 \quad \text{Eq. S3}$$

i: is the number of months in the year (1-12) with January = 1,

R_A : is the extra-terrestrial radiation [$\text{MJ m}^{-2} \text{d}^{-1}$]; the simplified calculation given in by Valiantzas (2013) in Eq. S4

$$R_A \approx 3N \sin(0.131N - 0.95\phi) \quad \text{for } |\phi| > \frac{23.5\pi}{180} \quad \text{Eq. S4}$$

Where:

\emptyset : latitude of the site [radians]

Salinity index of Lake Urmia estimated by Schulz et al. (2020) is given in Eq. S5. Here, the corresponding values of the lake volume for our time series (1998 to 2020) were inserted into the Salinity index equation.

$$S = -0.62 \times V + 37.2 \quad \text{Eq. S5}$$

Where;

S: Salinity [%], V: lake volume [km³].

Empirical evaporation coefficient (α) of Lake Urmia as a function of salinity, estimated by Schulz et al. (2020), is given in Eq. S6.

$$\alpha = -0.012 \times S + 1.13 \quad \text{Eq. S6}$$

Where;

S: Salinity [%].

Table S3-2. Averaged lake volume, water level of the lake and the saltwater evaporation coefficient as ratio between saline and freshwater evaporation.

| Year (Dry season*) | Lake volume [km ³] | Salinity index [%] | Evaporation coefficient ratio (α) |
|-----------------------|--------------------------------|--------------------|---|
| 1998 | 31.06 | 18.0 | 0.89 |
| 1999 | 24.20 | 22.3 | 0.86 |
| 2000 | 19.42 | 25.2 | 0.82 |
| 2001 | 15.02 | 27.9 | 0.79 |
| 2002 | 13.31 | 29.0 | 0.77 |
| 2003 | 14.01 | 28.5 | 0.76 |
| 2004 | 13.58 | 28.8 | 0.76 |
| 2005 | 12.47 | 29.5 | 0.76 |
| 2006 | 10.85 | 30.5 | 0.75 |
| 2007 | 10.45 | 30.7 | 0.74 |
| 2008 | 7.94 | 32.3 | 0.73 |
| 2009 | 5.99 | 33.5 | 0.72 |
| 2010 | 5.47 | 33.8 | 0.71 |
| 2011 | 4.38 | 34.5 | 0.70 |
| 2012 | 3.48 | 35.0 | 0.69 |
| 2013 | 2.99 | 35.3 | 0.69 |
| 2014 | 2.01 | 35.9 | 0.68 |
| 2015 | 2.01 | 35.9 | 0.68 |
| 2016 | 3.14 | 35.2 | 0.68 |
| 2017 | 2.54 | 35.6 | 0.68 |
| 2018 | 2.54 | 35.6 | 0.68 |
| 2019 | 5.47 | 33.8 | 0.69 |
| 2020 | 5.17 | 34.0 | 0.70 |

* June, July and August

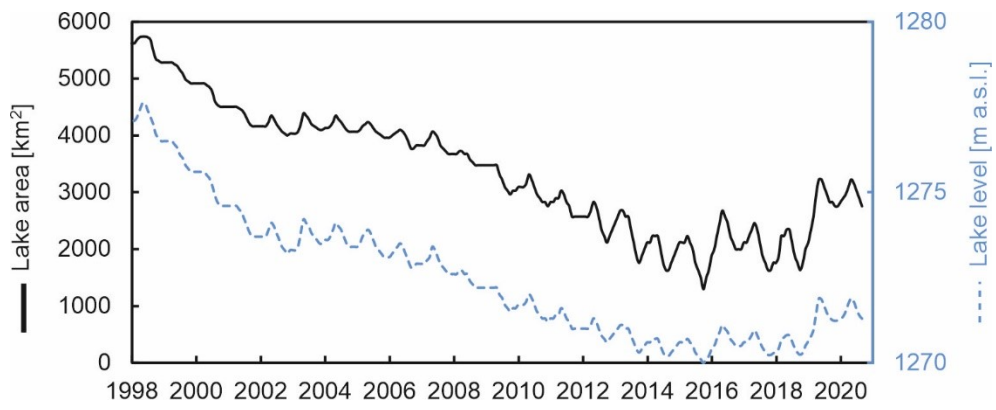


Fig. S3-4. Lake Urmia level compared to lake area (monthly mean) from 1998 to 2020.

Influence of temperature on sensors (Sealed column experiment)

To test the influence of temperature on the sensors or the apparent wiggling observed in Fig. 4, we have conducted an additional experiment with sealed columns to avoid evaporative losses. The columns then exposed to diurnal temperature and relative humidity changes (Fig. S5a). The simulated diurnal temperature cycles lead to corresponding variations in apparent water level (Fig. S5b).

During the controlled experiment, we also tested the influence of temperature variations on the scales. In this temperature range we observed ± 4 g changes while weighing samples of approximately 25,000 and 27,000 g (Fig. S5c). We observed similar variations in weight as in the main experiment, confirming that the observations were most likely due to a temperature effect on the sensors.

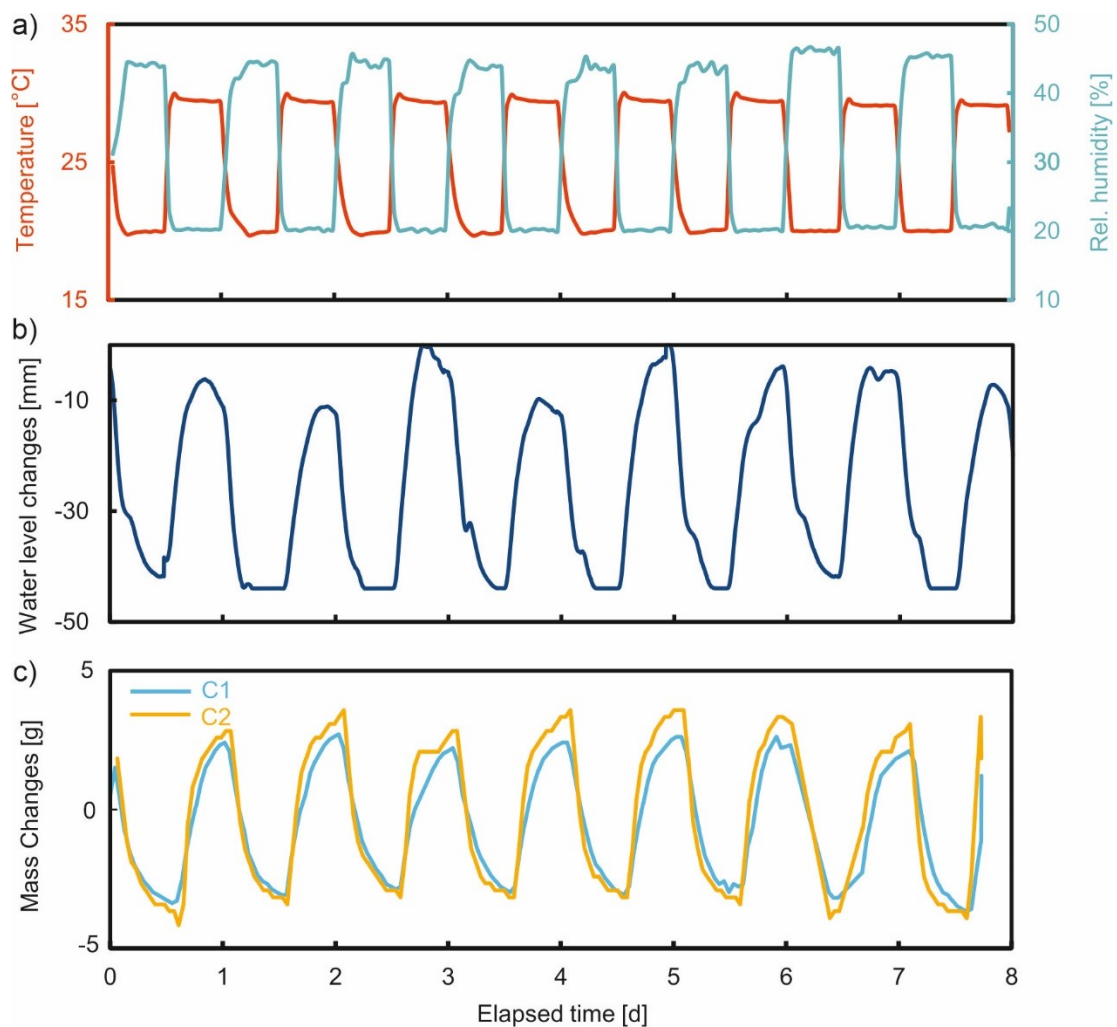


Fig. S3-5. Influence of temperature on sensors; (a) simulated diurnal temperature and humidity, corresponding (b) water level changes and (c) weight changes.

Annual and seasonal evaporation

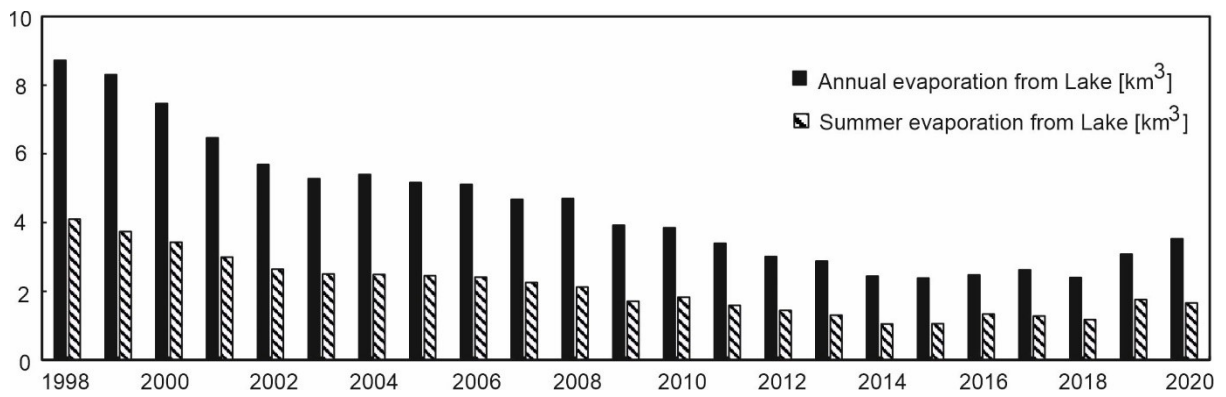


Fig. S3-6. Estimated yearly evaporation compared to summer (June, July and August) evaporation from the open lake surface.

Table S3-3. Estimated evaporation amounts from lake surface and dried up lakebed area of the Lake Urmia for three summer months (June, July and August) in the period 1998–2020)

| Year (Dry season) | Lake area [km ²] | Dried up lakebed [km ²] | Evaporation from lake surface [km ³] | Evaporation from dried up lake bed based on column 1 [km ³] | Evaporation from dried up lake bed based on column 2 [km ³] |
|-------------------------|------------------------------------|---|---|--|--|
| 1998 | 5718.4 | 0.0 | 4.10 | 0.00 | 0.00 |
| 1999 | 5156.2 | 543.8 | 3.73 | 0.01 | 0.01 |
| 2000 | 4743.2 | 956.8 | 3.43 | 0.01 | 0.02 |
| 2001 | 4375.4 | 1324.6 | 2.99 | 0.01 | 0.02 |
| 2002 | 4207.1 | 1492.9 | 2.64 | 0.02 | 0.03 |
| 2003 | 4279.8 | 1420.2 | 2.50 | 0.02 | 0.03 |
| 2004 | 4230.7 | 1469.3 | 2.49 | 0.02 | 0.03 |
| 2005 | 4133.8 | 1566.2 | 2.46 | 0.02 | 0.03 |
| 2006 | 3989.5 | 1710.5 | 2.41 | 0.02 | 0.03 |
| 2007 | 3942.7 | 1757.3 | 2.25 | 0.02 | 0.03 |
| 2008 | 3595.7 | 2104.3 | 2.12 | 0.02 | 0.04 |
| 2009 | 3212.1 | 2487.9 | 1.71 | 0.03 | 0.04 |
| 2010 | 3095.5 | 2604.5 | 1.83 | 0.03 | 0.05 |
| 2011 | 2851.3 | 2848.7 | 1.59 | 0.03 | 0.05 |
| 2012 | 2559.4 | 3140.6 | 1.44 | 0.03 | 0.06 |
| 2013 | 2346.4 | 3353.6 | 1.30 | 0.04 | 0.06 |
| 2014 | 1799.9 | 3900.1 | 1.06 | 0.04 | 0.07 |
| 2015 | 1799.9 | 3900.1 | 1.06 | 0.04 | 0.07 |
| 2016 | 2422.4 | 3277.6 | 1.33 | 0.04 | 0.06 |
| 2017 | 2115.6 | 3584.4 | 1.28 | 0.04 | 0.06 |
| 2018 | 2115.6 | 3584.4 | 1.18 | 0.04 | 0.06 |
| 2019 | 3095.5 | 2604.5 | 1.76 | 0.03 | 0.05 |
| 2020 | 3029.7 | 2670.3 | 1.66 | 0.03 | 0.05 |

References

- Alipour, S., 2006. Hydrogeochemistry of seasonal variation of Urmia Salt Lake, Iran. *Saline Systems* 2, 9. <https://doi.org/10.1186/1746-1448-2-9>
- Allen, R., Smith, M., Pereira, L., Perrier, A., 1994. An update for the calculation of reference evaporation. *ICID Bull.* 43. 35–92.
- Salhotra, A.M., Adams, E.E., Harleman, D.R.F., 1985. Effect of Salinity and Ionic Composition on Evaporation: Analysis of Dead Sea Evaporation Pans. *Water Resources Research*. 21, 1336–1344. <https://doi.org/10.1029/WR021i009p01336>
- Schulz, S., Darehshouri, S., Hassanzadeh, E., Tajrishy, M., Schüth, C., 2020. Climate change or irrigated agriculture – what drives the water level decline of Lake Urmia. *Scientific Reports* 10, 1–10. <https://doi.org/10.1038/s41598-019-57150-y>
- Shuttleworth, W.J., 1993. Evaporation. An Update for the Calculation of Reference Evapotranspiration In: *Handbook of hydrology*, D.R. Maidment (Ed.), McGraw-Hill, New York, USA (Chapter 4, 4.1-4.53)
- ULRP, 2021. Urmia Lake Restoration programme. Daily Lake Urmia level data. Available at: <https://www.ulrp.ir/fa/آرشیو-تراز-دریاچه-ارومیه/>, (accessed 26 November 2021)
- Valiantzas, J.D., 2013. Simplified forms for the standardized FAO-56 Penman-Monteith reference evapotranspiration using limited weather data. *Journal of Hydrology* 505, 13–23. <https://doi.org/10.1016/j.jhydrol.2013.09.005>
- Valiantzas, J.D., 2006. Simplified versions for the Penman evaporation equation using routine weather data. *Journal of Hydrology* 331, 690–702. <https://doi.org/10.1016/j.jhydrol.2006.06.012>
- WRMC, 2021. Water Resources Management Company (WRMC) of Iran Ministry of Energy